2007-07-19

Elliptical Rolling Link Toggle Mechanisms for Passive Force Closures with Self-Adjustment

Jacob Ross Montierth
Brigham Young University - Provo

ELLIPTICAL ROLLING LINK TOGGLE MECHANISMS FOR PASSIVE FORCE CLOSURES WITH SELF-ADJUSTMENT

By

Jacob R. Montierth

A thesis submitted to the faculty of

Brigham Young University

in partial fulfillment of the requirements for the degree of

Master of Science

Department of Mechanical Engineering

Brigham Young University

August 2007

BRIGHAM YOUNG UNIVERSITY

GRADUATE COMMITTEE APPROVAL

of a thesis submitted by

Jacob R. Montierth

This thesis has been read by each member of the following graduate committee and by majority vote has been found to be satisfactory.

_____	_____
Date	Robert H. Todd, Chair
_____	_____
Date	Larry L. Howell
_____	_____
Date	Spencer P. Magleby

BRIGHAM YOUNG UNIVERSITY

As chair of the candidate's graduate committee, I have read the thesis of Jacob R. Montierth in its final form and have found that (1) its format, citations, and bibliographical style are consistent and acceptable and fulfill university and department style requirements; (2) its illustrative materials including figures, tables, and charts are in place; and (3) the final manuscript is satisfactory to the graduate committee and is ready for submission to the university library.

_____ _____

Date

Robert H. Todd
Chair, Graduate Committee

Accepted for the Department

_____

Matthew R. Jones
Graduate Coordinator

Accepted for the College

_____

Alan R. Parkinson
Dean, Ira A. Fulton College of
Engineering and Technology

ABSTRACT

ELLIPTICAL ROLLING LINK TOGGLE MECHANISMS FOR

PASSIVE FORCE CLOSURES WITH SELF-ADJUSTMENT

Jacob R. Montierth

Department of Mechanical Engineering

Master of Science

This thesis presents elliptical rolling contact joints as an alternative to circular rolling contact and conventional revolute joints where high quality force transmission—low friction and backlash—with variable output are desired. Parameters specific to the joint and its position are developed in terms of relative link angles and elliptical surface geometry. These parameters are used to generate the basic forward kinematics for elliptical rolling link toggle mechanisms with oscillatory motion and high mechanical advantage. As large compressive loads are characteristic of such mechanisms, stress conditions are identified and principles for joint stability with variable, precision outputs are discussed. Finally, application is made to self-adjusting passive force closures with a case study of the MUSCLE Brake (Multi-toggle Self-adjusting Connecting-Linked Electromechanical) disc brake caliper.

Elliptical rolling contact joints are shown to offer several benefits over circular rolling contact, including: reduced Hertz contact stresses and flexure bending stresses, variable output velocity, maximum use of contact interface by distributing small rotations across surfaces of small curvature, reduced forces on stabilizing members, increased mechanical advantage due to eccentricity, and no-slip pure rolling provided exclusively by connecting links (or flexures) without the need for gear teeth or friction.

ACKNOWLEDGMENTS

This work represents the contribution and sacrifice of many individuals. I appreciate the guidance, encouragement, and wisdom of my advisor, Dr. Robert Todd. His faith in my potential never waned, and his example of persistence and determination continues to motivate me to “do good work”. I also want to thank Dr. Larry Howell for his expertise in mechanism design and Dr. Spencer Magleby for product insights and mentoring throughout my graduate career. I count it a privilege to have attended Brigham Young University and studied under these great professors.

Funding for my research was provided by the Utah Center of Excellence Program and the Department of Mechanical Engineering at BYU; both are appreciated. I’m grateful for the ideas and input of fellow Compliant Mechanisms Research lab members, in particular Brian Winder for feedback on early design iterations and prototype generation. Nick Hawkins is also acknowledged for his technical expertise in manufacturing prototype hardware.

I acknowledge the inspiration received from my Father in Heaven, for all that is light comes from Him. I thank my parents for teaching me how to work and granting me every opportunity to succeed in whatever I chose to do. Finally, I’m grateful to my loving wife Laura and three sons Ryan, Caden, and Andrew who are my biggest fans and have supported me throughout.

TABLE OF CONTENTS

LIST OF TABLES

LIST OF FIGURES

CHAPTER 1 INTRODUCTION

Rolling contact joints may benefit designs that require low friction and backlash; however, the circular contact surfaces and associated kinematics developed to date are characterized by large Hertz contact stresses, large bending stresses (if contact-aided compliant flexures are used between the surfaces to stabilize the joint), and added complexity for pure rolling where two constraints—no-slip (e.g. gear teeth) and engagement (connecting link)—are required (see Figure 1.1).

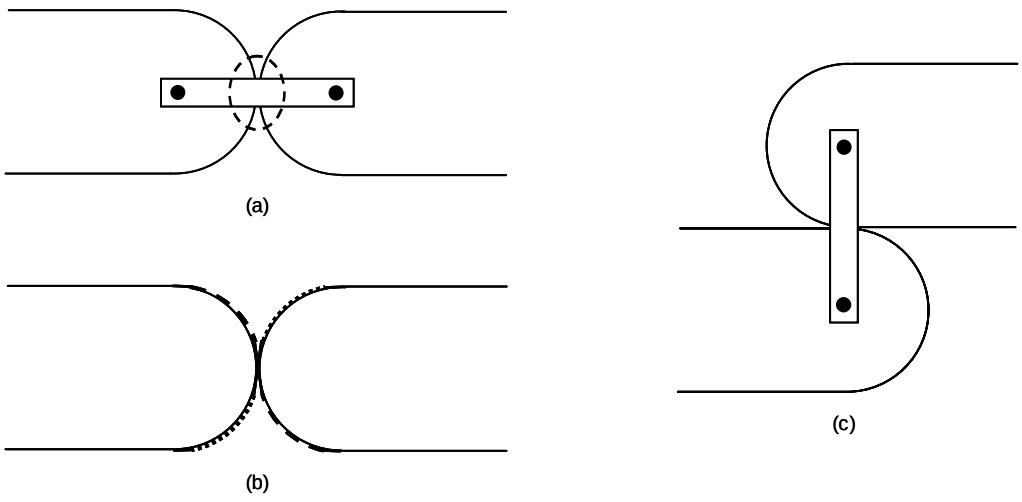

Figure 1.1 Undesirable characteristics of circular rolling contact joints: (a) large Hertz contact stresses; (b) large bending stresses, if flexures are used; and (c) gear teeth or other no-slip provision required for tractive rolling.

This thesis presents elliptical rolling contact joints as an alternative to circular rolling contact and conventional revolute joints where high quality force transmission—low friction and backlash—with variable output are desired. Parameters specific to the joint and its position are developed in terms of relative link angles and elliptical surface geometry. These parameters are used to generate the basic forward kinematics for elliptical rolling link toggle mechanisms with oscillatory motion and high mechanical advantage. As large compressive loads are characteristic of such mechanisms, stress conditions are identified and principles for joint stability with variable, precision outputs are discussed. Finally, application is made to self-adjusting passive force closures with a case study of the MUSCLE Brake (MUlti-toggle Self-adjusting Connecting-Linked Electromechanical) disc brake caliper.

The sections that follow present the motivation for this work and the objectives of the thesis including the research justification and contributions made to this area of study. An outline of the thesis is then provided.

1.1 Motivation

Many electromechanical brake caliper designs use discrete velocity ratios, stop-and-go motion, and active feedback to provide the required output. Large forces are generated by expensive, high-performance motors, and adjustment is achieved through the use of embedded sensors and central computer systems. The field of mechatronics integrates the required mechanical and electronic components, but some designs might be better served with a purely mechanical solution, incorporating electronics for actuation only. The mechanisms developed in this thesis may represent a more efficient solution to such seemingly sophisticated designs. Further, it is anticipated that the guiding principles developed herein will ex-

tend beyond the transportation industry to other applications that require similar functionality.

Automotive systems technology is in constant flux, and nowhere is that more apparent than in the area of automotive brakes. With the increasing cost of fuel, OEMs are adopting new technologies to reduce weight and thermal losses. Electrohydraulic brakes (EHB) are being implemented along with regenerative braking to lighten the load and harness some of this wasted energy [1]. By 2010, Siemens will have an energy-efficient electromechanical brake (EMB) called the Electronic Wedge Brake (EWB) out on the market [2], and other brake suppliers continue to iterate on initial EMB designs to develop the brake of the future. This move to "Brake-by-Wire" will be accompanied by the adoption of other "by-wire" vehicular systems such as steering and suspension, although brakes are one of the lead technologies [3].

Electromechanical brakes offer several advantages over hydraulic brakes. Some of these advantages are listed below [4]:

- Faster response times (shorter stopping distances, optimized stability)
- Environmentally friendly (no brake fluid, improved fuel economy)
- Less parts; simplified assembly
- Low maintenance (no park brake adjustment, brake fluid fill, or hoses)
- Pedal decoupled from brake (consistent pedal feel; customizable)
- Greater packaging efficiency and architectural flexibility
- Integrated safety features (collision avoidance, stability control, adaptive cruise control, and panic brake assist)

While current EMB designs already provide the required functionality, this thesis will apply rolling contact principles to develop a design solution that might be advantageous in

this and other applications. “Good” designs, like the Siemens EWB, are less complex (reduced part count/electronics) and require lower actuation forces (greater mechanical advantage) while still emulating the behavior of a more traditional hydraulic brake caliper. Such improvements reduce overall product cost and therefore make these solutions accessible to other applications like snowmobiles or even machine tools.

1.2 Thesis Objective

The purpose of this research is to develop the kinematics for rolling link mechanisms with elliptical contact surfaces, identifying the benefits, challenges, and tradeoffs as applied generally and to a specific product idea, the electromechanical disc brake caliper. Mechanisms that are self-adjusting and generate high mechanical advantage are of particular interest given the application to automotive disc brakes.

1.2.1 Research Justification

Although much has been written about circular rolling link mechanisms, little is found in the literature on elliptical rolling link mechanisms. However, several authors acknowledge the possibility of using non-circular surfaces joined in rolling contact, and many of them explicitly recommend that future research analyze the potential benefits of elliptical or other non-circular shapes.

1.2.2 Contributions

The primary contribution of this work is the development of elliptical rolling contact joint parameters in terms of generalized coordinates from the parent mechanism. These relationships enable elliptical rolling contact joints to be incorporated into vector loop summations that are used in kinematic analysis. Notably, elliptical rolling contact is the more general case of which circular rolling contact is a subset.

Another key contribution is the synthesis of several sources on the thesis subject matter as provided in the literature review. The integration of many related but heretofore scattered design principles is a benchmark for future work in this area.

The treatise on self-adjustment, including classification of specific examples and derivations of governing equations for tip before slip, provides a starting point for the application of self-adjustment in other mechanical devices. It is anticipated that the self-adjustment methods cited and developed in this thesis, as used in conjunction with passive force closures, will be applicable and transferable to other product development projects where active location sensing and/or positioning can be displaced by such mechanisms.

Another significant product of this thesis is the development of a mechanical brake caliper that requires relatively little actuation energy when properly adjusted. The first prototype of the MUSCLE Brake using production-level materials provides lessons learned for subsequent iterations, and the test apparatus can be used for future development and design validation.

1.3 Thesis Outline

This section outlines the topics discussed in the various chapters of the thesis, providing a brief overview of the rest of the document.

Chapter 2 presents background information and related research to acknowledge what has already been done and to set up the analysis in the following chapters. Constraining mechanisms are classified and passive force closures selected as the subset of mechanisms to be analyzed. Prior work with passive force closures is summarized and examples are presented. Underactuation is explained and examples of differential mechanisms are provided. Next, self-adjusting grasping mechanisms are classified and the equations for self-locking behavior are derived. Recent advances in joint design are then reviewed, including rolling contact joints and associated stresses. Finally, the topics of pressure angles, transmission angles, mechanical advantage, and elastic deflections are presented as they relate to rolling contacts and toggle linkages.

In Chapter 3, elliptical rolling contact joints are developed and joint parameters defined in terms of relative link angles and elliptical surface geometry. The complex motion of elliptical rolling contact is described as a combination of rotation and translation, and equations for displacement are provided. Several characteristics of the contact surface profile are then discussed, including: radius of curvature, curvature, contact angles, and stabilization constraint stress conditions.

Chapter 4 provides a case study for applying learning from Chapters 2 and 3 and further expanding understanding of elliptical rolling contact to mechanisms comprised of multiple elliptical rolling contact joints. First, a brief background is provided on disc brake applications including bicycles and automobiles. Siemens' Electronic Wedge Brake is then

presented as an example of a future electromechanical brake technology. The focus then shifts to the development of the MUSCLE Brake. The design boundaries are established and the need for self-adjustment is identified. Concepts are then narrowed down to the final multi-toggle design. Forward kinematics are developed, which leads to a discussion on how much force is actually needed versus how much is provided by the MUSCLE Brake. A final self-adjustment method is selected and applied, with reliability and actuator mobility identified and discussed as potential challenges. Finally, stresses and deflections are quantified and output stroke confirmed.

Chapter 5 presents some of the benefits and challenges of using elliptical rolling link mechanisms. Guiding principles and key takeaways are provided. Finally, the thesis concludes with recommendations for future work.

CHAPTER 2 BACKGROUND AND LITERATURE SEARCH

This chapter provides background information for this thesis including a review of prior work. Although references are made to the theoretical possibility of elliptical rolling link mechanisms, very little has been written on the subject. Thus, this review lays the foundation for subsequent development of elliptical rolling link mechanisms. First, the scope is narrowed to passive force closures that are self-centering, force-balanced, and resolve a single input into multiple outputs. Self-adjustment is reviewed as a potential functional requirement, and recent publications on rolling contact joints and joints in compression are examined. Finally, topics important to the development of mechanisms that exhibit high quality force transmission and precision displacement are discussed.

2.1 Constraining Mechanisms

Any mechanism that restricts the motion of an object either kinematically or dynamically can be called a "constraining mechanism" or closure [5]. These closures can be further categorized as active, passive, or a combination of the two. Active closures have dynamic

actuation at each of the contacting surfaces; thus, motion is restricted only when the value of all forces is known and a control algorithm with continuous feedback acts to balance these forces (Figure 2.1a). Passive force closure implies that the balancing force counteracting the applied external force is produced by the mechanism itself (Figure 2.1b). When there is no applied external force—if geometry alone restricts motion, such as in fixtures and bearings—the constraining device is called a passive form closure (Figure 2.1c). It should be noted that friction forces will only restrict motion in the tangential direction if the applied force at the contact point lies within the friction cone (or "friction wedge" for planar motion) described by the coefficient of friction.

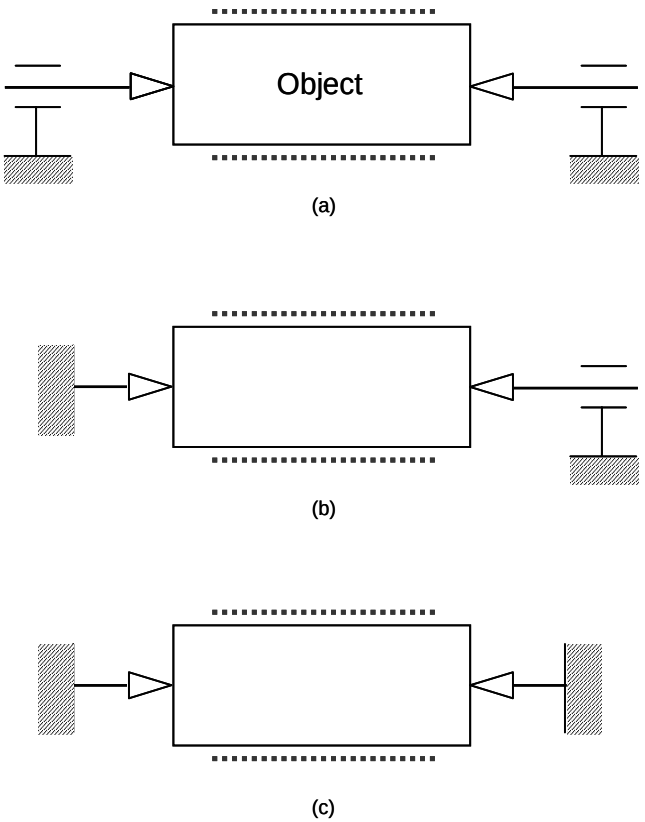

Figure 2.1 Constraints in one-dimensional motion: (a) active closure, (b) passive force closure, and (c) passive form closure [5].

2.2 Self-centering Force-balanced Grasping Mechanisms

Brooks [6] identified and developed several grasping mechanisms that are both self-centering and force-balanced (see Figure 2.2). Four postulates were developed with regard to the successful design of such mechanisms. In summary, these postulates state that self-centering, force-balanced mechanisms: 1) require a minimum of two degrees of freedom to actuate the mechanism, 2) deviate from ideal behavior because of finite link lengths, variations in rotation angles, etc., 3) must have at least one compliant link or "potential energy storage device" for each degree of freedom in order to maintain a stable "off" position, and

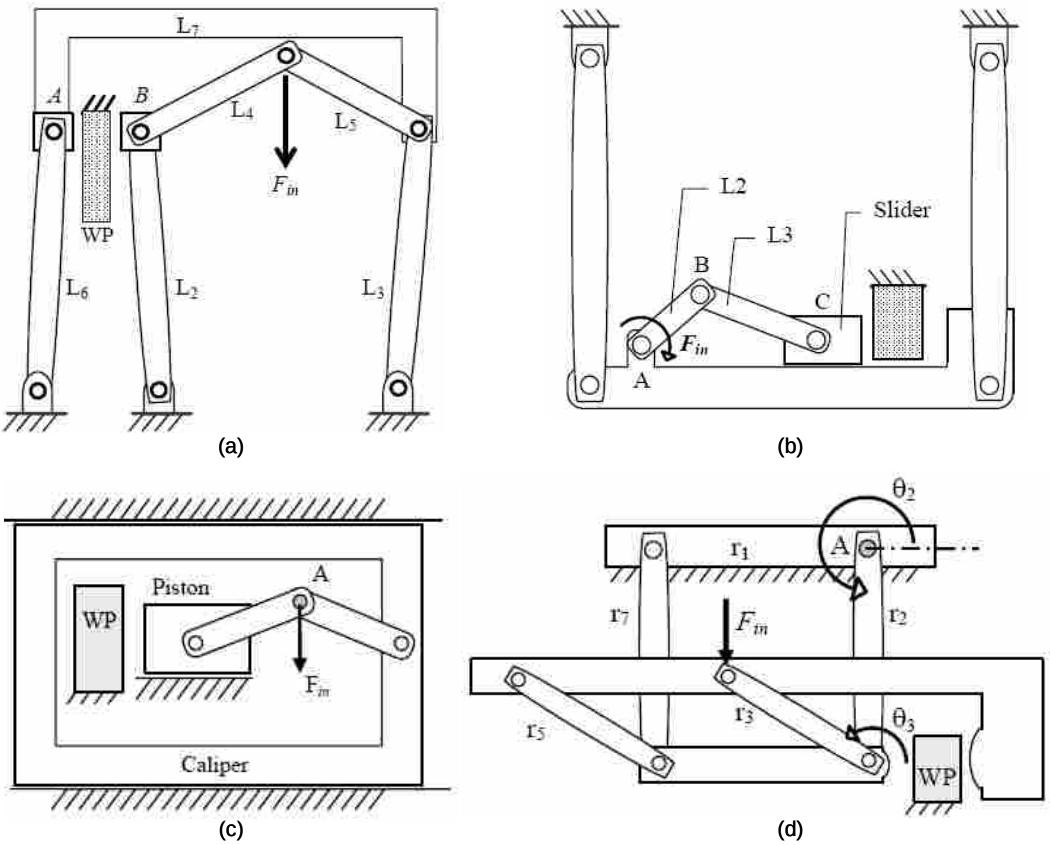

Figure 2.2 Self-centering, force-balanced grasping mechanisms developed by Brooks [6].

4) are separate rigid link embodiments that each have multiple compliant mechanism equivalents [7].

In Yoshikawa's classification of constraining mechanisms, Brooks' mechanisms would be considered passive force closures since the balancing force counteracting the applied external force is produced by the mechanism itself. The Brooks mechanisms were developed to demonstrate that one could replicate the behavior of a hydraulic disc brake caliper—self-centering, force-balanced grasping—in a purely mechanical (fluid-less) system. A toggle linkage was used in place of the conventional hydraulic pressure source, although Brooks acknowledges there are other mechanisms that could provide similar function. The toggles have the benefit of high mechanical advantage near the toggle point and, when applied in these particular kinematic configurations, energy transfer from a single input into two outputs, thus controlling a 2-DOF mechanism with a single actuator. This idea of underactuation—when a mechanism has fewer actuators than degrees of freedom [8]—is the subject of the next section.

2.3 Differential Mechanisms

Advances in the development of the robotic hand provide the backdrop for a discussion on underactuation. The artificial hand and other multi-DOF robotic grippers are able to function with a minimal number of actuators through the combined use of differential mechanisms and spring elements. A differential mechanism is a two-DOF mechanism that resolves a single input into two outputs [9]. Spring elements are used to stabilize the device in the "off" position and thus constrain it kinematically.

Birglen and Gosselin [9] provide several examples of differential mechanisms, including: planetary and bevel gear differentials, the fluidic T-pipe, the movable pulley, and the seesaw mechanism. These mechanisms are illustrated below and examples of each are provided.

2.3.1 Planetary and Bevel Gear Differentials

The bevel gear differential found in automotive drivelines is what first comes to mind when discussing differential mechanisms. On the rear drive of an automobile, the differential transfers torque evenly from the driveshaft to each half-shaft (see Figure 2.3). When the vehicle is driving straight ahead, the planet pinions do not rotate; both half-shafts turn at the same rate. However, when the vehicle is turning a corner, the planet pinions rotate to allow

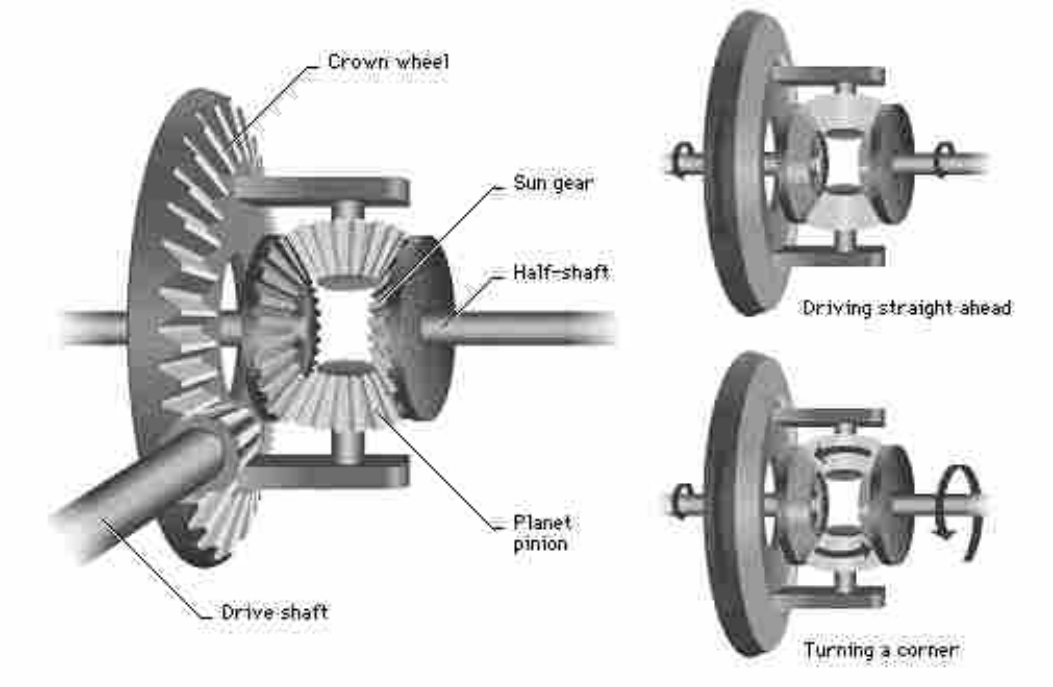

Figure 2.3 Bevel gear differential on the rear axle of an automobile [10].

the outside wheel to turn faster than the inside wheel. The bevel gear differential is a special case of the more general planetary gear differential found in automotive transmissions.

One of the benefits of gear systems is that torque transmission is constant and independent of output position with respect to actuation position. Further, mechanical advantage can be achieved through gear reduction. Unfortunately, gear trains can become overly complex in order to achieve the desired reductions. In many applications, rotational energy must ultimately be converted into linear motion, which further complicates the design.

2.3.2 Fluidic T-pipe

Due to pressure equilibrium and the deformability of a fluid, the T-pipe is perhaps the simplest differential mechanism and is therefore used in a variety of applications, including automotive brake systems. The fixed caliper design in particular implements a fluidic T-pipe to channel brake fluid from a single input port to pistons on both sides of the rotor (see Figure 2.4a). The result is a 2-DOF self-centering, force-balanced output from a single input.

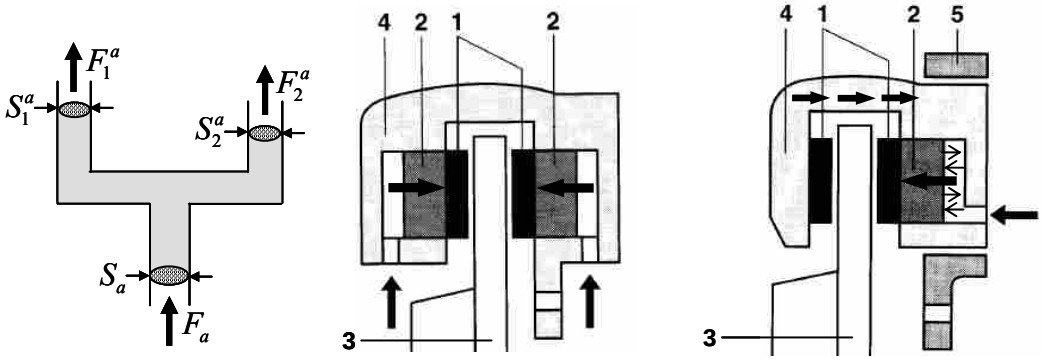

(a) Fluidic T-pipe, Fixed Caliper (b) Floating Caliper

Figure 2.4 Fixed and floating hydraulic disc brakes, with the following components shown: (1) brake pads, (2) pistons, (3) rotor, (4) caliper, and (5) support for floating caliper ([11], arrows added). Fluidic T-pipe reproduced from [9].

Like the gear differentials mentioned above, the output force on the fluidic T-pipe is independent of actuation position. Also, large mechanical advantages can be obtained by controlling the area of the output section relative to the input. However, the use of hydraulics requires several "wet" components (accumulators and hoses, not to mention the hydraulic fluid itself and its associated volatility) that are either not compatible with some applications or just simply not worth the effort when a suitable "dry" alternative is available.

2.3.3 Movable Pulley

The movable pulley is one of the most commonly used differential mechanisms in robotics because it employs a single output tendon (one cable that wraps around the pulley as two outputs) that can transmit actuation forces to the rest of the phalanges (see Figure 2.5). Multiple pulleys are often combined in series or parallel to actuate multi-fingered hands. Outside of robotics, the movable pulley is used in such everyday applications as cantilever bicycle brakes and fitness equipment.

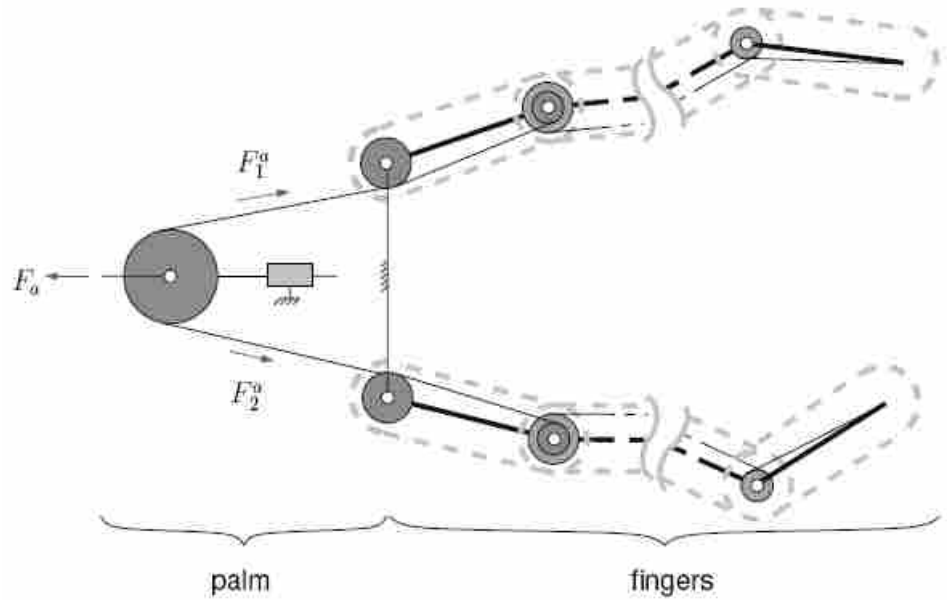

Figure 2.5 Movable pulley driving two underactuated fingers [9].

The two degrees of freedom of a movable pulley are in-plane translation and rotation about the central axis orthogonal to the plane of the pulley. It can be shown that an input force, or horizontal translation, will constrain one output, at which point further translation will cause the pulley to rotate until the other output is constrained. Since the tension in the outputs—a common cable—is the same, this mechanism is force-isotropic, like the bevel gear differential and the fluidic T-pipe. However, the mechanical advantage (output force relative to input force) is highly dependent on the angles of the output tendon relative to the input force.

2.3.4 Seesaw Mechanism

Figure 2.6 illustrates the use of a "seesaw mechanism" in a two-fingered robotic gripper. Like the movable pulley, the seesaw "bar" has two degrees of freedom: in-plane translation and rotation about an axis orthogonal to the plane of the mechanism. Its function is similar to the movable pulley: an input force, or translation, will constrain one end of the bar, at which point further translation will cause the bar to rotate until the other end is constrained.

In automobiles, a seesaw mechanism is used on the hand (parking) brake. When you manually set the parking brake, the parking brake lever pulls on a cable that is attached to the middle of a seesaw bar or "equalizing bar". Each end of the bar is attached to and pulls the respective left or right side rear parking brake cable, actuating the parking brake.

The seesaw mechanism is similar to the movable pulley except it has push/pull capability—when linkages are used—while the movable pulley is pull only (i.e. can't push a cable). Further, larger forces can be achieved because rigid links are used instead of tendons,

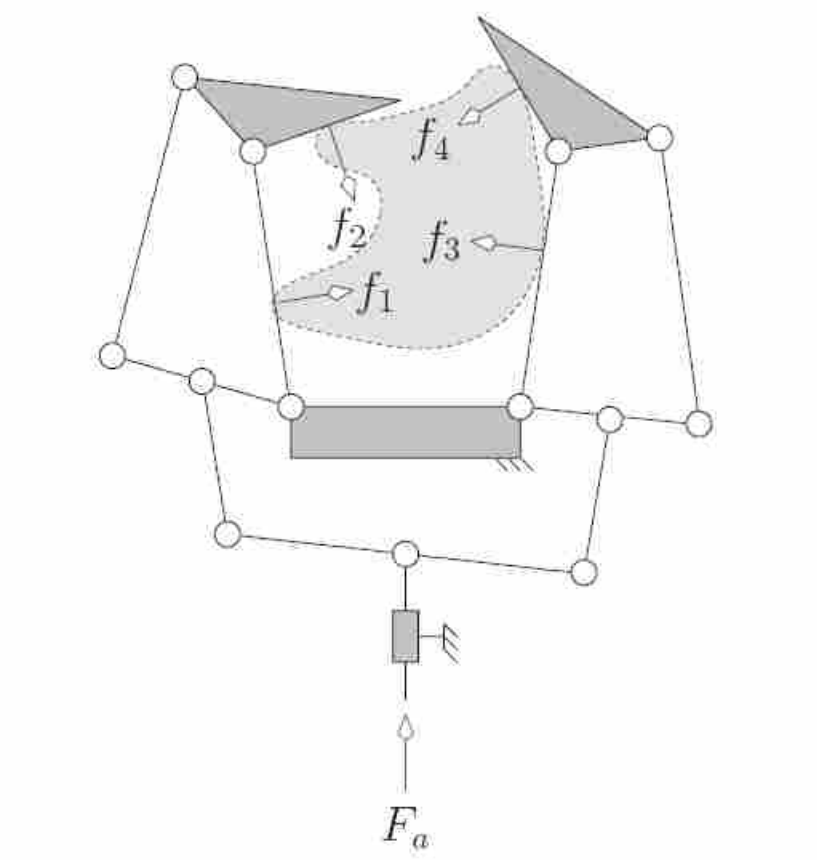

Figure 2.6 Seesaw mechanisms used in robotic gripper [9].

but mechanical advantages still vary significantly over a limited range of motion. Another challenge with designing seesaw mechanisms is that they have undesirable singular configurations; this, of course, is not a problem with pulleys and tendons, fluidic T-pipes, or planetary gear differentials [12].

2.4 Self-adjustment

One of the characteristics of hydraulic disc brake calipers that Brooks did not address is self-adjustment. As discussed in section 2.3, some mechanisms provide consistent mechanical advantage independent of position. The planetary gear system (e.g. bevel gear dif-

ferential) and fluidic T-pipe (e.g. hydraulic brakes) are examples of such mechanisms. However, the mechanical advantage on the movable pulley, the seesaw mechanism, and the toggle linkages used in Brooks' mechanisms will vary significantly with changing transmission angles and, in general, are more likely to require self-adjustment in order to provide consistent performance over the service life of the mechanism.

Self-adjustment can be classified as either discrete or continuous, with input stroke dependent on object size or independent of size, resulting in either incremental adjustment or total (full range) adjustment with each and every actuation (see Figure 2.7). In the sections that follow, definitions and examples of each are provided. In Chapter 4, self-adjustment will be incorporated into a self-centering, force-balanced grasping mechanism as a case study.

2.4.1 Discrete

Mechanisms with discrete adjustment have a finite number of levels, settings, or speeds to improve performance. For example, an automobile might have a 6-speed transmission, meaning there are six different gear ratios to deliver the torque demands of the driver and his vehicle. While 6-speeds are smoother than four, there are still discrete steps between each gear that are felt by the passengers and tradeoffs made when selecting one gear over another. In most cases, these step changes are acceptable to the customer if not unnoticed; in others, suboptimal performance between adjustments is an unwelcome compromise.

Adjustable pliers provide several examples of discrete adjustment and are worthy of review. With tongue-and-groove pliers like those made by Channellock, Inc. (Figure 2.8a), the user can manually select which groove the jaws will pivot in to accommodate various

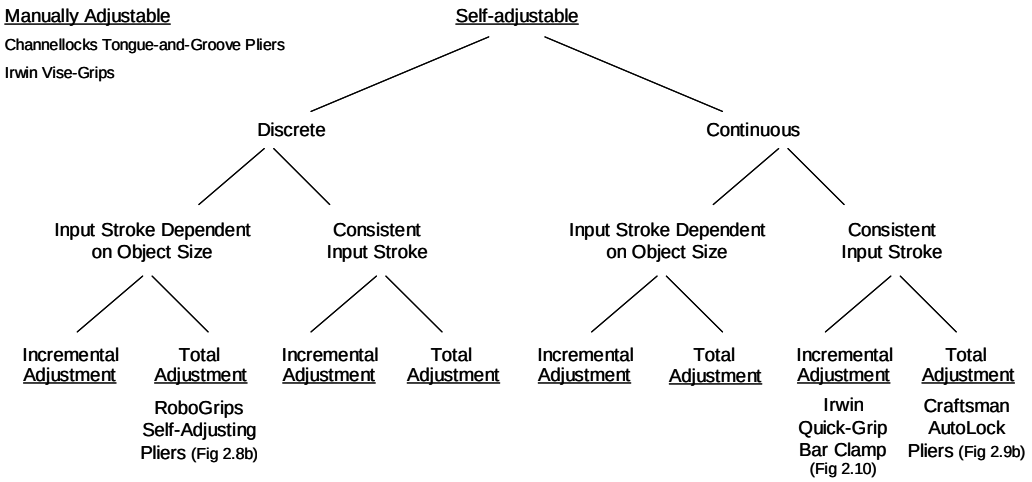

Figure 2.7 Self-adjustment classification tree derived from adjustable pliers and clamps.

sizes of grasped objects. RoboGrips self-adjusting pliers (Figure 2.8b) automatically adjust for workpiece size variation. As the user squeezes the handles, the jaws close by pivoting about the fulcrum in the handle (class 1 lever). Once contact has been made and the workpiece is fully constrained, the RoboGrips become a class 2 lever, and further actuation pivots the jaws about the workpiece until the self-adjusting teeth are engaged at the traditional pivot location. A firm grip then increases the clamping force as the jaws pivot about the engage-

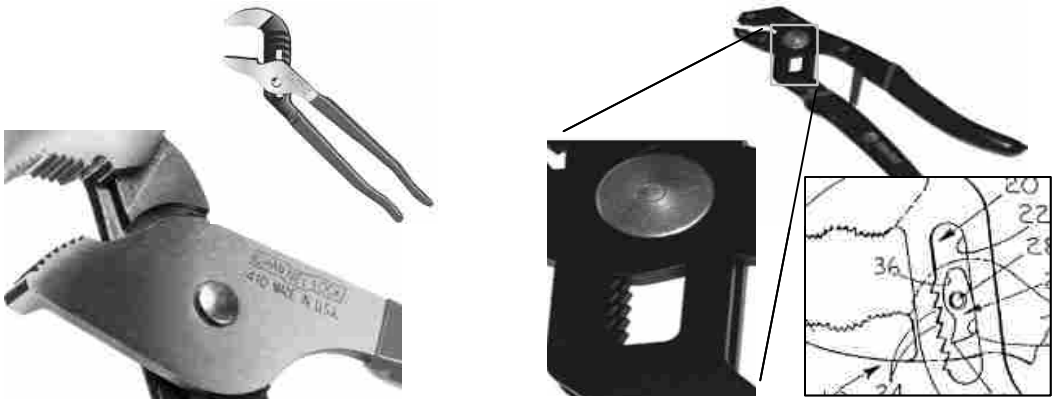

Figure 2.8 Examples of discrete adjustment: (a) Channellocks manually adjustable Tongue-and-Groove Pliers, and (b) RoboGrips Self-Adjusting Pliers [13].

ment at the teeth. Thus, the RoboGrips' function is best explained by the movement of the fulcrum from the handles, to the workpiece, to the teeth. The location of tooth engagement in the self-adjusting pivot is, of course, dependent on the size (thickness) of the workpiece (i.e. the input stroke is not consistent with each and every actuation). Further, the actuation stroke covers the full range of possible output strokes each and every time.

While RoboGrips provide greater resolution than tongue-and-groove pliers, there are still a discrete number of adjustments available, limited by the number of teeth at the pivot point. However, one of the advantages these discrete adjustments provide—the grooves on the one and the teeth on the other—is positive, locking engagement so the mechanism can then operate as if kinematically constrained at that location and in that configuration. Continuous adjustments can sometimes be less stable and thus less reliable.

2.4.2 Continuous

Where mechanisms with discrete adjustment have a finite number of levels, settings, or speeds, the possible adjustments for a mechanism with continuous adjustment are infinite. Keeping with the example of transmissions, a Continuously Variable Transmission (CVT) provides an infinite number of transmission ratios. This is accomplished by using a V-shaped belt to transmit torque from one V-shaped "pulley" or clutch to another. The sheaves of each pulley move together or apart to vary the relative diameters of the pulleys (for a given belt width) and thereby control the transmission ratio. Some of the benefits realized by incorporating CVTs in automotive drive systems include smooth shifting and improved gas mileage.

Adjustable pliers also offer several examples of continuous adjustment. Irwin's Vise-Grip self-locking pliers (Figure 2.9a) allow users to clamp down on objects of varying size by changing the location of the pivot point at the end of the toggle linkage with a manual screw adjustment. Other designs adjust automatically, but whether manually-adjustable or self-adjusting, most designs accommodate objects of varying size by moving the pivot point at the end of the toggle linkage either closer to the jaws for small/thin objects or further down the handle for large/thick objects.

One example of continuously self-adjusting pliers is found in US Patent #3,116,656 (Figure 2.9b, [14]), and a similar design solution is implemented in the Craftsman AutoLock Pliers (also shown in Figure 2.9b). In this design, the toggle link (46) is attached to a triangular wedge (60) in the handle (42). This wedge-shaped link (60) stacks up against another wedge-shaped link (62) that combine to form a rectangle (or rectangular prism), which slides back and forth inside the handle (42 and 76) to accommodate large and small objects, respectively.

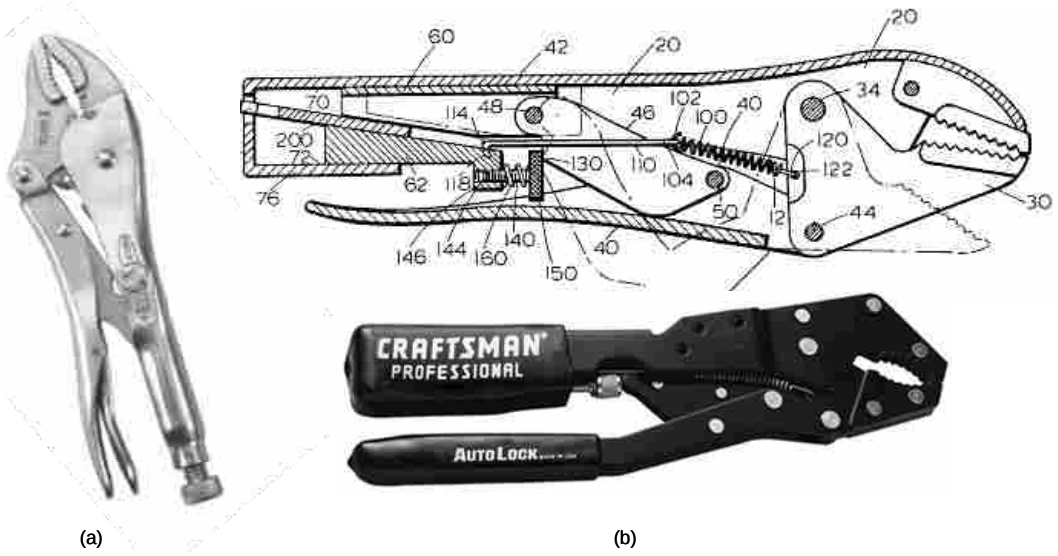

Figure 2.9 Examples of continuous adjustment: (a) Irwin Vise-Grips, and (b) Craftsman AutoLock Pliers [14].

The invention functions as follows. Grasping contact is made and the workpiece and jaws of the pliers (20 and 30) become fully constrained. Further actuation (i.e. squeezing of the handles, 40 and 42) slides the wedges (60 and 62) down the length of the handle (42 and 76; inner surfaces 70 and 72) and consequently rotates the toggle linkage (46) into a near-toggle position with the handle (40). The toggle link (46) is also connected to one of the wedges (60) at a pin joint (48) and has a cammed protrusion (130) that passively "joins" it to the other wedge (62); however, as the actuation of the handle (40) rotates the toggle link (46) into a toggle position, the cam profile (130) creates relative motion between the two wedges (60 and 62) that causes them to widen as they wedge against each other and become jammed inside the confines of the handle (70 and 72). Just as the translation of the wedges (60 and 62) and, it follows, the pivot point of the toggle link (48) are stopped, the toggle link (46) toggles into a locked position with the handle (40) and the workpiece is clamped tightly between the jaws of the pliers. The screw mechanism (150) simply allows the user to increase or decrease the length of wedge link 62, thus forcing the wedges to jam just before toggle (low MA) or well before toggle (high MA).

The functional description above shows that Crafstman AutoLock Pliers have a consistent input stroke every time, regardless of the size of the grasped object. Also, these pliers demonstrate "total adjustment" because the input stroke covers the full range of possible output strokes each and every time.

Another example of continuous adjustment is the bar clamp, as shown in US Patent #4,926,722 (see Figure 2.10; [15]). Parallel jaws are mounted to a length of bar stock, one that is fixed and one that is movable. Sliding of the movable jaw back and forth on the bar stock is controlled by two self-locking plates (146 and 132). Backward movement of the

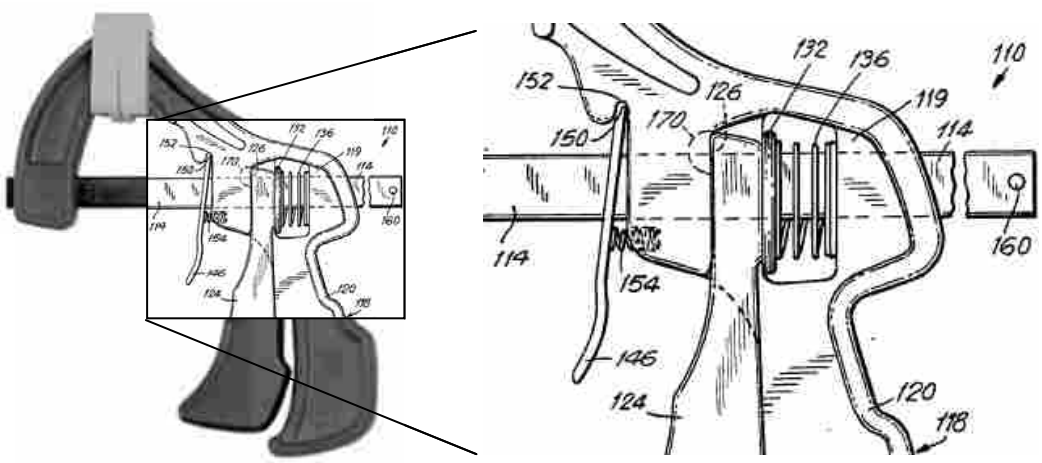

Figure 2.10 The “Quick-Action Bar Clamp” implements continuous adjustment [15].

movable jaw is limited by the braking plate (146) while forward movement is controlled by locking plate 132. Springs 136 and 154 maintain each plate on the verge of lock/slide.

Compared to other self-adjusting mechanisms, the function of the bar clamp is relatively simple. Squeezing handles 124 and 118 together causes plate 132 to rotate counterclockwise and bind on the slide bar (114). Further actuation incrementally advances the slide bar and the fixed jaw to the right, bringing the two jaws together. The braking plate (146) allows the bar (114) to slide through left to right because this motion acts to “unbind” the plate, making it perpendicular with the bar and allowing the plate to slide through freely. However, as the jaws make contact with and clamp down on the workpiece, reaction forces act to drive the jaws apart, but the braking plate resists these forces since bar translation right to left only further binds and tightens braking plate 146 against the slide bar.

The Quick-Action Bar Clamp uses a consistent input stroke every time and incrementally adjusts for object size variation. Incremental adjustment is most useful when size variation between grasps is less than the output stroke of the mechanism; otherwise, multiple actuation strokes will be required to constrain the workpiece. In the case of the bar clamp,

manual adjustment across the full range of the mechanism is provided by releasing—depressing—the braking plate lever (146).

2.4.2.1 Self-Locking and Tip before Slip

The idea of using a locking plate to control movement seems so simple, yet there are several parameters that determine whether or not a plate sliding on a bar will self-lock. Some bar clamp designs obtain positive engagement through geometry and localized deformation of the slide bar. This solution would be unacceptable in many applications where the design is expected to sustain an extended service life and would drive questions of long-term reliability, wear, and a host of other tribological issues.

In the literature surrounding problems on dry friction, this locking versus sliding condition is often described as "tip before slip". The criteria for tip before slip can be derived from the equations of equilibrium for a rigid body, which for two dimensional motion in a plane are

$$\begin{aligned} \Sigma F_x &= 0 \\ \Sigma F_y &= 0 \\ \Sigma M &= 0 \end{aligned} \tag{2.1}$$

Applying Equation 2.1 to Figure 2.11, we can derive the conditions for tip before slip. (Note that the weight of the self-locking plate is negligible when compared to the forces involved and will be ignored for this analysis.)

$$\Sigma F_x = 0; \qquad P\cos\theta - F_A - F_B = 0$$

Where $F_{A,B}$ are the friction forces resisting sliding at points A and B, and $F = \mu N$, we have

$$P\cos\theta - \mu N_A - \mu N_B = 0 \tag{2.2}$$

where $N_{A,B}$ are the normal forces acting at points A and B. Summing forces in the y-direction, we have

$$\Sigma F_y = 0; \qquad N_B - N_A - P\sin\theta = 0$$

$$N_A = N_B - P\sin\theta \tag{2.3}$$

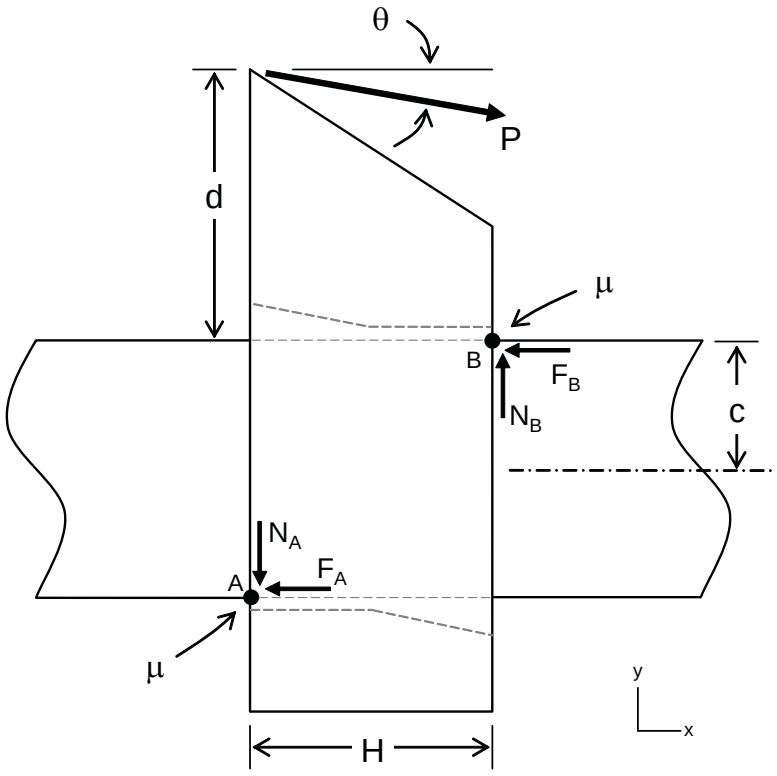

Figure 2.11 Self-locking plate with thickness H, lever arm d, slide bar height $2c$, input force P, and reaction forces as shown at points A and B.

Substituting Equation 2.3 into Equation 2.2, we arrive at an expression for P

$$P\cos\theta - \mu\left(N_B - P\sin\theta\right) - \mu N_B = 0$$

Simplifying, we have

$$P = \frac{2\mu N_B}{\cos\theta + \mu\sin\theta} \tag{2.4}$$

Summing the moments about point A we get

$$\Sigma M_A = 0; \qquad N_B H + F_B 2c - P\cos\theta\left(d + 2c\right) = 0 \tag{2.5}$$

where H is the thickness of the self-locking plate, d is the lever arm from the location of the input force to the slide bar, and $2c$ is the height of the slide bar. We can now substitute $F_B = \mu N_B$ and Equation 2.4 into Equation 2.5

$$N_B H + \mu N_B 2c - \frac{2\mu N_B\cos\theta}{\cos\theta + \mu\sin\theta}\left(d + 2c\right) = 0$$

Dividing by N_B and adding the last term to both sides yields

$$H + 2\mu c = \frac{2\mu\cos\theta}{\cos\theta + \mu\sin\theta}\left(d + 2c\right)$$

Isolating d and simplifying, we have the criteria for tip before slip

$$d \geq \left(\frac{H}{2} + \mu c \right) \tan\theta + \frac{H}{2\mu} - c \tag{2.6}$$

Equation 2.6 provides required values for lever arm d as a function of the angle of the input force θ and the three design variables H, μ, and c. Note that tip before slip is solely dependent on the geometry of the mechanism; it is not dependent on the magnitude of the input force.

A simplified version of Equation 2.6 reveals sensitivities to the different design variables. For the case where $\theta = tan\ \theta = 0$, we have

$$d \geq \frac{H}{2\mu} - c \tag{2.7}$$

Thus we see tip before slip (i.e. binding or self-locking) is more likely with large values of lever arm d, small values of plate thickness H, large coefficients of friction μ, and large slide bar height c. While Equation 2.7 helps to explain what determines lock versus slide, Equation 2.6 should be used to confirm the prescribed functionality over the relevant range of input force angle θ and potential variations in other design variables (e.g. coefficient of friction, μ).

2.5 Joints

An exhaustive review of kinematic joints is beyond the scope of this research, but recent work on flexible joints used in compression as well as advances in the development of rolling contact joints and rolling link mechanisms provide perspective for the chapters ahead.

2.5.1 Rigid-link Mechanisms

Mechanisms transfer motion and forces from a power source to an output [16]. Traditionally, mechanisms consist of rigid links connected by movable joints. Mechanisms that are designed to move in a single plane (two-dimensional motion) are called planar mechanisms. Each link in a planar mechanism has freedom to translate in two coordinate directions and to rotate about an axis orthogonal to the plane of the mechanism. Joints control relative motion between adjacent links in a planar mechanism by constraining one or two of these degrees of freedom (DOF). The four joints that are applied in traditional kinematics include: pin joints, sliders, cam joints, and gears. The first two are often referred to as lower pair because they allow just one DOF (rotation and 1-D translation, respectively) while the latter are considered higher pair because they allow two DOF (rotation and 1-D translation for both). The mobility (DOF) of a planar mechanism comprised of multiple links and joints is calculated using Gruebler's equation, below

$$DOF = 3(n-1) - 2j_L - j_H \tag{2.8}$$

where n is the number of links in the mechanism, j_L is the number of lower pair joints, and j_H is the number of higher pair joints.

Rigid-link mechanisms are used in most of the mechanical devices we interact with on a day-to-day basis. Many of these devices are relatively complex with multiple parts (links) and interfaces (joints). Unfortunately, increased part count is highly correlated to cost, weight, wear, maintenance, and (low) reliability. The performance of pin joints, sliders, gears, and cams is compromised due to friction, which creates thermal losses, excessive wear, and inconsistent force transmission. Mechanisms that incorporate these joints have to compensate for frictional losses and erratic behavior through lubrication and feedback control. Positioning accuracy is limited due to static friction forces. Mobility requires clearance at the joints which equates to backlash in the overall mechanism; thus, motion transmission is difficult to reproduce. While this lack of precision and overall inefficiency of traditional rigid-link mechanisms is acceptable in most applications, it is inadequate in others.

2.5.2 Compliant Mechanisms

Compliant mechanisms can be a good alternative to rigid link mechanisms as they mitigate several of the undesirable attributes of their rigid-link counterparts. Unlike rigid-link mechanisms, compliant mechanisms gain some or all of their mobility from the deflection of flexible members rather than from movable joints only [17]. Consequently, mobility can be achieved with fewer parts (links) and fewer traditional interfaces (joints), which reduces backlash and friction while improving cost, weight, wear, maintenance, and reliability. Also, we remember from section 2.2 that Brooks' third postulate states that a self-centering, force-balanced grasping mechanism must have at least one compliant link or "potential en-

ergy storage device" for each degree of freedom in order to maintain a stable "off" position. In other words, compliant members store energy and act as a restoring force to return an oscillating mechanism to its initial position.

2.5.3 Compression vs. Tension

Among the challenges inherent to designing with compliant mechanisms is their propensity to buckle when loaded in compression. For a given material, the quick solution would be to increase the moment of inertia of the cross section or decrease the length of the member; unfortunately, this is the very geometry that makes the member flexible, so there would appear to be a tradeoff between compliance and compressive load bearing.

Guérinot [18] shows that using the principles of isolation and inversion, one can design a compliant joint that retains flexibility in high compressive load situations. Isolation (Figure 2.12a) decouples compression and compliance by suggesting the use of a passive rest

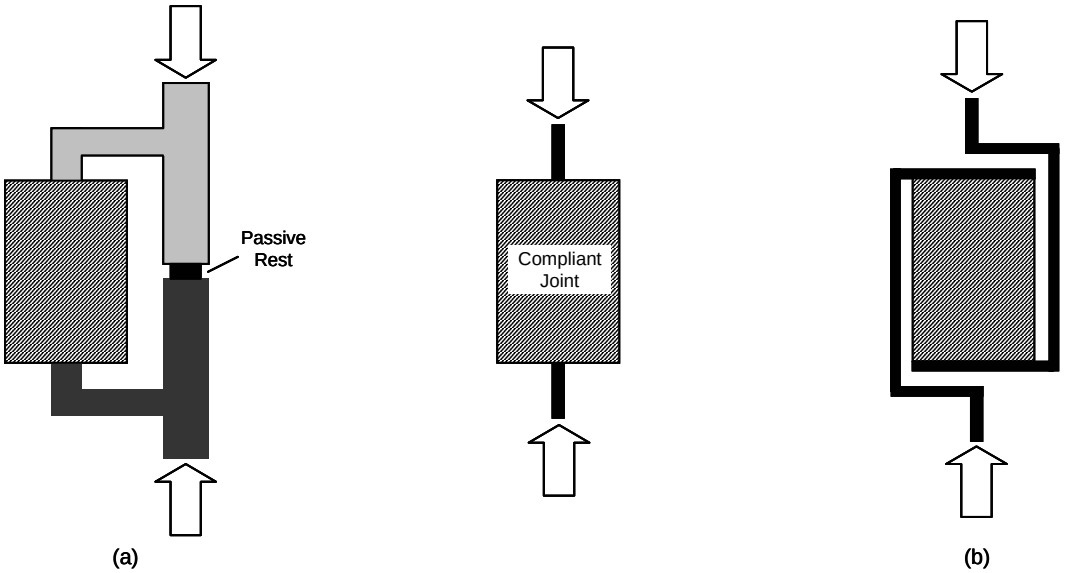

Figure 2.12 Principles for designing compliant joints that bear high compressive loads: (a) isolation, and (b) inversion [18].

to bear the compressive forces while allowing the flexible members to provide the benefits of compliance, thus the flexible members are isolated from the compressive load. Inversion (Figure 2.12b) recommends that, rather than use opposing compressive forces to push on an intermediate joint from each of their respective sides, the designer should couple each link to the opposite side of the intermediate joint, effectively pulling the joint apart (loading it in tension).

2.5.4 Rolling Contact Joints

Another joint that minimizes friction and backlash is the rolling contact. The sections that follow review some relatively recent contributions to this area of research, and then conclude with a discussion on relevant stresses.

2.5.4.1 Rolamite (Wilkes, 1967)

One of the most basic mechanical inventions of the 20th Century, Rolamite was designed by Sandia engineer Donald F. Wilkes as a suspension system to be used in subminiature components of nuclear weapons [19]. Figure 2.13 illustrates how this mechanism works. The flexible strip between the rollers allows relative motion without slip, which creates a very efficient bearing device (friction as low as 0.0005—better than ball bearings and no need for lubricant). Billed as a precision device that does not require precision tolerance machining to manufacture, the Rolamite technology has been used in everything from prosthetic knee joints to inertial sensors for air bag deployment. More importantly, its reuse has spawned further rolling contact developments, including the research conducted by Kuntz and Herder that follows.

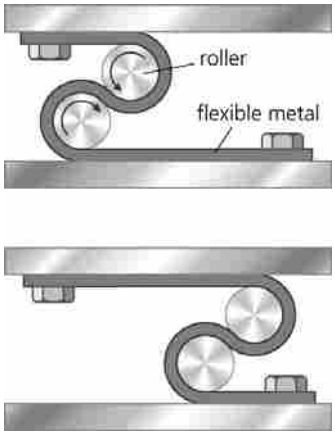

Figure 2.13 Rolamite virtually eliminates friction and backlash as parallel cylinders roll horizontally left to right without slip [19]. (Figure created by Precision Graphics)

2.5.4.2 Rolling Link Mechanisms (Kuntz, 1995)

When multiple links in a kinematic chain are joined in rolling contact the mechanism is called a Rolling Link Mechanism [20]. The thesis of Kuntz' work is that direct rolling contact leads to highly efficient mechanisms *if* a proper control system is added to stabilize the mechanism and extend its range of motion. Stabilization bands like those shown in Chironis and Sclater (Figure 2.14, [21]) are recommended.

It is worth noting a few differences in nomenclature when discussing stabilizing constraints. The common names for all rigid or compliant links that are used to stabilize a roll-

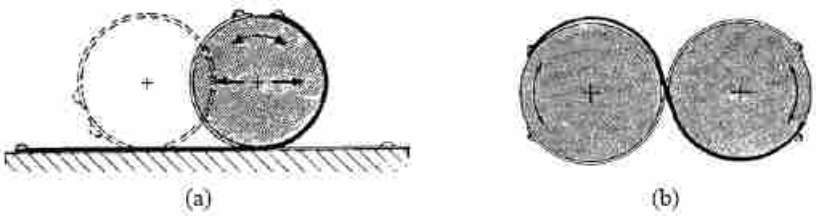

Figure 2.14 Direct rolling contact with the addition of stabilization bands: (a) between a cylindrical and flat surface, and (b) between identical cylindrical surfaces [21].

ing contact joint are stabilization (or stabilizing) member or stabilization (or stabilizing) constraint. Stabilization members that are deflected across contacting surfaces are called *bands* or *flexures*, with the "stabilization" or "stabilizing" adjective often preceding either term. Stabilization members that join centers of curvature (circles) or foci (ellipses) are called *connecting links*. The connecting links discussed in this thesis are assumed to be rigid, but a compliant link could also be used.

The design of Rolling Link Mechanisms (RLMs) is complex. Unlike conventional joints, the points of rotation on the contact surface between adjacent links move in the direction of rolling, effectively creating a mechanism with varying link lengths through its range of motion. Also, rolling contact joints are not form-closed but force-closed. Geometry alone does not guarantee a connection; the joint is dependent on a compressive force within the friction wedge (see Figure 2.15) to hold the links together. Thus, RLM design requires that kinematics and forces be analyzed in parallel.

The following RLM design guidelines can be summarized from Kuntz' work:

- To maintain contact, the normal component of the contact force must be a compressive force.

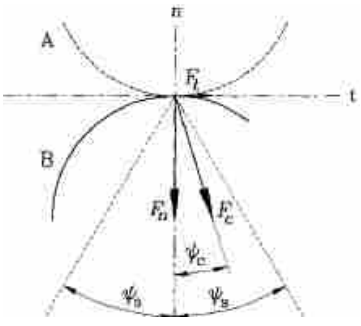

Figure 2.15 The contact force, F_c, resolved into normal component, F_n, and tangential component, F_t. The direction of the contact force, ψ_c, must lie within the "friction wedge" defined by the maximum slip angle, ψ_s [20].

- To maintain pure rolling and joint stability in the absence of a stabilizing constraint, the contact angle ψ_c must always be smaller than the slip angle ψ_s (see Figure 2.15), where $\psi_s = \arctan \mu$.
- To maximize the operational range of the mechanism, the line of action of the contact force and the normal at the contact point should rotate in the same direction during the rolling motion (Figure 2.16).
- If rolling axes are non-parallel, lateral creepage equal to the angle—in radians—will reduce the efficiency of the rolling contact. Creepage is the difference in velocities divided by the average velocity.
- Convex-convex contact is feasible provided stabilization bands—or a similar control system—are used to provide support over an extended range of motion. These bands provide a no-slip condition (see Figure 2.17), restrict skew of rolling axes, preserve a reproducible back-and-forth motion, increase the operational range, and protect the system against shocks.
- Just as compliant joints use the principle of inversion to be loaded in compression, rolling contact joints can implement inversion to be loaded in tension (Figure 2.18).
- A convex-convex contact is limited by Hertzian contact stresses. When stabilization bands are used, the joint is also limited by the maximum allowable stress in the band ($\sigma_y > \sigma_{bending} + \sigma_{tension} + \sigma_{compression}$).

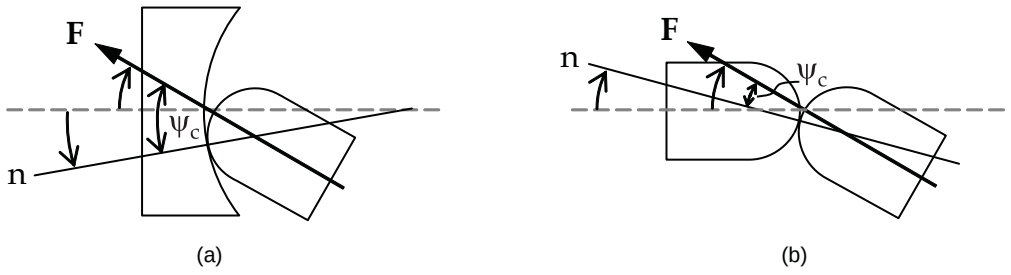

Figure 2.16 Although the links in both examples experience the same relative rotation, (a) will have much larger contact angles (ψ_c) because the normal line through the contact rotates away from the force rather than with the force.

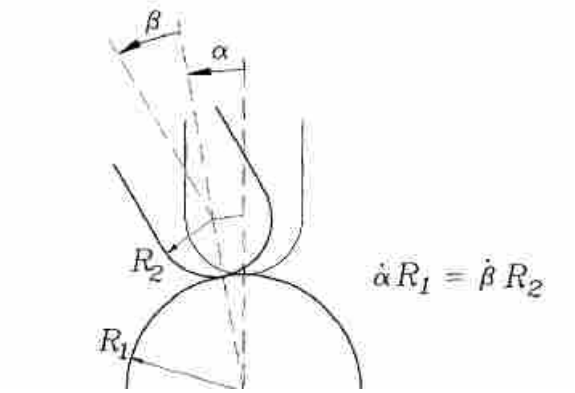

Figure 2.17 Pure rolling (no-slip) kinematic rolling constraint [20].

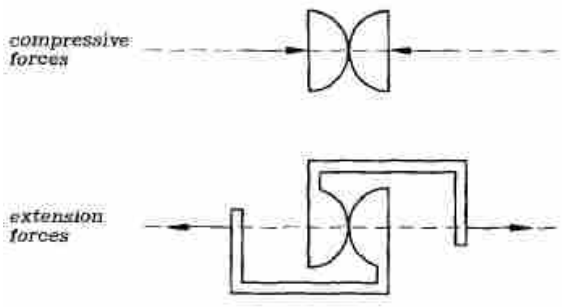

Figure 2.18 The principle of inversion can be used to load a rolling contact joint in tension [20].

RLMs provide many benefits, but Kuntz also identifies several challenges. For example, the manufacture and attachment strategy of the stabilization bands is not optimized. For small radii of curvature, the "metal bands" are merely foils only a few thousandths of an inch thick. The effects of corrosion may also limit their influence in some practical applications. The kinematics of RLMs are relatively complex; so, computer programs have been created (Kuntz' ROLMEX, for example) to understand their motion.

2.5.4.3 Kinematics of Circular Rolling Contact Joints (Collins, 2003)

Although rolling contact joints do increase the kinematic complexity of a mechanism, researchers have begun to develop the equations that define their motion. Collins investigates the use of rolling contact joints in robotic fingers [22]. The focus of his paper is position and rate kinematics of planar mechanisms with links connected in series, each having circular profiles joined in rolling contact.

Figure 2.19a shows two links joined in rolling contact, similar to Figure 2.17 but with Collins' subscript convention, which will be important as we begin to look at multiple links connected in a chain. For the given rolling contact joint with rolling contact angle θ_{10}, the '1' refers to the link the angle is defined on (Link 1), while the '0' refers to the adjacent link that forms the rolling contact joint (Link 0). True to conventional kinematic notation, the relative angle between the two links is simply denoted θ_1. Based on geometry and the no-slip condition, we know that

$$\theta_1 = \theta_{01} + \theta_{10} \tag{2.9}$$

and

$$r_{01}\theta_{01} = r_{10}\theta_{10} \tag{2.10}$$

where r is the radius of the respective contact surface. We can combine Equations 2.9 and 2.10 to develop equations for the rolling contact angles (θ_{01} and θ_{10}) in terms of the relative angle between the links (θ_1) and the respective radii of the contact surfaces (r_{01} and r_{10}).

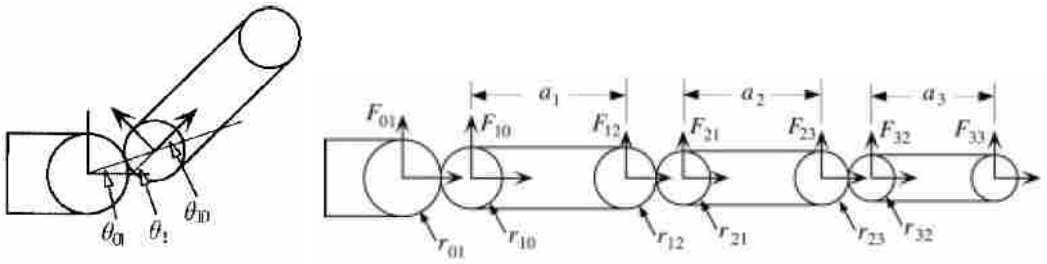

Figure 2.19 (a) Rolling contact joint with angular displacement, and (b) four link, three joint chain joined in rolling contact [22].

$$\theta_1 = \left(1 + \frac{r_{01}}{r_{10}}\right)\theta_{01} = \left(\frac{r_{10}}{r_{01}} + 1\right)\theta_{10}$$

or

$$\theta_{01} = \left(\frac{r_{10}}{r_{01} + r_{10}}\right)\theta_1 \tag{2.11}$$

$$\theta_{10} = \left(\frac{r_{01}}{r_{01} + r_{10}}\right)\theta_1 \tag{2.12}$$

(Note that $\theta_{01} = \theta_{10} = \theta_1/2$ if and only if contacting radii are equal.) We can now apply Equations 2.11 and 2.12 more generally for each successive joint and develop the forward kinematics for a chain of links connected in circular rolling contact. Equations 2.13 and 2.14 apply to four link, three joint rolling link mechanisms like that shown in Figure 2.19b, where $r_1 = r_{01} + r_{10}$, $r_2 = r_{12} + r_{21}$, $r_3 = r_{23} + r_{32}$ and $\theta_{01,\ldots,ij}$ represents the absolute angle of each link or joint radius, as summed from the first link θ_{01} up the chain to θ_{ij}. It should be noted that these equations find the position of reference frame F_{33}, the center of the tip of the last link.

$$x = a_1 \cos(\theta_{01,10}) + a_2 \cos(\theta_{01,\ldots,21}) + a_3 \cos(\theta_{01,\ldots,32}) + r_1 \cos(\theta_{01}) + r_2 \cos(\theta_{01,\ldots,12}) + r_3 \cos(\theta_{01,\ldots,23}) \quad (2.13)$$

$$y = a_1 \sin(\theta_{01,10}) + a_2 \sin(\theta_{01,\ldots,21}) + a_3 \sin(\theta_{01,\ldots,32}) + r_1 \sin(\theta_{01}) + r_2 \sin(\theta_{01,\ldots,12}) + r_3 \sin(\theta_{01,\ldots,23}) \quad (2.14)$$

Collins also develops the inverse and rate kinematics, and then applies these and other methods to the solution of a two joint robot finger. These methods will not be discussed here.

2.5.4.4 Compliant Rolling Contact Joints (Herder, 1998-2004)

Herder suggests that a *force directed design* approach requires the engineer to consider the effects of friction up front, whereas the more conventional *movement directed design* tends to account for friction only after the mechanism has been developed and actuation methods, forces, and stresses are considered [23]. He also argues that force directed design often yields mechanisms that are simpler and more efficient.

Herder's research has been applied to several concepts including laparoscopic forceps [24], hand prostheses [25], and the X_U-joint [26], all of which use some form of compliant rolling contact to join links together, delivering high quality force transmission with minimal friction and backlash. The last of these is based on his X_R-joint, which is shown in Figure 2.20 (the X_U-joint being two X_R-joints stacked in series—three links total—but acting in planes orthogonal to each other).

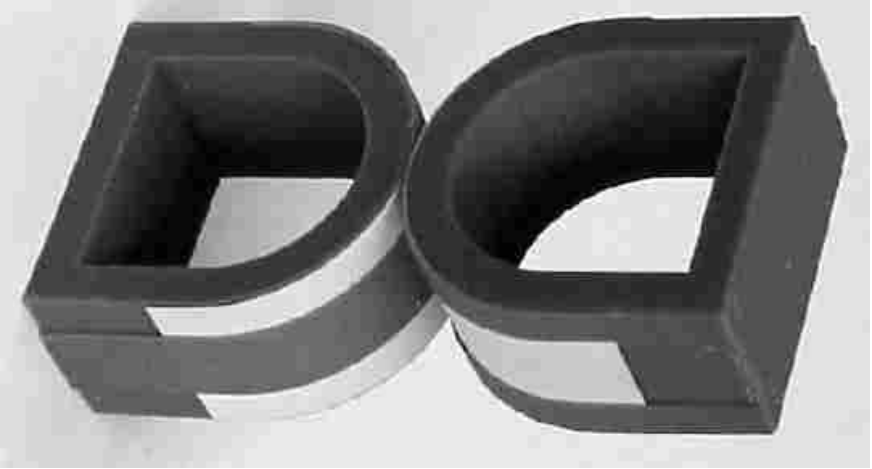

Figure 2.20 Compliant rolling contact joint developed by Herder and manufactured by Laliberté using rapid prototyping [26].

In the configuration shown in Figure 2.20, Laliberté uses rapid prototyping to deposit ABS plastic layer by layer to ultimately create a monolithic joint and thus avoid the complexities discussed previously of accurately attaching the flexible bands. Methods for tightening the bands are recommended, and Jeanneau and Gosselin develop the kinematics—based on Collins' prior work [27]—for a 3-DOF planar parallel mechanism that incorporates multiple X_R-joints.

2.5.4.5 Elliptical CORE Bearing (Cannon, 2004)

Cannon [28] independently developed a compliant rolling contact joint called CORE (from "COmpliant Rolling-contact Element"), shown in Figure 2.21a. While the CORE may resemble the joint developed concurrently by Herder, its manufacture and assembly is unique. Figure 2.21b shows the three layers that comprise the CORE prior to assembly. Like the Herder joint, the flexures and the cylindrical contact surfaces are a single, monolithic piece, thereby avoiding the need to develop an attachment strategy that is both accurate

(a) (b)

Figure 2.21 The Compliant Rolling-contact Element (CORE) in its assembled configuration (a) and pre-assembly (b) [28].

and permanent. Assembly is achieved by aligning and fastening the three lower surfaces as shown in Figure 2.21b, then deflecting the straight flexures around the lower surfaces in order to align and fasten the three upper surfaces.

Kuntz identified the relevant loading and stresses in a rolling contact joint with stabilization bands [20], but Cannon further develops the bending aspect for both straight and initially curved flexures. Based on the Bernoulli-Euler equation, it can be shown that the bending stress in a rectangular beam deflected over a surface with effective radius of curvature R' is a function of the modulus of elasticity E of the material, its thickness h, and R', as shown in Equation 2.15.

$$\sigma_{bending} = \frac{Eh}{2R'} \tag{2.15}$$

R' varies from the radius of the cylindrical surface when 1) the curvature of the rolling contact changes along its surface (e.g. ellipses), and 2) the flexures themselves have some initial curvature, per the following equation

$$R' = \left(\frac{1}{R_s} - \frac{1}{R_0} \right)^{-1} \tag{2.16}$$

where R_s is the radius of curvature of the surface constraining the flexure's shape and R_0 is the initial radius of curvature of the flexure. Equations 2.15 and 2.16 assume: 1) the material is linearly elastic, homogenous, and isotropic, 2) the transverse shear component of deflection is small compared to that due to bending, and 3) the flexure's thickness h is small relative to R_s (so that the neutral and centroidal axes can be assumed coincident for initially curved beams).

As discussed by Kuntz, the tensile stress in the flexures is

$$\sigma_{tension} = \frac{F_t}{Lh} \tag{2.17}$$

where L is the width of the flexure. The stress in the flexures due to compression of the two surfaces at the contact point is

$$\sigma_{compression} = \frac{F_n}{(2b)L} \tag{2.18}$$

where $2b$ is the width of the contact area from Equation 2.24, discussed in the next section. Note that the stress on the flexures due to compression is offset by the absence of bending stress at the contact point for initially straight flexures (i.e. no bending stress at the inflection point).

Circular rolling contact surfaces are the most fundamental in that they are relatively easy to design and manufacture; however, they are limited because of the stresses inherent to their small radii. One solution explored by Cannon is an elliptical rolling contact joint as implemented in his elliptical CORE bearing. He suggests that ellipses, with larger radii at their minor axes, can reduce the stresses in the flexures used to stabilize rolling contact.

As shown in Figure 2.22, the motion of an ellipse is derived from the antiparallelogram (also known as a crossed four-bar with non-parallel equal cranks) which means a link running from the focus of one ellipse to the diagonally opposite focus of an adjacent identical ellipse will always be the same length, *2a*, throughout its motion, just as the center to center distance between two circular profiles in rolling contact remains constant. Therefore, rigid links of length *2a* can connect diagonally opposite foci—one link on each side of mating elliptical cylinders—and create a no-slip condition. As one ellipse rolls without slip around the circumference of the other, its foci trace circular paths of radius *2a* (see Figure 2.22b). Note that unlike rigid links connected by conventional pin joints, this motion is both a rotation and translation of one elliptical gear relative to the other. Cannon provides the angular displacement of the connecting link as a function of the Cartesian coordinates x and y, as follows

$$\theta = \tan^{-1}\left(\frac{y}{c-x}\right) \tag{2.19}$$

where θ for ellipses is typically measured at one of the foci, from the major axis to the connecting link (contact point), as shown in Figure 2.22a.

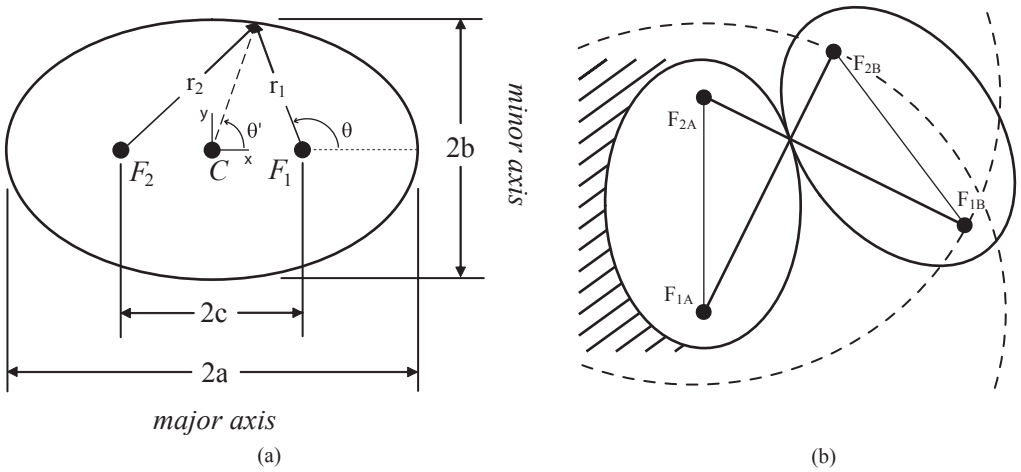

Figure 2.22 (a) Basic elements and dimensions of an ellipse. (b) The motion of the elliptical gear is derived from the antiparallelogram, where $d(F_{1A}, F_{2B}) = d(F_{1B}, F_{2A}) = 2a$ and $d(F_{1A}, F_{2A}) = d(F_{1B}, F_{2B}) = 2c$.

Of course, if full rotation is not required, the no-slip condition can come from flexible bands. Once again, bending stress is a function of the radius of the surface over which the flexure will be deflected, and Equation 2.15 applies. However, for an elliptical contact surface, R_s varies according to the following equation, where x is the rectangular coordinate (along the major axis) of the surface point in question

$$R_s(x) = \frac{a^2}{b}\left[1 + \left(\frac{b^2}{a^2} - 1\right)\left(\frac{x}{a}\right)^2\right]^{3/2} \tag{2.20}$$

For initially straight flexures, $R' = R_s$ so Equation 2.20 can be plugged into Equation 2.15 to find the bending stress at any point along the surface.

An important characteristic of ellipses is eccentricity, defined as "the position of the focus as a fraction of the semi-major axis" [29]. The distance between the geometric center of an ellipse and either focus is c, so the eccentricity, ε, is defined as

$$\varepsilon = \frac{c}{a} = \sqrt{1 - \frac{b^2}{a^2}} \tag{2.21}$$

and ranges from 0 to 1. An ellipse with ε approaching zero looks like a circle. As ε increases to 1, the radii of curvature across the semi-minor axes increase while the radii across the semi-major axes decrease. The visual equivalent would be to look down at the cross section of a cylinder (a circle), then rotate that cross section and watch how the circle flattens out (an ellipse). It is the eccentricity of an ellipse that makes it such a unique solution to so many design problems, from gear design to orbital mechanics.

2.5.4.6 Multi-stable CORE Bearings (Halverson, 2007)

Prior work has predominately dealt with continuous surfaces—circles and ellipses. However, Halverson [30] evaluates concepts that have multiple points of stable equilibrium—potential energy minima—throughout the CORE bearing's range of motion. The change in strain energy can be achieved by one of the following: placing the CORE flexure in tension; attaching flexible segments to the foci; or varying either the initial curvature of the flexure, the curvature of the CORE surface, the cross sectional area of the flexure, or the material properties of the contacts or flexures along their respective lengths. Using a Pugh scoring matrix, stability through tension was selected as the preferred method.

The contact-aided compliant flexures are placed in tension by deflecting them across a continuous (e.g. circular) surface while rolling the joint across an adjacent discontinuous cammed surface, as shown in Figure 2.23. Rolling through mating surfaces of relatively

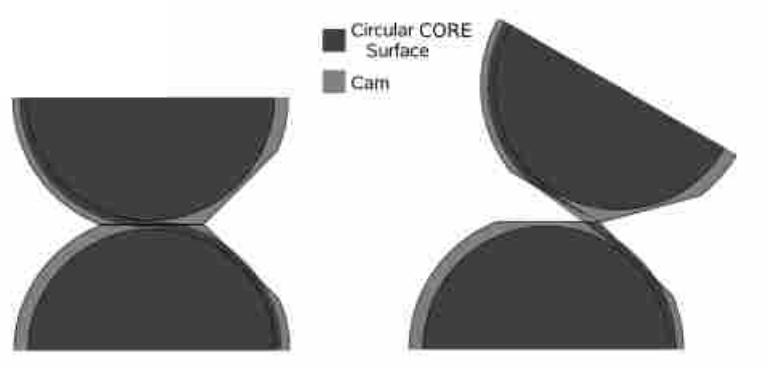

Figure 2.23 Tension-stable CORE in stable (left) and unstable equilibrium [30].

large radii places the flexures in increased tension, a range of instability. The flat surfaces between the peaks of larger radii are points of stable equilibrium.

The focus of this thesis is on continuous surfaces—ellipses—in rolling contact; Halverson's work is presented here only to provide an example of independent research in the area of non-linear rolling contact surfaces to achieve a particular functional characteristic: multi-stability.

2.5.4.7 Hertz Contact Stresses

When two curved prismatic surfaces (e.g. cylinders, elliptical prisms, etc.) are brought together in rolling contact under negligible compressive loads, the contact geometry between the two surfaces is a straight line. As the normal force increases, the materials elastically deform and the line contact becomes a rectangular contact of area *(2b)L*. Hertz contact theory says that the pressure distribution over this contact area is represented by a semielliptical prism with major axis *2b*, semi-minor axis p_0, and width *L*, as shown in Figure 2.24 [31]. The maximum pressure p_0 at the center of the distribution is given by

$$p_0 = 0.564\sqrt{\frac{P(1/R_1 + 1/R_2)}{L\Delta}} \tag{2.22}$$

where P is the normal force at the contact point, R_1 and R_2 are the radii of the contact surfaces, L is the width of the contact surface, and Δ is a combined measure of Young's modulus, E, and Poisson's ratio, ν, for both materials according to Equation 2.23, below

$$\Delta = \frac{1-\nu_1^2}{E_1} + \frac{1-\nu_2^2}{E_2} \tag{2.23}$$

Equation 2.22 is valid not just for parallel cylinders (convex-convex contacts) but also for a cylinder on a flat plate (R_2 is infinite) and a cylinder in a cylindrical groove (convex-concave; R_2 is negative). Applying this equation to these three cases, we see that, all else equal, Hertzian stresses are largest in convex-convex interactions and smallest in convex-concave interactions. The width of the contact area, 2b, is given in Equation 2.24.

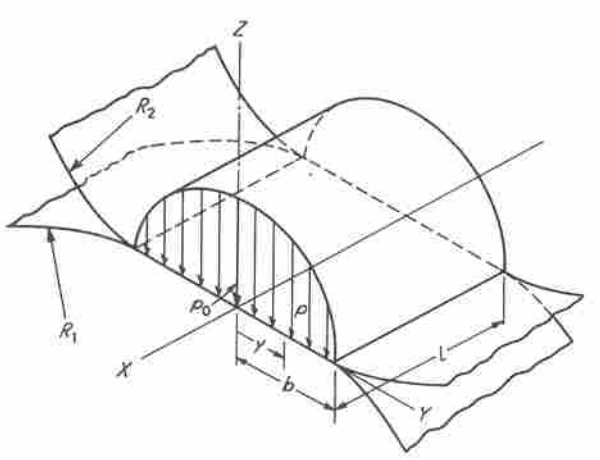

Figure 2.24 Hertz contact pressure distribution for two parallel cylinders [31].

$$2b = 2.26\sqrt{\frac{P\Delta}{L\left(1/R_1 + 1/R_2\right)}} \tag{2.24}$$

The presence of tangential forces due to friction and slip complicate the stress condition at the contact surface; however, Wittermans' research shows that Hertz contact theory is accurate for friction coefficients below 0.3 [20]. The use of stabilizing constraints—e.g. bands or rigid links—to counteract tangential forces and prevent slip will further mitigate the effects of tangential forces on the contact surface.

2.6 Pressure Angles and Transmission Angles

The contact angle, ψ_c, discussed in previous sections is often called the pressure angle, especially with regard to gearsets and cam-follower mechanisms. With mating gear teeth, for example, a 20º pressure angle is common [32]. Involute curves on teeth in contact create this constant pressure angle and allow them to mesh and roll through each other, transmitting torque with minimal wear. In contrast, contact angles in rolling link mechanisms usually change throughout their motion, so design guidelines developed by Kuntz to minimize contact angles and mitigate the effects of excessive rotation on joint stability were reviewed previously.

Another gauge on the quality of force transmission in a mechanism is the transmission angle. As a rule of thumb, the angle between any two driven links (e.g. the coupler and the driven in a four-bar linkage) should not exceed 90º ± 50º, with 90º being optimal for torque transmission. In [33], the transmission angle is cited from Alt as

$$\phi_{trans} = \tan^{-1} \frac{F_t}{F_b} \tag{2.25}$$

where F_t is the tangential force tending to rotate the driven link and F_b is the bearing force tending to apply pressure on the driven link. As transmission angles fall outside the recommended range, bearing forces on the driven link increase, torque on the driven link decreases, and—in the presence of friction—the mechanism may bind. Extreme transmission angles create noise and excessive wear and exacerbate sensitivity to manufacturing variation. These undesirable configurations cause jerky motion and promote bending and buckling failure.

2.7 Mechanical Advantage

The mechanical advantage or transmission ratio of a mechanism is a measure of what you put in versus what you get out, and the comparators are typically some ratio of force or velocity, with the velocity relationship being the reciprocal of the force relationship, as follows

$$MA = \frac{F_{out}}{F_{in}} = \frac{V_{in}}{V_{out}} \tag{2.26}$$

Mechanical advantage calculations for compliant mechanisms incorporate energy terms for the compliant elements of the mechanism. Salamon and Midha [34] provide the derivations for these metrics.

Equation 2.26 provides the generic definition of mechanical advantage; however, the equations for certain applications may be more specific. For example, the mechanical advantage for toggle linkages—like those implemented in Brooks' self-centering, force-balanced

grasping mechanisms, Figure 2.2—is provided by Chironis and Sclater (Figure 2.25 and Equation 2.27 [21]).

$$MA = \frac{F_B}{F_A} = \frac{1}{2}\frac{x}{y} = \frac{1}{2}\tan\alpha = \frac{V_A}{V_B} \tag{2.27}$$

Toggle linkages achieve large mechanical advantages near the toggle point and are thus used in a variety of applications from self-locking pliers to stone crushers.

2.8 Elastic Deflections

Failure mechanisms are often characterized by physical changes that can be catastrophic: fracture, shear, and buckling, to name a few. However, failure in one mechanism doesn't necessarily constitute failure in another. Many compliant mechanisms, for example, are designed to buckle to achieve stability in multiple positions [17]. Elastic deflections are one of the potential failure mechanisms that are acceptable in many applications, but not in others. In most cases they are relatively small, but where material deflections under prescribed loads rival desired displacements, they must be accounted for and designed into the kinematics of the mechanism.

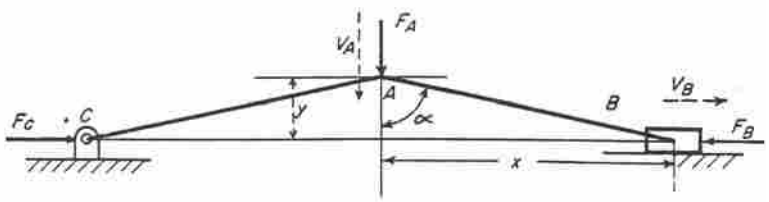

Figure 2.25 Basic elements and dimensions of a toggle linkage. Mechanical advantage is given by Equation 2.27 [21].

Elastic deflections can be calculated using energy methods such as Castigliano's method or the principle of virtual work. Although neither will be discussed in detail here, a brief summary of each is provided. Castigliano's method is amply explained by Juvinall [31], and Howell [17] provides a step-by-step approach for applying the principle of virtual work.

Castigliano's method says that the elastic deflection at any point in any direction at that point is equal to the partial derivative of the strain energy with respect to a load at that point in that direction. Loads, or systems of loads, are categorized as either axial, bending, torsion, or transverse shear and the appropriate strain energy equations are applied, differentiated with respect to each associated load, and summed to arrive at the overall deflection at that point in that direction. Imaginary loads can be applied at any location, carried through, and set to zero at the end to determine the deflection due to that "load" (at that point).

The principle of virtual work states [35]: "The net virtual work of all active forces is zero if and only if an ideal mechanical system is in equilibrium." In an ideal mechanical system, the constraints do no work, so they are ignored. To summarize the process, position vectors for each force and angular displacement vectors for each moment are differentiated with respect to a chosen generalized coordinate, resulting in the virtual displacements of both. Virtual work for forces and moments is then found by taking the dot product of each and their respective virtual displacements. Virtual work for any potential energy sources not yet accounted for is determined by differentiating them with respect to the generalized coordinate and multiplying by $-\delta q$. The unknown can then be calculated by summing the virtual work due to forces, moments, and other potential energy sources, setting this equal to zero, and solving for the unknown.

The principle of virtual work is straightforward and efficient. Unlike conventional methods, only the active forces are considered. Together with the pseudo-rigid-body model, the virtual work due to compliant members can be easily analyzed as well. The principle of virtual work is also flexible; it can be adapted to *n*-DOF mechanisms by choosing any *n* generalized coordinates.

CHAPTER 3 ELLIPTICAL ROLLING CONTACT JOINTS

Linkages that undergo high compressive forces must be comprised of joints that can bear these forces without yielding or causing excessive wear and without becoming unstable in tension. Circular rolling contact joints have been successfully used in robotic fingers [22] but are limited in high compression applications because 1) the radius of curvature for the required link size is often too small, causing excessive Hertzian contact forces in the links and bending stresses in the flexures (if used), and 2) if flexures aren't used, circular rolling contact joints must have another provision for tractive rolling (e.g. gear teeth or adequate friction) and a link joining their respective centers to maintain engagement or compression.

Ellipses, on the other hand, have larger radii of curvature across the semi-minor axis (along the semi-major axis) and thus can withstand larger loads. Additionally, links connecting diagonally opposite foci force pure rolling, regardless of the friction condition at the contact surface. Thus, elliptical surfaces joined in rolling contact with flexible bands or connecting links will have lower Hertzian contact stresses, lower bending stresses in the flexures, and won't roll over or slip past each other.

The aforementioned characteristics of elliptical surfaces joined in rolling contact make them well-suited for use in linkages that undergo high compressive forces; however, to date, the motion of mechanisms comprised of these elliptical rolling contact joints has not been clearly described. In section 3.1, the angles of the connecting links for the elliptical rolling contact joint will be derived as a function of the relative angle between the two rolling contact links and the elliptical eccentricity of the contacting surfaces. These angles are required for kinematic analysis. Once these angles are known, a vector loop through a mechanism containing multiple elliptical rolling contact joints can be created and the forward kinematics for the mechanism can be developed. In section 3.2, motion is described as a combination of rotation and translation, and equations for displacement are provided. In section 3.3, the radius of curvature, curvature, and stabilizing member stresses resulting from excessive contact angles will be presented.

3.1 Connecting Link Angles

When the two adjacent elliptical surfaces of links L_i and L_j join in rolling contact as shown in Figure 3.1, where $j = i + 1$, their semi-major axes intersect at some angle θ_j. Assuming this joint is part of a mechanism comprised of multiple rigid links and joints, we can follow the vector loop defining the position of the mechanism in clockwise fashion and pass through each joint of this type, for $i = 1, 2, 3, \ldots n$, where n is the total number of links in the mechanism. If we look at each joint separately and in succession, i represents the link in question and j indicates the next link in the loop; therefore, θ_j denotes the angle the next link makes with the link in question, which follows conventional kinematic notation (e.g. θ_2 is the angle between L_1 and L_2).

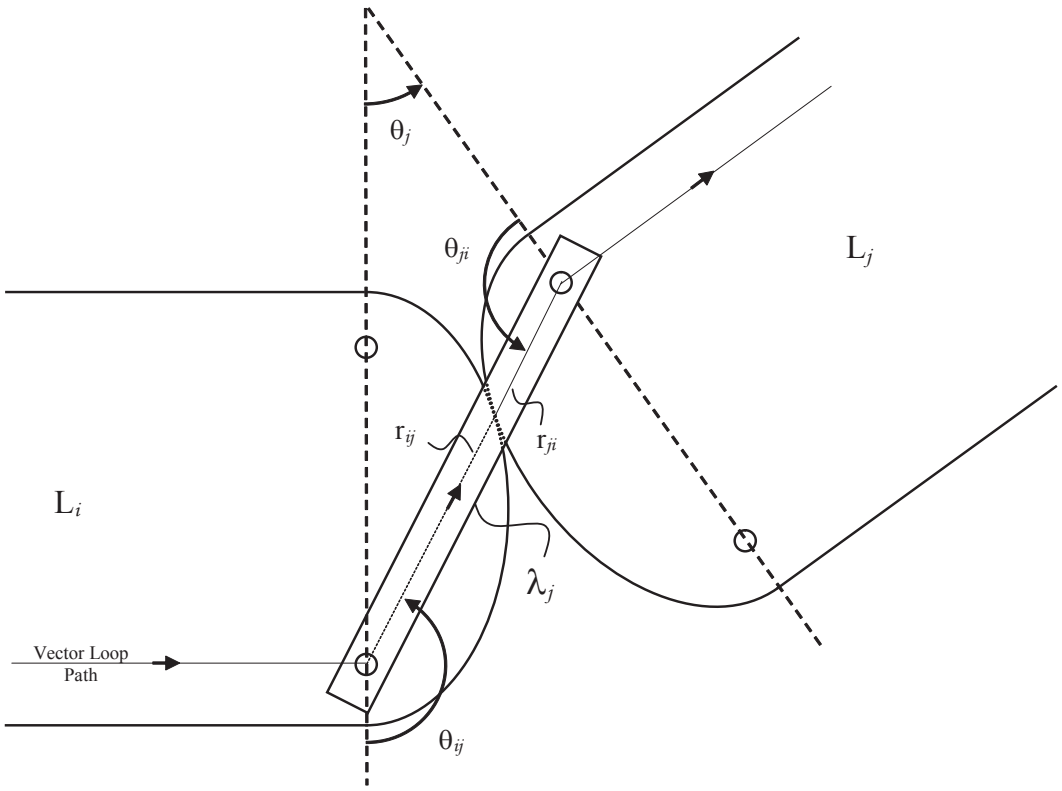

Figure 3.1 Vector loop path through elliptical rolling contact joint (ε = 0.762, *a* = 1.06 in.).

When we join both sets of diagonally opposite foci on ellipses in rolling contact with pinned-pinned rigid links λ_j (only one connection shown in Figure 3.1 for simplicity), we create an elliptical gear with a no-slip condition. From the two-center bipolar coordinate equation, we know that

$$\lambda_j = r_{ij} + r_{ji} = 2a \tag{3.1}$$

Note that when variables carry two subscripts, the first subscript refers to the link the variables are defined on, while the second refers to the adjacent link that forms the rolling contact joint, similar to the notation used by Collins [22].

In Figure 3.1, it is clear that this *connecting link*, λ_j, is one side of a triangle whose other two sides are formed by the semi-major axes that intersect at θ_j. The notable exception is when the two elliptical surfaces are in contact at the semi-minor axes—the toggle point—and thus have parallel semi-major axes, crossing at infinity. In this case, any rotation between the two ellipses causes the semi-major axes to intersect and form a triangle. This topic will be further discussed at the end of this section.

Since θ_j is known throughout the range of motion of the mechanism, we are left with two unknown angles. These angles, which we will denote θ_{ij} and θ_{ji} and call the *connecting link angles*, represent the angles between the connecting link and the semi-major axis of L_i and the connecting link and the semi-major axis of L_j, respectively. (Note that the term "connecting link angle" will be used throughout, regardless of whether connecting links are used to join diagonally opposite foci or stabilization bands are attached to and deflected across elliptical contacting surfaces with no physical link between the foci. Either way, a no-slip condition is created and the angles between the line joining diagonally opposite foci and the semi-major axes remain the same.)

What follows is a derivation of the equations that define these connecting link angles, which are simply a function of the eccentricity of the ellipses, ε, and the included angle, θ_j. Each joint consists of two identical elliptical surfaces (i.e. $a_{ij} = a_{ji}$, $\varepsilon_{ij} = \varepsilon_{ji}$), although this geometry can change from joint to joint within the same mechanism. From the polar equation of an ellipse, we have

$$r_{ji} = \frac{a\left(1-\varepsilon^2\right)}{1+\varepsilon\cos\theta_{ji}} \tag{3.2}$$

Since $r_{ij} + r_{ji} = 2a$, it follows that

$$r_{ij} = 2a - \frac{a\left(1-\varepsilon^2\right)}{1+\varepsilon\cos\theta_{ji}} \tag{3.3}$$

or

$$r_{ij} = a\left[\frac{1+2\varepsilon\cos\theta_{ji}+\varepsilon^2}{1+\varepsilon\cos\theta_{ji}}\right] \tag{3.4}$$

From the polar equation of an ellipse, we also know that

$$r_{ij} = \frac{a\left(1-\varepsilon^2\right)}{1+\varepsilon\cos\theta_{ij}} \tag{3.5}$$

Solving for θ_{ij}, we get

$$\theta_{ij} = \cos^{-1}\left[\frac{a\left(1-\varepsilon^2\right)-r_{ij}}{\varepsilon r_{ij}}\right] \tag{3.6}$$

Substituting Equation 3.4 into Equation 3.6 and simplifying, we have

$$\theta_{ij} = \cos^{-1}\left[\frac{\left(-1-\varepsilon^2\right)\cos\theta_{ji}-2\varepsilon}{2\varepsilon\cos\theta_{ji}+1+\varepsilon^2}\right] \tag{3.7}$$

From geometry, we know that

$$\theta_{ij} = \theta_{ji} + \theta_j$$

or

$$\theta_{ji} = \theta_{ij} - \theta_j \tag{3.8}$$

We can now substitute Equation 3.8 into Equation 3.7 and numerically solve for the connecting link angles using Equation 3.9 (θ_{ij}) and then Equation 3.8 (θ_{ji}). Note that these angles are simply a function of the relative link angle, θ_j, and the elliptical eccentricity of the contact surfaces, ε.

$$\theta_{ij} - \cos^{-1}\left[\frac{\left(-1-\varepsilon^2\right)\cos\left(\theta_{ij}-\theta_j\right)-2\varepsilon}{2\varepsilon\cos\left(\theta_{ij}-\theta_j\right)+1+\varepsilon^2}\right] = 0 \tag{3.9}$$

When using Equations 3.8 and 3.9, it is important to remember that θ_j can be positive or negative since it represents the relative position of L_j with respect to L_i using generalized polar coordinate angles. In the configuration shown in Figure 3.1 and comparing this with Equation 3.8, we can see θ_j is positive because $\theta_{ij} > \theta_{ji}$. At the toggle point, $\theta_{ij} = \theta_{ji}$ and $\theta_j = 0$. If the linkage were to travel through the toggle point, $\theta_{ij} < \theta_{ji}$ and θ_j would then be negative. Note also that, given some fixed linkage position, switching the connecting link so that it joins the other two diagonally opposite foci and analyzing the vector loop path through the connecting link in this new orientation would also change the sign on θ_j. In short, it is critical that the designer check each joint angle (θ_j) in the linkage to verify that the correct sign has been used and thus ensure that the connecting link angles in the vector loop are correct.

3.2 Elliptical Rolling Link Motion

Unlike rigid links connected at pin joints, adjacent links joined in rolling contact experience complex relative motion that is a combination of both rotation and translation. The connecting link angles developed in the previous section enable position analysis and a better understanding of elliptical rolling link motion.

Chasles' theorem, cited in [36], states: "Any displacement of a rigid body is equivalent to the sum of a translation of any one point on that body and a rotation of the body about an axis through that point." From Figure 3.2, the rectangular components of the position vector from one of the foci of the reference link (F_1 of L_i, in this case) to an arbitrary point P on adjacent link L_j are

$$x_P = 2a\sin\theta_{ij} + c\sin\theta_j + u\cos\theta_j + v\sin\theta_j \tag{3.10}$$

$$y_P = -2a\cos\theta_{ij} - c\cos\theta_j + u\sin\theta_j - v\cos\theta_j \tag{3.11}$$

Thus, the relative rotation of link L_j at point P is simply θ_j, and the magnitude of the associated translation of P is given by the position difference

$$R_{P_f P_i} = \sqrt{(x_{P_f} - x_{P_i})^2 + (y_{P_f} - y_{P_i})^2} \tag{3.12}$$

while the angle of the position difference vector is given in Equation 3.13.

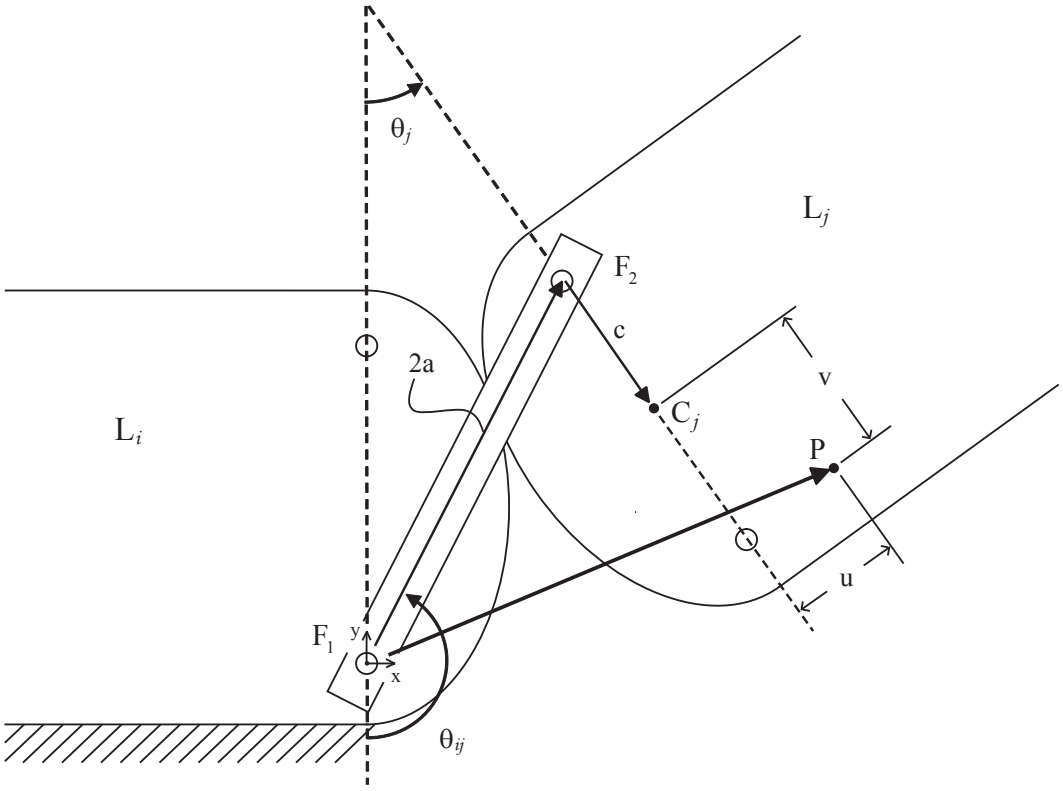

Figure 3.2 Geometric parameters defining a point *P* on adjacent elliptical rolling links.

$$\theta = \arctan\left(\frac{y_{P_f} - y_{P_i}}{x_{P_f} - x_{P_i}}\right) \tag{3.13}$$

Care should be taken when using the inverse trigonometric functions to ensure the proper solution is used (e.g. *tan 150° = tan -30°* and *tan 210° = tan 30°*).

As discussed in Chapter 2, focus F_2 traces a circular arc as it rotates about F_1. How ever, the motion of center C_j of elliptical prism L_j is shown in Figure 3.3a for two different eccentricities (ε = 0.762 and 0.333), while Figure 3.3b describes the motion of point *P* (*u = 0.5a*, *v = 0.7a*) where the position of *P* is measured from C_j. In both cases, position is normalized as a function of semi-major axis length *a*. Note that displacement is a function of

the relative location of point P on link L_j and, for elliptical rolling links, is also a function of the eccentricity. It can also be seen that, for a finite range of motion and for certain eccentricities and point locations, the point experiences straight line motion (C_j with $\varepsilon = 0.762$, which varies 0.01 in. from straight line motion between 0º and 65º) or motion that closely approximates a circular path (R_P, with $\varepsilon = 0.333$, deviates just 0.003 in. from a circular path between θ_j = 130º and 150º).

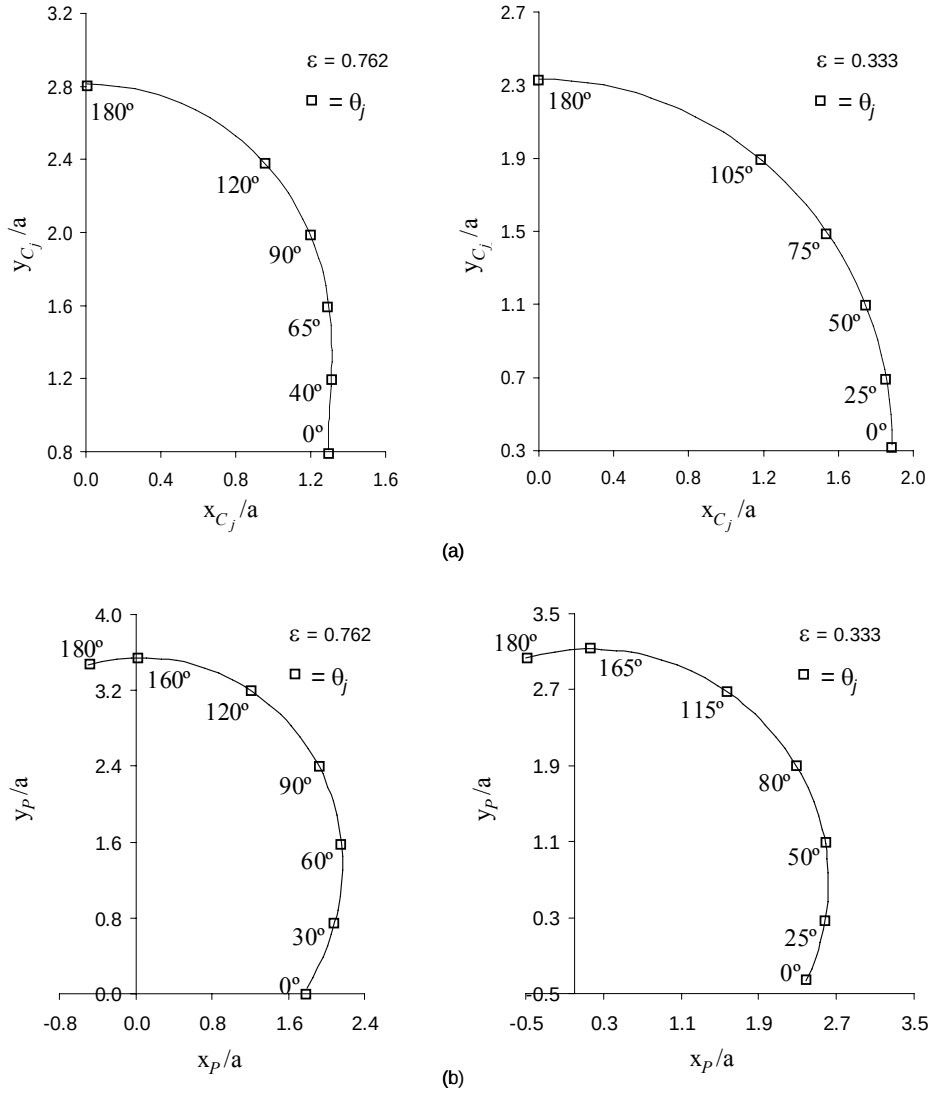

Figure 3.3 Motion path of ellipse center C_j (a) and point P ($u=0.5a$, $v=0.7a$) (b) given two different eccentricities.

In sections 3.1 and 3.2, connecting link angles (rotation) and translation have been described for a given joint as a function of relative link angle θ_j and elliptical link geometry ε and a. In Chapter 4, the displacement of a kinematic chain comprised of multiple elliptical rolling contact joints will be analyzed. It will be shown that total output displacement is simply the summation of the individual rotations and translations of each of the links in the mechanism.

3.3 Characteristics of the Contact Surface Profile

The connecting link angles θ_{ij} and θ_{ji} developed in section 3.1 are the characteristic angles of elliptical rolling contact joints and can be used to derive dimensions that are critical to understanding stresses and motion through the joint. The following sections discuss radius of curvature, curvature, and flexure stresses resulting from excessive contact angles.

3.3.1 Radius of Curvature

Hertz contact stresses and bending stresses in the flexures are a function of the changing radius of the elliptical surface. For a given r_{ij} and θ_{ij}, the x coordinate of the contact point can be found from

$$x = c + r_{ij} \cos \theta_{ij} \tag{3.14}$$

This equation can be substituted for x in Equation 2.20 to calculate the radius of the surface, R_s, at the contact point.

Polar coordinates measured from the center of the ellipse are sometimes preferred over Cartesian coordinates, especially with large rotations. Using the Law of Cosines to find r' and then the Law of Sines to find θ' (Figure 3.4), we have

$$\theta' = \sin^{-1}\left(\frac{r_{ij}\sin\theta_{ij}}{\left(c^2 + r_{ij}^{\ 2} + 2cr_{ij}\cos\theta_{ij}\right)^{1/2}}\right) \tag{3.15}$$

Equation 3.16 [29] provides the radius of the surface, R_s, at the contact point as a function of the parameter t

$$R_s(t) = \frac{\left(b^2\cos^2 t + a^2\sin^2 t\right)^{3/2}}{ab} \tag{3.16}$$

where t is defined as

$$t = \tan^{-1}\left(\frac{a}{b}\tan\theta'\right) \tag{3.17}$$

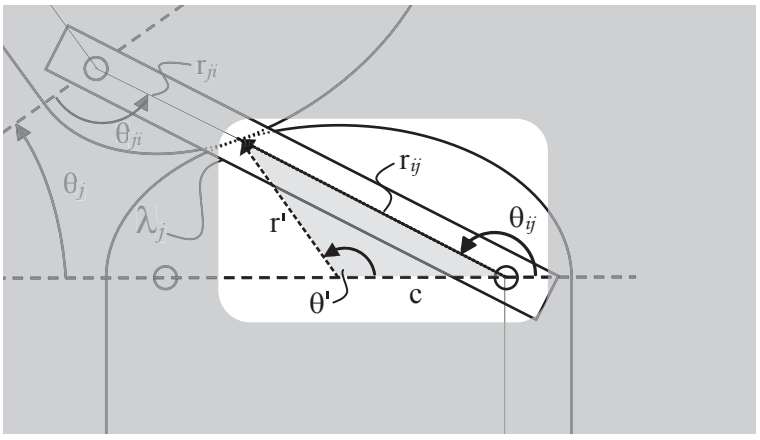

Figure 3.4 Dimensions used to derive the polar coordinates from the ellipse center.

Looking at the extreme values of R_s for both Equations 2.20 and 3.16 we see that

…smallest radius… $$R_s(a) = R_s(0°) = \frac{b^2}{a} \tag{3.18}$$

…largest radius… $$R_s(0) = R_s(90°) = \frac{a^2}{b} \tag{3.19}$$

The results from Equation 2.20 or 3.16 can be plugged into Equation 2.22 to find the Hertzian stress at the contact point. A force directed design approach would allow large compressive forces near θ' = 90º (x = 0), and would minimize contact forces at θ' = 0º and 180º (|x| = a). In application, the large radius can deliver high-powered force transmission while the small radius accelerates displacement.

Similarly, Equation 2.20 or 3.16 is used in combination with the bending stress equation, Equation 2.15, to ensure flexure stresses aren't excessive across small radii. For oscillatory motion, it is often unnecessary to extend the range of motion or deflect stabilization bands over the small radius; these equations would confirm that stresses are within the elastic range.

3.3.2 Curvature

The "instantaneous rate $d\alpha/ds$ at which the tangent vector is turning, in radians per unit of arc length, is called the curvature" [37]. Curvature is usually denoted by the Greek letter κ and is equal to the reciprocal of the radius of curvature, in this case R_s. From Equations 2.20 and 3.16 we have

$$\kappa = \frac{d\alpha}{ds} = \frac{1}{R_s(x)} = \frac{b}{a^2\left[1+\left(\frac{b^2}{a^2}-1\right)\left(\frac{x}{a}\right)^2\right]^{3/2}} \tag{3.20}$$

and

$$\kappa = \frac{d\alpha}{ds} = \frac{1}{R_s(t)} = \frac{ab}{\left(b^2\cos^2 t + a^2\sin^2 t\right)^{3/2}} \tag{3.21}$$

The relative rotation θ_j of convex-convex parallel cylinders in rolling contact, L_i and L_j in Figure 3.1 for example, is simply the sum of the individual $\theta_j/2$ rotations of each, assuming the elliptical cylinders are identical. If α is the integral sum of all the infinitesimally small rotations $d\alpha/ds$ around the perimeter of a single ellipse, then $\alpha = \theta_j/2$. Equations 3.20 and 3.21 indicate how quickly θ_j is changing as the surfaces roll across each other. In the reference frame of L_i (i.e. L_i "grounded"), L_j will rotate 180º when rolled 90º from the large radius (minor axis) to the small radius (major axis) of L_i. However, the "distribution of rotation" will depend on the eccentricity of the elliptical surfaces. While circles ($\varepsilon = 0$) exhibit uniform rotation, ellipses with eccentricities approaching 1 undergo most of their rotation over a small fraction of the arc length, near the major axes.

Figure 3.5 shows a plot of the curvature, $d\alpha/ds$, versus the polar coordinate at the ellipse center, θ', and introduces a term called the *curvature ratio*. If Equations 3.18 and 3.19 represent the smallest and largest radii, respectively, for an elliptical surface at some coordinate x or θ', then the corollary maximum and minimum values of curvature would be

…largest curvature… $$\kappa(a) = \kappa(0°) = \frac{a}{b^2} \tag{3.22}$$

…smallest curvature… $$\kappa(0) = \kappa(90°) = \frac{b}{a^2} \tag{3.23}$$

The curvature ratio is found by dividing the largest curvature, Equation 3.22, by the smallest curvature, Equation 3.23, and is thus defined by

$$\kappa_{ratio} = \left(\frac{a}{b}\right)^3 = \left(1-\varepsilon^2\right)^{-3/2} \tag{3.24}$$

Curvature ratio is offered to complement velocity ratio. Using the example of links L_i and L_j in Figure 3.1 again, if the connecting link between the two elliptical surfaces were the driving input (i.e. ground L_i and apply a constant angular velocity to the connecting link) as in planetary gear systems, the velocity ratio accurately characterizes the motion—ω_{min} at

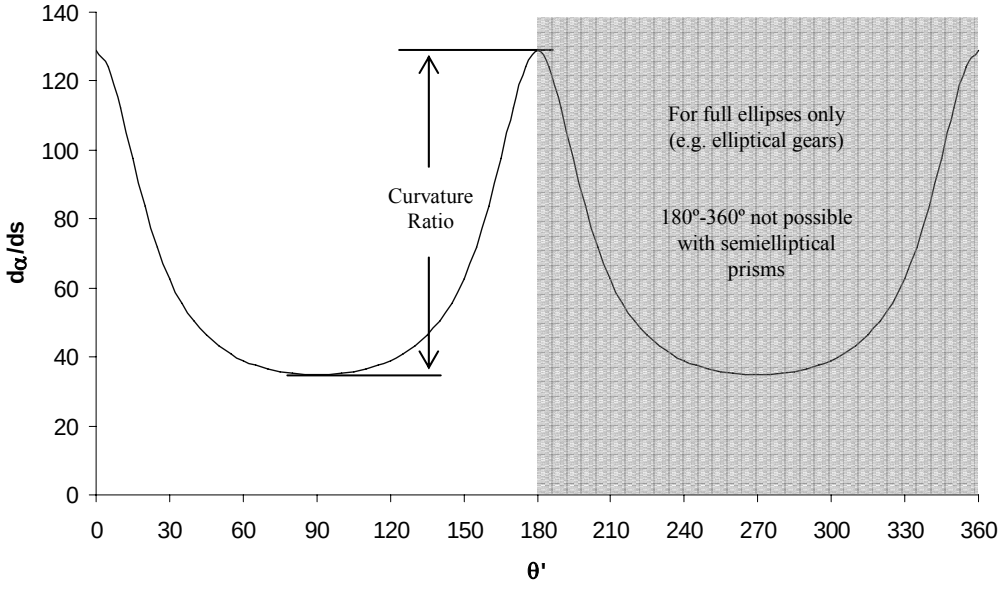

Figure 3.5 Curvature for the elliptical contact surfaces shown in Figure 3.1 (ε = 0.762, a = 1.06 in.) as a function of the polar angle at the ellipse center.

$\theta_{ij} = 0^o$, ω_{max} at $\theta_{ij} = 180^o$, and $\omega_{ratio} = (r_{max}/r_{min})^2 = [(a+c)/(a-c)]^2$. However, when the input is the rotation of one of the elliptical surfaces rather than the connecting link, the relative rotation between the two surfaces is best described by their curvatures. This comparison of how quickly θ_j is changing as the surfaces roll across each other at the major axes (large curvature) versus the minor axes (small curvature) measures the "distribution of rotation" mentioned previously. Rolling contact joints with a small curvature ratio will distribute rotation evenly across the surface, while elliptical rolling contact joints with larger curvature ratios will undergo most of their rotation between the foci and the major axes.

Light compression, quick rotation across areas of large curvature and heavy compression, slow rotation over areas of small curvature are preferred. It follows that equal distribution—as provided by circular cylinders in rolling contact—may be a compromised solution but is often pursued to limit complexity.

3.3.3 Contact Angles and Constraining Member Stresses

The contact angle ψ_c for identical convex-convex parallel cylinders in rolling contact is simply half the relative rotation between the two cylinders, or $\theta_j/2$ (see Figure 3.6). When ψ_c is greater than the slip angle (ψ_s), stabilization bands or connecting links are required. When two bands are used, one will be loaded in compression and the other loaded in tension. (Note that reversing motion—switching the driving and driven links—changes which member is in tension and which is in compression.) Since the flexure loaded in compression will just buckle—i.e. it won't support a load—the flexure loaded in tension is used to confirm the joint's resistance to tangential loads. The force in the flexure, however, is not the full tan-

gential component of the contact force, because some of this force is resisted by friction. Building upon Equation 2.17, the tensile stress in the flexure, reduced by the friction force, is

$$\sigma_{tension} = \frac{F_c\left(\sin\psi_c - \cos\psi_c \tan\psi_s\right)}{Lh} \tag{3.25}$$

or

$$\sigma_{tension} = \frac{F_c\left(\sin\frac{\theta_j}{2} - \mu\cos\frac{\theta_j}{2}\right)}{Lh} \tag{3.26}$$

Unlike stabilization bands, links connecting diagonally opposite foci are not collinear with the tangential force at the contact point; thus, the geometry is more complex. Figure 3.6 illustrates this configuration. As with flexures, the loading places one of the connecting links in compression and one in tension. In the general case of potentially low stiffness, the link in compression is susceptible to buckling, so the connecting link in tension is assumed to bear the tangential load. By inspection, the angle γ between the tensile connecting link and the tangent to the contact point is found from Equations 3.27 and 3.28

…for θ_j positive… $$\gamma = 180° - \theta_{ji} - \frac{\theta_j}{2} \tag{3.27}$$

…for θ_j negative… $$\gamma = 180° - \theta_{ij} - \frac{\theta_j}{2} \tag{3.28}$$

and the tensile stress in the connecting link, reduced by the friction force, is

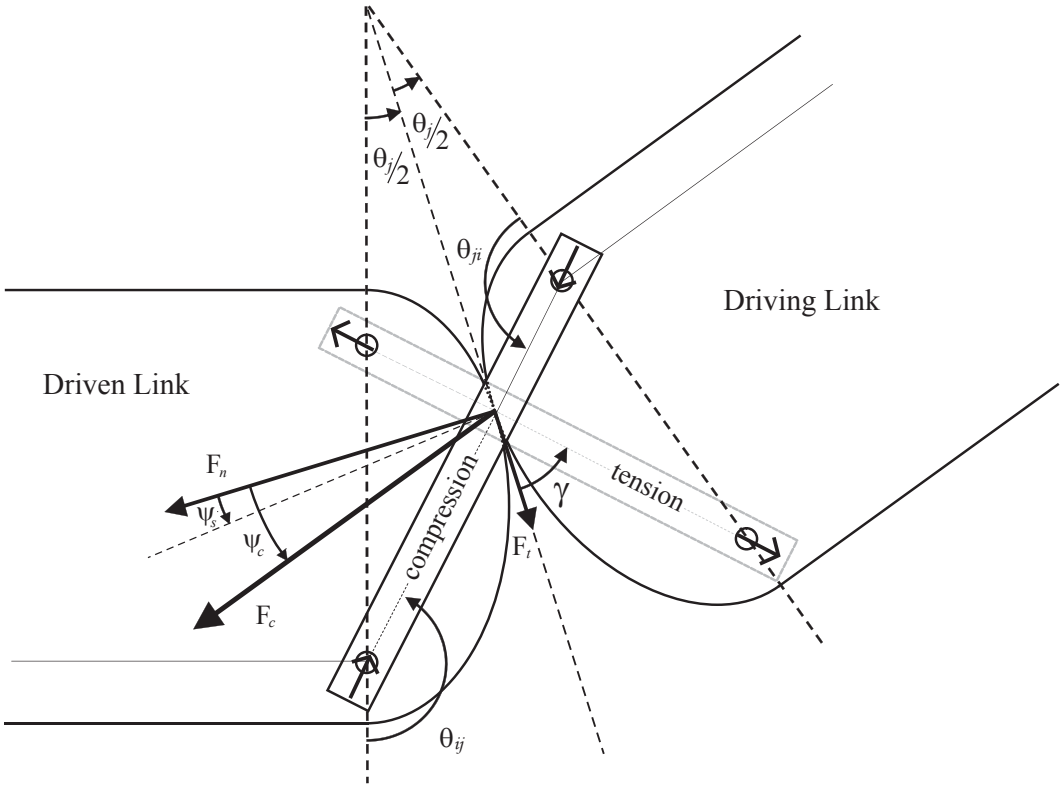

Figure 3.6 Dimensions and forces required to calculate the component loads in the stabilizing flexures or connecting links of an elliptical rolling contact joint (ε = 0.762, *a* = 1.06 in.).

$$\sigma_{tension} = \frac{F_c\left(\sin\psi_c - \cos\psi_c \tan\psi_s\right)}{A_{CL}\cos\gamma} \tag{3.29}$$

or

$$\sigma_{tension} = \frac{F_c\left(\sin\frac{\theta_j}{2} - \mu\cos\frac{\theta_j}{2}\right)}{A_{CL}\cos\gamma} \tag{3.30}$$

For $\theta_j = 0^o$, $\gamma = 180^o - \theta_{ij}$ and, by inspection, $\cos\gamma = c/a = \varepsilon$. Thus when plotted versus θ_j, $\cos\gamma$ starts at ε and slopes concave down toward $\theta_j = 180^o$, as shown in Figure 3.7.

Note that Equation 3.30 is identical to Equation 3.26 except for the $\cos\gamma$ in the denominator (the cross sectional area A_{CL}, versus Lh for the bands, may also vary). Whether

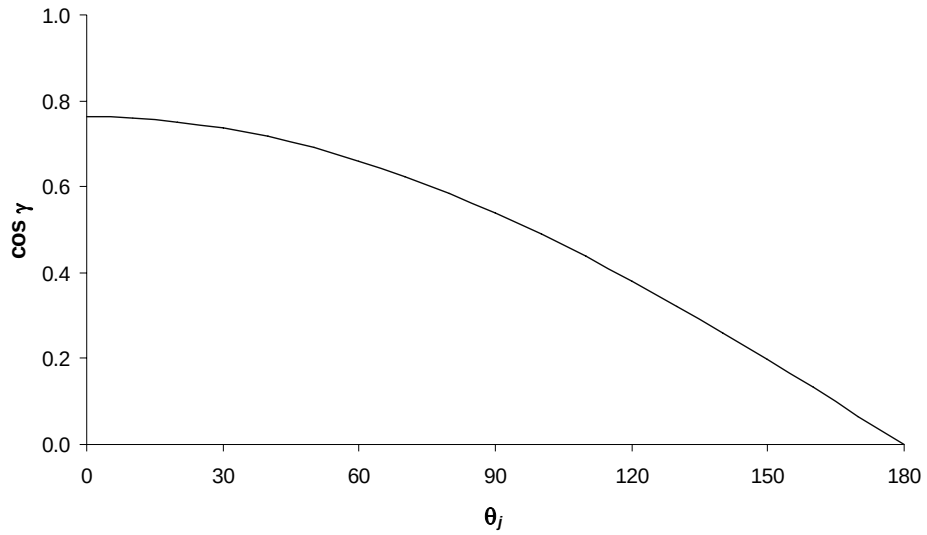

Figure 3.7 The tangential force is divided by *cos* γ to obtain the component in the direction of the connecting link. Notably, *cos* $\gamma = \varepsilon$ when $\theta_j = 0$.

flexures or connecting links are used, the tensile stress increases as θ_j (and consequently, F_t) increase; however, dividing by *cos* γ results in even larger forces in the latter (see Figure 3.8). Depending on how the connecting links are executed, these large forces can cause tensile failure, shear at the foci, or just excessive friction and wear that either binds the mechanism or causes premature failure. As we approach the limit of $\varepsilon = 0$ (a circle), the forces in the connecting link(s) go to infinity. These large tangential forces and large stresses in the connecting links can be interpreted as a tendency for the contacting surfaces to slip past each other rather than roll. At the limiting case of two circular cylinders connected at their centers, the only resistance to slip is some form of friction or gear teeth.

Equations 3.27 through 3.30 have important implications when designing elliptical rolling link mechanisms. Although flexures and bands allow large rotations under light loading, heavy compression is not supported at large angles due to high tangential forces. Additionally, designs that employ connecting links may require larger eccentricities or limited range of motion to sustain smooth force transmission.

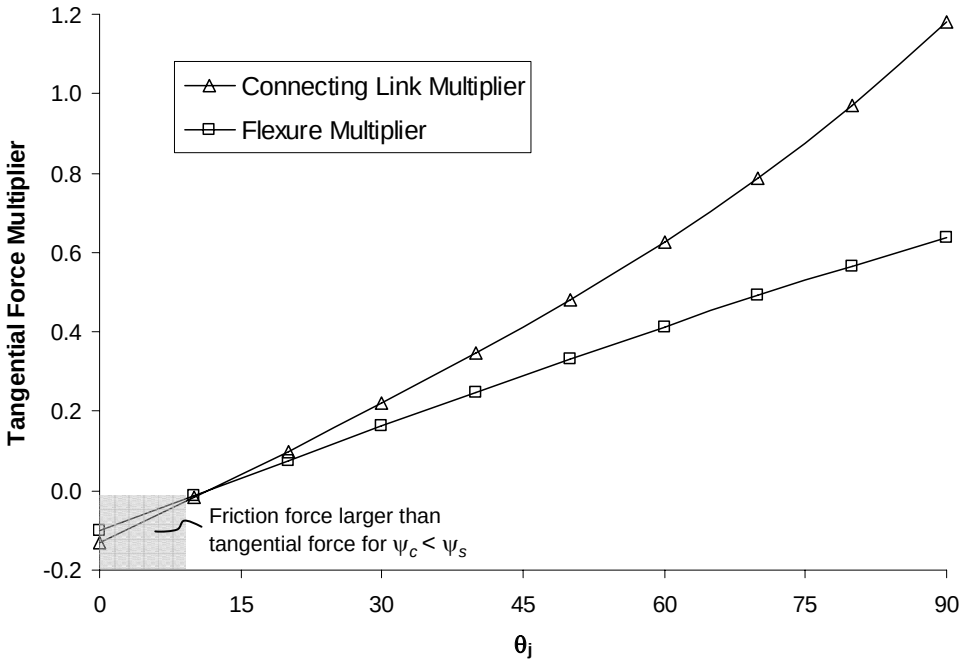

Figure 3.8 The tangential force at the contact resisted by the constraining members is a function of the contact angle $\theta_j/2$ and (for connecting links) *cos* γ, where γ is also a function of the eccentricity ($\varepsilon = 0.762$ and $\mu = 0.1$ in this case).

This chapter, in conjunction with Chapter 2, has provided the basic principles for developing an elliptical rolling link mechanism. However some topics, such as forward kinematics, mechanical advantage, and self-adjustment, are best understood when applied to a specific design problem. In Chapter 4, the design of a mechanical brake caliper as conceived by Brooks is further developed as design guidelines from Chapters 2 and 3 are applied.

CHAPTER 4 BRAKE CALIPER CASE STUDY

This chapter provides an example of how to implement elliptical rolling contact and continuous self-adjustment in a floating disc brake caliper mechanism where large forces and precision displacement are required. While the manufacture is relatively difficult, the mechanics of a disc brake are easily understood, making it a good candidate for this analysis. Although the different aspects are presented in series, they are not independent, consecutive steps but rather interrelated parameters of a large, complex design problem, the solution of which is amenable to spreadsheet analysis with numerical solutions that are obtained through an iterative process.

4.1 Disc Brakes

From the time wheels began to turn man has tried to stop them. While the technology has matured significantly since early artisans began using their feet to stop the potter's wheel, the basic principle is the same: pressure applied to a rotating disc, in the presence of friction, creates a force that opposes motion and slows the rotation of the disc. If the disc is

attached to a potter's wheel, the clay stops turning, and if the disc is clamped to the wheel of an automobile, it slows down.

The sections that follow provide background on the use of disc brakes in various applications. First, bicycle disc brakes are reviewed as an example of a purely mechanical system. Automotive disc brakes are then discussed and the basic equations used to size a brake system are provided. Finally, the Electronic Wedge Brake technology being developed by Siemens is shared as an example of a viable electromechanical alternative to hydraulic systems.

4.1.1 Disc Brakes on Bicycles

In 1969, disc brakes were applied to production line motorcycles for the first time [38]. More recently, bicycle manufacturers have also incorporated disc brakes on some of their models. Unlike conventional bike brakes that rely on the friction interface between the wheel rim and a rubber brake pad lining (a design with erratic performance results given the varying terrain and weather conditions), disc brakes are reliable and consistent in brake torque and performance.

Avid is an example of one company that produces a bicycle disc brake with a method of actuation that is typical of other bike disc brake designs (see Figure 4.1). The actuation mechanism consists of a circular fixed cam that can rotate about an axis of symmetry through its center point, with a mating cam that is allowed to travel along this axis. The two cams have matching, tapered grooves that, as the cams experience relative rotation, allow for three small bearings to push the movable cam out in a direction along the axis of cam rotation, thus transforming a rotational force into a linear axial force.

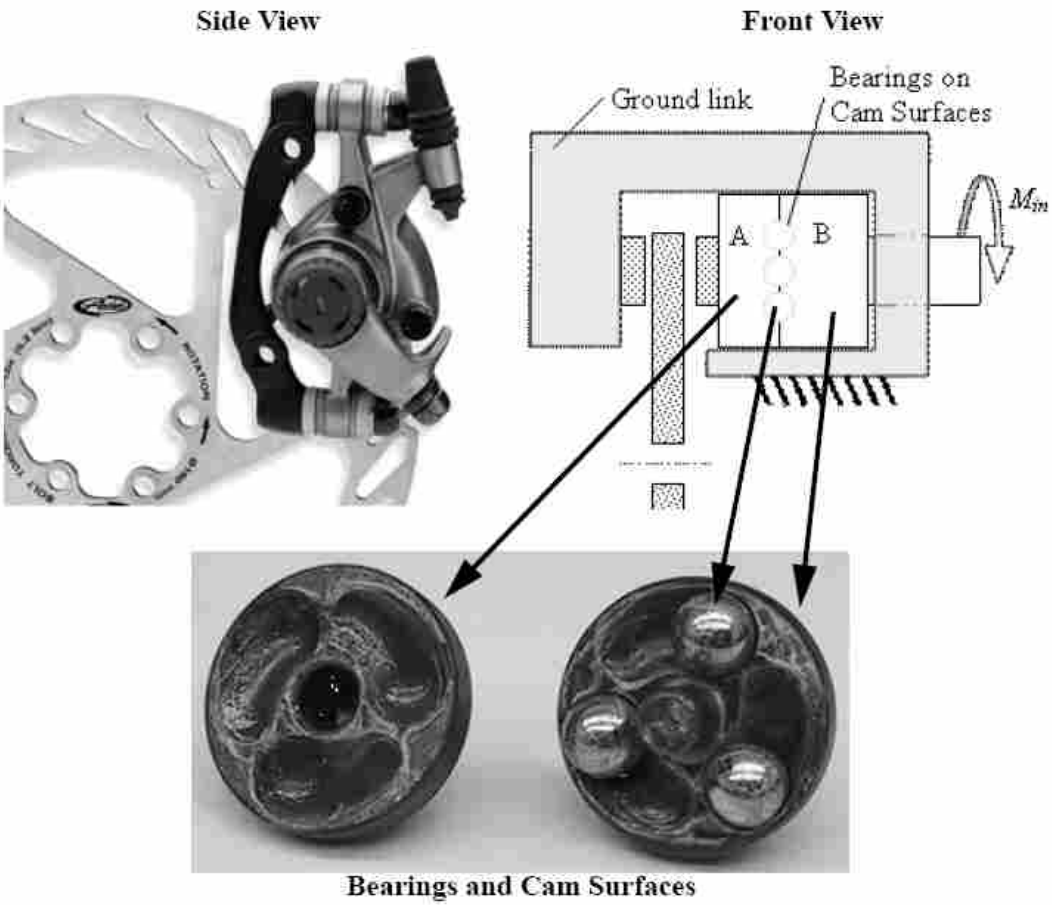

Figure 4.1 Avid bicycle mechanical disc brake (side view). Front view shows the internal wedge mechanism (cams and sliders A and B) used to actuate a single pad into contact with the rotor [6].

In most bike brake designs, including the Avid design described here, the actuating mechanism pushes one pad against the rotor and then the rotor deflects until it makes contact with the other pad; thus, the system does not produce balanced forces on both sides of the rotor since it relies on rotor deflection to realize contact between both pads. A review of the United States Patent and Trademark Office (USPTO) website reveals a patent for a product very similar to this one [39].

4.1.2 Automotive Disc Brakes

Although disc brakes have been around since the early days of the automobile, they have only recently become the standard. The first automobiles used various forms of mechanical braking and engine braking. Hydraulic drum brakes became standard equipment in the 1930's, and self-adjustment was introduced in the 1940's [40, 41]. Figure 4.2 shows basic components of both types of brakes, and Figure 2.4 in Chapter 2 illustrates the use of hydraulic pressure to actuate both fixed and floating caliper disc brakes.

Drum brakes were relatively easy to manufacture when compared to disc brakes, which may explain their adoption as the standard, but the mechanics are more complex and their performance was unpredictable [38]. In 1953, Dunlop equipped the Jaguar XK 120 with hydraulic disc brakes, a historic event which is usually regarded as the first implementation of disc brakes on cars. Three of these vehicles went on to take 1st, 2nd, and 4th in the Le Mans 24-hour race. It wasn't long after this that disc brakes became the standard on European cars, although Americans didn't latch on until the 60's and 70's [40, 41].

The equations for sizing a brake system are developed from [42]. Figure 4.3 illustrates the relevant dimensions. First, we start with the "DNA of the vehicle", the non-dimensional values ψ and χ. These values locate the center of gravity, where ψ is the weight over the rear axle, F_{zR}, compared to the overall weight, W, of the vehicle (in a static situation—parked on level ground, zero velocity), and χ is the height, h, of the center of gravity compared to the wheelbase, L (see Equation 4.1).

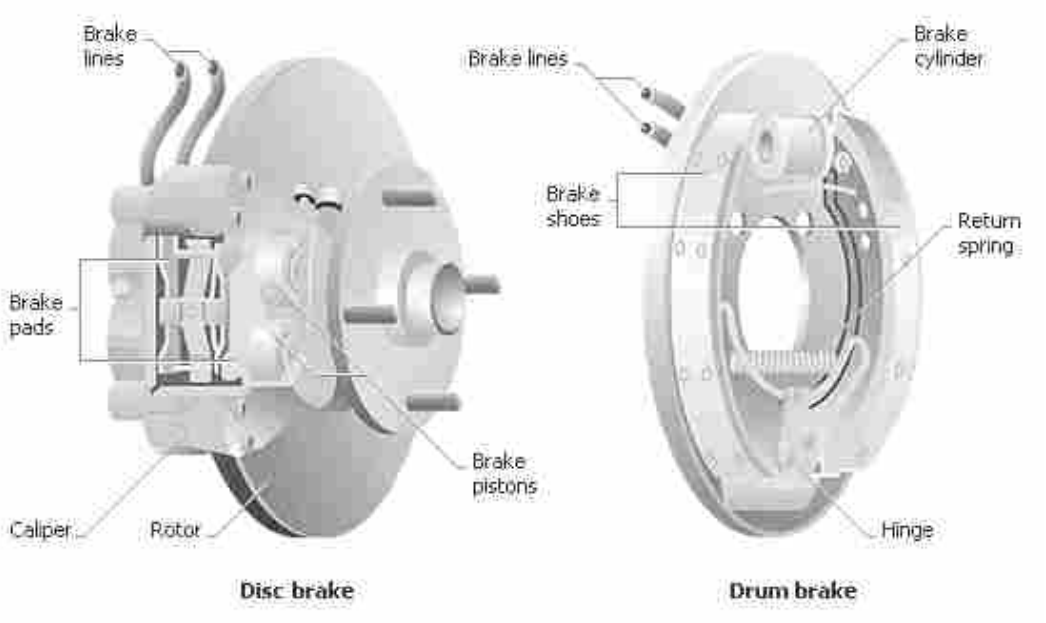

Figure 4.2 Basic components of hydraulic brakes [10].

$$\psi = \frac{F_{zR}}{W} \qquad \chi = \frac{h}{L} \tag{4.1}$$

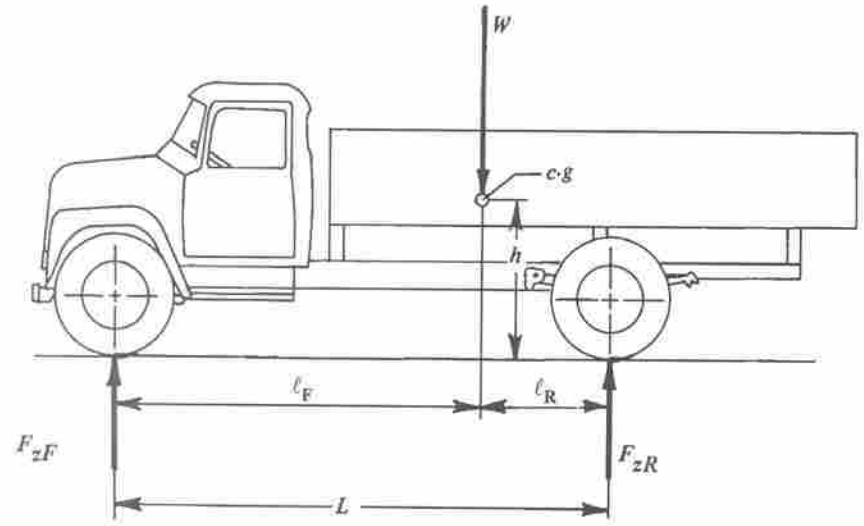

Figure 4.3 Basic loads and dimensions for sizing a brake system on a vehicle [42].

The dynamic axle loads are then

$$F_{zF,dyn} = \left(1 - \psi + \chi \frac{a}{g}\right) W \tag{4.2}$$

$$F_{zR,dyn} = \left(\psi - \chi \frac{a}{g}\right) W \tag{4.3}$$

These equations represent the normal force in a dynamic situation at the tire-road interface (per axle; divide by 2 to find per tire). Multiplying Equations 4.2 and 4.3 by the coefficient of friction at the tire-road interface, μ_{TR}, would then tell us how much dynamic braking force is available (e.g. large available braking force on dry pavement, small available braking force on ice). The dynamic axle torque is found by multiplying Equations 4.2 and 4.3 by the rolling radius of the tires (*rr*) and the deceleration in g's (*a/g*), as follows

$$T_{F,dyn} = rr\left(\frac{a}{g}\right)\left(1 - \psi + \chi \frac{a}{g}\right) W \tag{4.4}$$

$$T_{R,dyn} = rr\left(\frac{a}{g}\right)\left(\psi - \chi \frac{a}{g}\right) W \tag{4.5}$$

With the weight shift due to the height of the center of gravity and deceleration, the torque on the front axles, Equation 4.4, represents the "worst case" loading. Any mechanism that will replace the hydraulic brake system on the front end of an automobile must be able to produce the brake torque necessary to counteract these dynamic loads.

4.1.3 Electronic Wedge Brake (Siemens)

Siemens VDO Automotive AG is finalizing the development of an electromechanical brake called the Electronic Wedge Brake (EWB), slated to come to market in 2010 [2]. Its name is descriptive of how this brake works. A wedge fixed to the back of the brake pad is "wedged" in between the rotor and the caliper, where the motion of the rotor provides the additional self-reinforcement required to stop the vehicle. Although the current embodiment is much more detailed, Figure 4.4 shows the underlying principle that prescribes the brake's function.

One of the key drivers for a design solution like the EWB was the need to generate very large actuation forces in an electromechanical system. The power required to initiate and sustain these high forces pushes these actuators to the limit and is a significant drain on the vehicle's 12V system [44]. While there has been some speculation about an industry-wide move to 42V systems that would enable competitive EMB designs [45], this brake does not require any additional power.

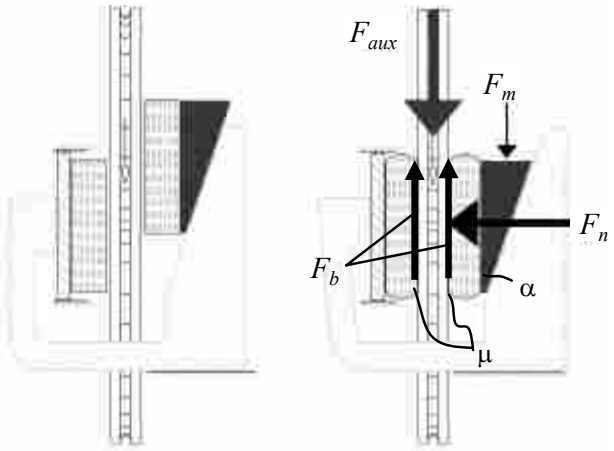

Figure 4.4 The wedge principle leveraged by Siemens' Electronic Wedge Brake (EWB) uses self-reinforcement from the rotor to achieve high normal forces, F_n, for a relatively small actuator input, F_m (figure adapted from [43]).

It has been shown that the EWB delivers many of the benefits anticipated from EMB applications [2, 46, 47], but the idea of self-reinforcement came with its own set of challenges. Chief among these is accurately controlling the actuation to deliver adequate braking force without locking the wheels, across a range of varying friction conditions (e.g. rusted rotors, glazed pads, etc.). It can be shown that the characteristic brake factor for a floating caliper actuated by the EWB is given by [43]

$$C^* = \frac{F_b}{F_m} = \frac{2\mu}{\tan\alpha - \mu} \tag{4.6}$$

where F_b is the pad braking force and F_m is the brake actuation force. A positive value of C^* ($tan\ \alpha > \mu$, or "large" wedge) means a pushing force is required, while a negative value of C^* ($tan\ \alpha < \mu$, or "small" wedge) requires a pulling force to prevent jamming. It follows that for $tan\ \alpha = \mu$, C^* is infinite and neither a pushing nor pulling force is required. Thus, the key is to provide controls that modulate the actuation force so that it operates around this point of neutral stability in the face of changing temperatures and friction conditions [44].

Another challenge presented by using the wedge principle is that self-reinforcement is direction dependent, so you either need two wedges per wheel or a "double-wedge" and actuation system that can reverse direction when you drive backward (or even just for stopping on a hill) [47]. This not-so-small detail is characteristic of revolutionary designs; while new ideas provide many improvements over previous designs, they often create their own unique set of problems.

4.2 Design Boundaries

In developing the MUSCLE brake, the decision was made early on to use established front corner architecture. In other words, this design had to be interchangeable with conventional brake calipers, and like the prior art, it had to compensate for wear. This section identifies the design boundary and develops the initial concept within those dimensions.

4.2.1 Physical Space

Hydraulic disc brakes have evolved into a complex system of pistons, seals, caliper housing, guide pins, skid plates, and pads, all mounted to the steering knuckle of the automobile. For a given size vehicle, this geometry is relatively fixed and any sort of disruptive, innovative technology likely needs to fit into this design space. Consequently, the MUSCLE Brake was designed to fit the steering knuckle of a compact car the size of a Ford Focus, a design space that is 120 mm (4.724 in.) from center to center on the mounting bolts and about 90 mm (~3.5 in.) inboard from this same mounting bolt/steering knuckle surface (Figure 4.5).

4.2.2 Adjustment Needed

Due to pad and rotor wear over their service life, brake calipers and actuation devices have to be able to extend their range of motion to compensate (approximately 0.70 in. from new pads, new rotor to old pads, old rotor on a compact car). In hydraulic brakes, the master cylinder and the extra brake fluid in the reservoir compensate for this pad and rotor wear, effectively adding the required volume of fluid to the closed part of the system as necessary.

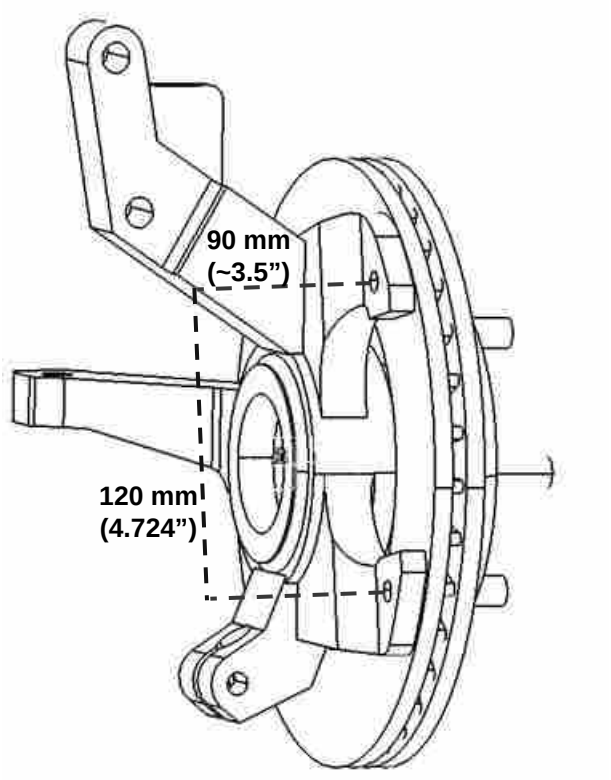

Figure 4.5 Physical space in which the MUSCLE Brake design must fit. For a compact car, this is 120 mm (4.724 in.) from center to center on the mounting bolts and about 90 mm (~3.5 in.) inboard.

Purely mechanical systems that exhibit self-adjustment have also been developed, and a review of the US Patent and Trademark Office website reveals no fewer than 13 patents for self-adjusting mechanical brakes in the last 30 years.

Related to the issue of self-adjustment but more specific to brakes is what some authors call "clearance management" [48] or "air gap management" [49]. In hydraulic brakes, the gap between the pads and rotor is maintained at some minimum value, usually about 0.003 in. per side or 0.006 in. total, which is close enough so that contact can be made as soon as the brakes are applied yet not so close so as to provide an undesirable drag force on the rotor. This is accomplished by the piston seal, which fits snugly around the piston cylinder circumference and deflects and retracts during brake actuation (see Figure 4.6). The hy-

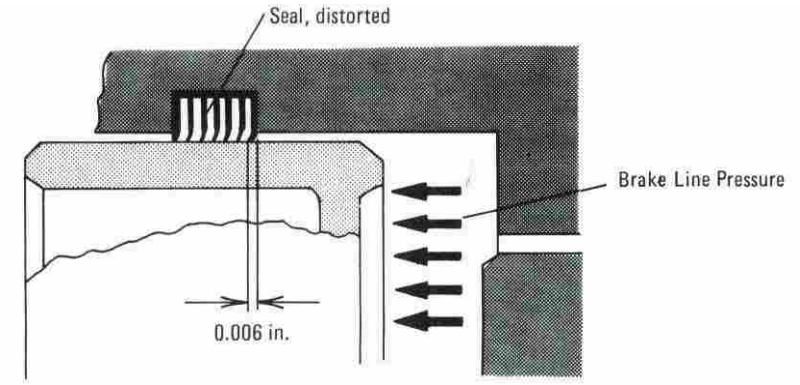

Figure 4.6 Disc brake clearance adjustment [42].

draulic pressure in the wheel cylinder pushes the piston toward the rotor until contact is made. This pressure easily exceeds the pressure required to deflect the seal. However, when the driver's foot comes off the pedal, piston retraction is controlled by the seal, which springs back to its undistorted position, approximately 0.003 in. from the contact position.

"In contrast…electromechanical brakes [of the type associated with the prior art] have to actively adjust the clearance" [48]. Many of the electromechanical brake concepts reviewed use active sensing for both self-adjustment and clearance management. This thesis will decouple these two functional requirements and build on the work of Brooks to suggest that a minimal air gap (stable "off" position) can be maintained through compliant links or joints, similar to the compliance used in hydraulic seals to achieve the minimal rollback distance.

4.3 Concept Development

The Brooks mechanisms (Figure 2.2, [6]) illustrate the self-centering, force-balanced principles that he developed and support discussion and explanation of objective characteristics. This was the point of departure for his thesis, and he recommended that future work be

done to develop these ideas into proof of concept hardware that could be physically mounted to the disc brake of a mountain bike or automobile. Then the principles could be proven out and desired attributes and performance confirmed. That was the motivation and foundation upon which the concepts presented here were based, not a clean sheet of paper, but an incremental step further down the road toward designing a mechanical disc brake caliper that emulates the behavior of a hydraulic disc brake caliper.

Figure 2.2a, b, and d represent unique 7-bar configurations of a self-centering, force-balanced grasping mechanism. Each can be decomposed and evaluated as the "stacked" or "nested" combination of two more familiar mechanisms. *Stacked* combinations share one common link; *nested* combinations share two or more links. Therefore, Figure 2.2a is a 5-bar nested inside a 4-bar parallel mechanism, Figure 2.2b is a slider-crank stacked on a 4-bar parallel mechanism, and Figure 2.2d is a 4-bar parallel mechanism stacked on another 4-bar parallel mechanism. (Note that a slider-crank mechanism with linear actuation at the joint between the crank and the coupler is more commonly called a toggle mechanism.) Decomposition reduces the larger, complex mechanism into manageable chunks with known kinematic behavior and off-the-shelf analysis. Further, type synthesis has already been conducted for these common configurations, simplifying the task of enumerating all the non-isomorphic configurations of each. Thus, different combinations of compliant and kinematic joints can be implemented according to the design requirements. Ultimately, the mechanisms in Figure 2.2b and d were pursued further but modified so that all mounting points to ground were inboard of the rotor. A concept "drawing" of both is shown in Figure 4.7.

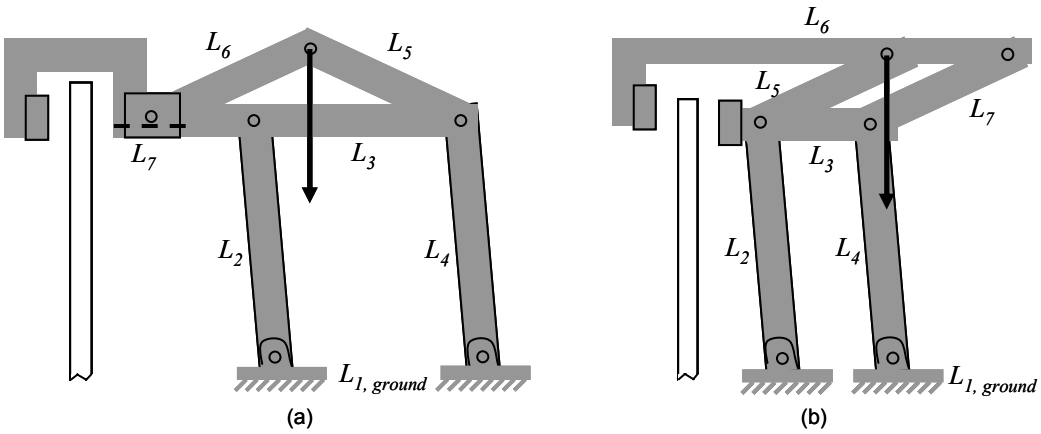

Figure 4.7 Two concepts developed as second iterations of the Brooks mechanisms in Figure 2.2b and d.

One of the enablers for the Electronic Wedge Brake being developed by Siemens is the large brake torque generated from relatively little actuation energy. The toggle linkages in Figure 4.7 provide similar gains, albeit not self-reinforcing. However, the next challenge of designing planar mechanisms is adapting them in a three-dimensional application. Looking at either mechanism in Figure 4.7, it became apparent that developing the third dimension would require at least two planar mechanisms working in parallel to sustain the large forces required to stop an automobile. After reviewing other devices that employ multiple toggle linkages, such as the stone crusher shown in Figure 4.8, it was determined that the

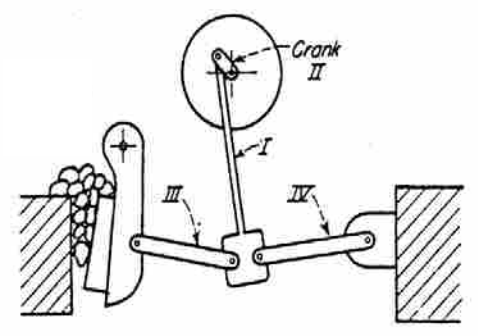

Figure 4.8 Multiple toggles are used in stone crushers like this one to achieve high mechanical advantage [21].

slider-crank chunk of the mechanism in Figure 4.7a (L_5 and L_6) could be rotated about L_3 90º onto its side such that two identical Figure 4.7a type mechanisms thus rotated would oppose each other, mirrored across a line of symmetry down the middle and actuated by a third toggle, as shown in the concept sketch in Figure 4.9.

With multiple toggles and large output forces over small displacements, the mechanism would be sensitive to friction. A review of the different kinematic and compliant joints

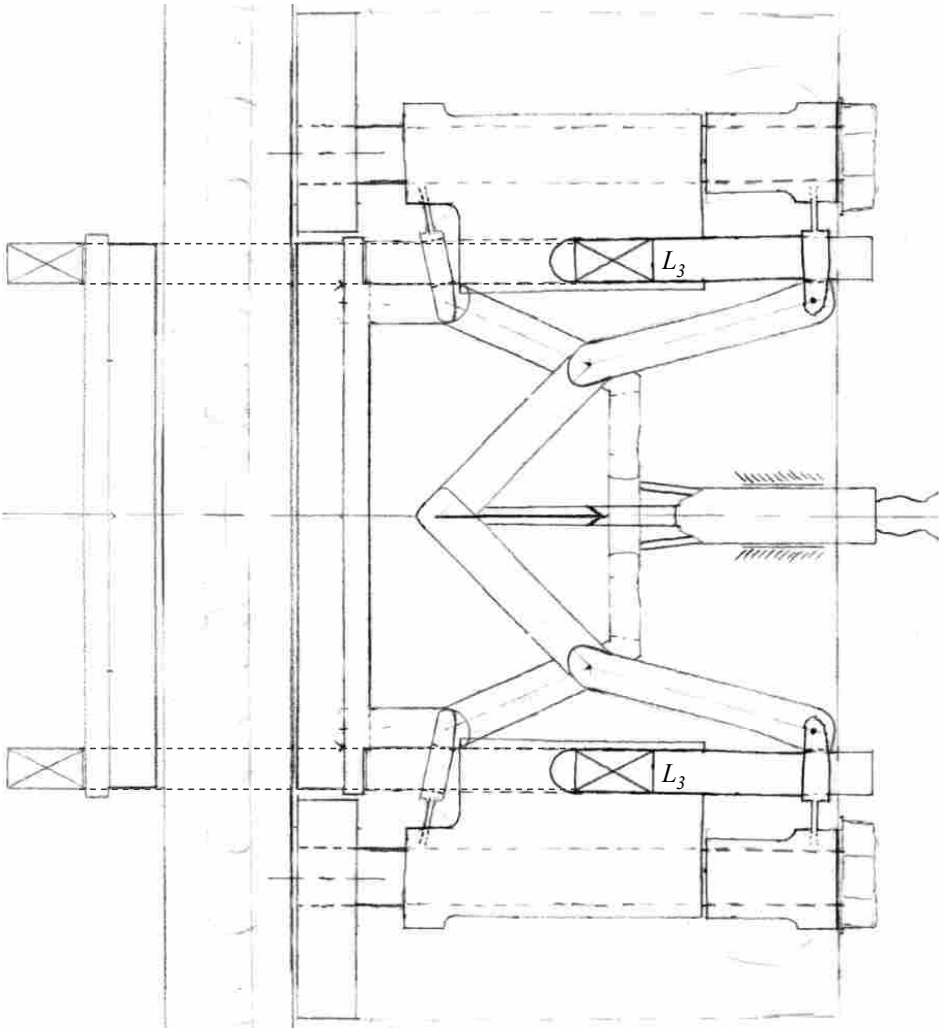

Figure 4.9 Early concept sketch showing the multi-toggle portion of the MUSCLE brake along with initial ideas for what was the 4-bar portion of Figure 4.7a. (Note that the two caliper arms, L_3, come out of the page, up and over the rotor at the cross sections marked with an 'X'.)

led to the selection of the elliptical rolling contact joint because of the many benefits it provides for mechanisms with similar design requirements (large compressive forces over small rotations; small output displacements; compliant stability in "off" position; etc.). Due to the difficulty of incorporating thin compliant flexures (both manufacture and assembly), connecting links were used as stabilizing constraints.

The toggle portion of the MUSCLE brake is shown in Figure 4.10, with the actuator toggles in the middle (white) and the caliper toggles on top and bottom (gray). In section 4.4, the forward kinematics of the toggles are developed. The 4-bar portion of the modified Brooks concept of Figure 4.7a will be discussed later in the chapter.

4.4 Forward Kinematics

The actuator and caliper toggles in Figure 4.10 can be moved to the fully actuated position—collinear actuator links, collinear caliper links—to identify the admissible link

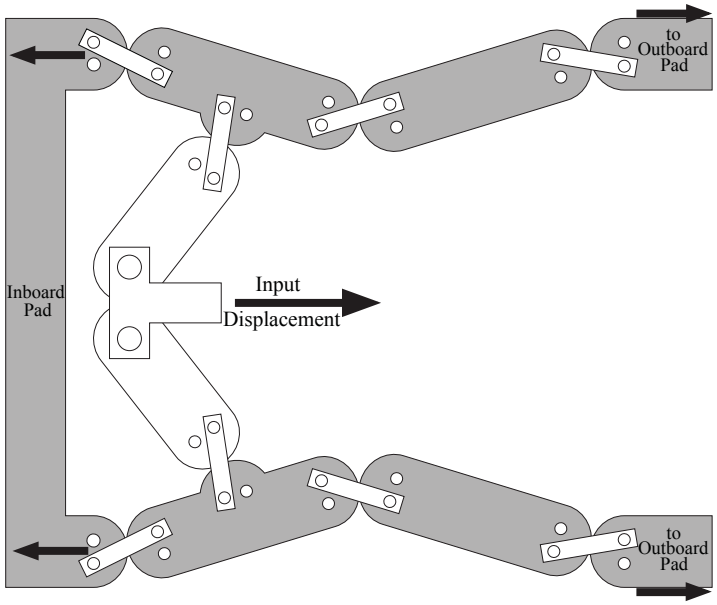

Figure 4.10 Concept drawing of the multi-toggle portion of the MUSCLE Brake with elliptical rolling contact joints ($\varepsilon = 0.333$) and connecting links as shown.

lengths based on the defined physical space from section 4.2 (i.e. the mechanism needs to fit between the mounting bolts when actuated). The total length of an elliptical rolling contact link is the perpendicular distance between the major axes plus the length of the minor axis. Since the latter is a function of the elliptical eccentricity (for a given link size, *a*), it becomes necessary to determine what eccentricity will provide the desired output stroke, not ignoring the fact that eccentricity will also affect Hertz stresses, elastic deflections, connecting link stresses, curvature ratio, and mechanical advantage.

The kinematics of an elliptical rolling link mechanism are relatively complex; however, with defined link lengths (both traditional links and connecting links), the connecting link angles can be used along with the link angles to determine the position of a mechanism throughout its range of motion. In the sections that follow, vector loops through the caliper toggles and actuator toggles are created to calculate output stroke for a given input. Factors contributing to required output stroke are also discussed.

4.4.1 Caliper Toggles

A vector loop through the caliper toggles defines the output stroke of the brake mechanism. Figure 4.11 shows what this loop might look like. With all link lengths and angles defined, one can solve for *x* (see Equation 4.7) at any position and compare that to the value of *x* at the final position to find the output stroke.

$$x = \lambda_3 \cos(\theta_{23} - 90) + L_3 \cos\theta_{3_{abs}} + \lambda_4 \cos(\theta_{3_{abs}} + 90 - \theta_{34}) + L_4 \cos\theta_{4_{abs}} + \lambda_5 \cos(\theta_{4_{abs}} - 90 + \theta_{45}) \tag{4.7}$$

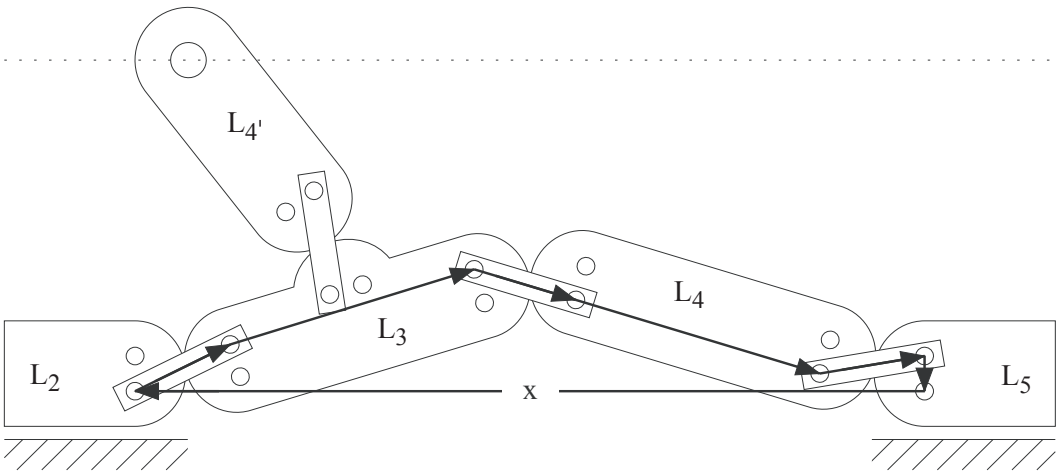

Figure 4.11 Vector loop through caliper toggles.

Solving for *x* at various initial positions shows us the effect of the initial caliper toggle position on the overall output stroke. The design engineer can then verify that the output stroke achieved by starting at some initial position is acceptable for the given application; otherwise, he can alter the angular range of motion for the links in the mechanism or change the size of the links (i.e. link lengths and elliptical eccentricities) to achieve the desired output stroke.

Figure 4.12 shows what the output stroke would be for the brake mechanism if we varied the elliptical eccentricity of the rolling contact joints and the initial angle of the caliper toggles, θ_3. As expected, the output stroke decreases as the initial angle of the toggles decreases. The effect of varying the elliptical eccentricity is more enlightening; there is little difference in output stroke when comparing elliptical eccentricities below 0.5, but a marked difference as ε approaches 1. In fact, for certain initial angles, the output stroke is actually negative! If you think of the bi-fold closet doors at home (or even a stack of wood at the lumber yard), this makes sense. These boards have an eccentricity of 1 (i.e. they are com-

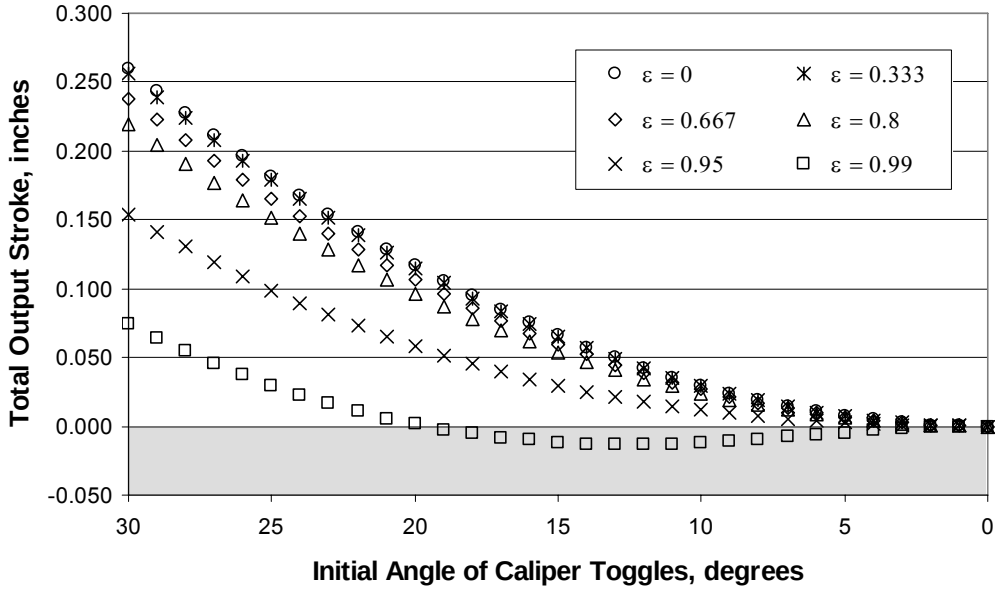

Figure 4.12 Effect of initial caliper toggle angle θ_3 and elliptical eccentricity ε on total available output stroke.

pletely flat ellipses or "rectangles") and toggle into a stable closed position only after brushing through the contact of the skewed boards.

4.4.2 Actuator Toggle

Now that we know the position of the links in the caliper toggles through each incremental degree of angular motion, we can use the position of L_2 and L_3, together with the links of the actuator toggle, to create a new vector loop. This loop will help us calculate the incremental actuator input stroke per degree of caliper toggle angular motion.

The vector loop for the actuator toggle is shown in Figure 4.13. Given the symmetry of the mechanism through its range of motion, *y* is a fixed value—1.177 in., in this case—defined by the physical design space identified previously. Unlike the caliper toggle vector loop where we solved for a single unknown, here there are two unknowns: *x* and $\theta_{4'}$. Remember that the equations for the connecting link angles assume the value of the included

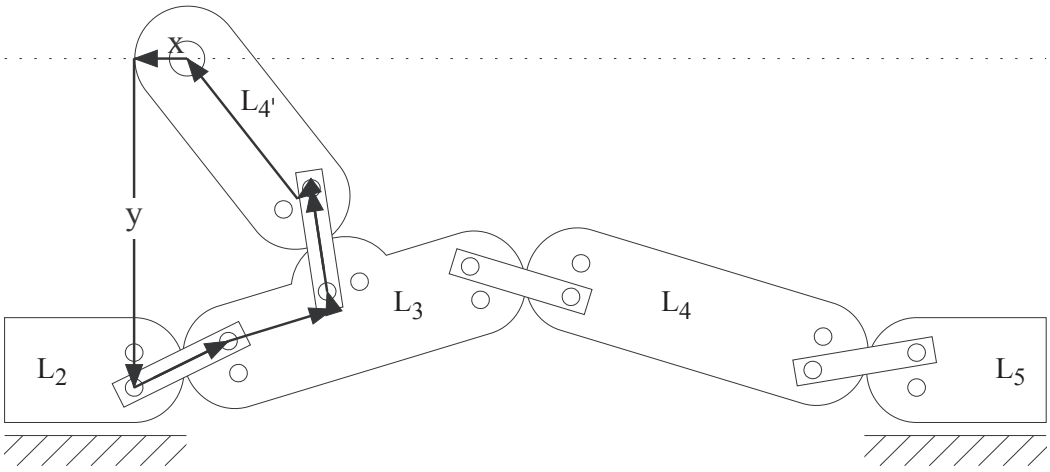

Figure 4.13 Vector loop through actuator toggle.

angle between the links in question is known; however, since we don't know the value of $\theta_{4'}$ in this case, we don't know the magnitudes of the connecting link angles.

Instead of using the equations derived in Chapter 3 to solve for the connecting link angles directly, these equations will have to be plugged into the y-direction vector loop summation. First, we'll use the y-direction equation (Equation 4.8) and the connecting link angle relationships (Equations 4.9 and 4.10) to solve for the unknown angles, and then we'll use the x-direction equation (Equation 4.11) to calculate the magnitude of *x*. Remember that *a*, *b*, and *c* in these equations define the shape of the ellipse used to generate the elliptical rolling contact surfaces. Resolving the vector loop summation in the y-direction, we get

$$\begin{aligned}&\lambda_3 \sin(\theta_{23} - 90) + (0.625 - b - c)\sin\theta_{3_{abs}} + (2a - 0.0625 - a - c)\sin(\theta_3 + 90) + \\ &\lambda_{4'} \sin(\theta_3 + 180 - \theta_{34'}) + c\sin(\theta_3 + \theta_{4'} + 180) + \\ &[1.177 - 2b - 2c - (2a - 0.0625 - a - c)]\sin(\theta_3 + \theta_{4'} + 90) = 1.177\end{aligned} \tag{4.8}$$

Equation 4.8 has two unknowns, $\theta_{4'}$ and $\theta_{34'}$, so we need to find one in terms of the other. With the orientation shown in Figure 4.13, we change the sign on Equation 3.8 and get

$$\theta_{ij} = \theta_{ji} - \theta_j$$

or

$$\theta_j = \theta_{ji} - \theta_{ij} \tag{4.9}$$

We can apply Equation 3.7 (just invert the subscripts on the angles) to find θ_{ji} in terms of θ_{ij} and then substitute this into Equation 4.9 to obtain this expression for θ_j in terms of θ_{ij}.

$$\theta_j = \cos^{-1}\left[\frac{\left(-1-\varepsilon^2\right)\cos\theta_{ij} - 2\varepsilon}{2\varepsilon\cos\theta_{ij} + 1 + \varepsilon^2}\right] - \theta_{ij} \tag{4.10}$$

Now we can substitute Equation 4.10 for $\theta_{4'}$ in Equation 4.8, solve for the only unknown ($\theta_{34'}$), and plug this into the x-direction vector summation to find *x* (Equation 4.11).

$$\begin{aligned}&\lambda_3\cos(\theta_{23} - 90) + \left(0.625 - b - c\right)\cos\theta_{3_{abs}} + (2a - 0.0625 - a - c)\cos\left(\theta_3 + 90\right) + \\ &\lambda_{4'}\cos\left(\theta_3 + 180 - \theta_{34'}\right) + c\cos\left(\theta_3 + \theta_{4'} + 180\right) + \\ &\left[1.177 - 2b - 2c - \left(2a - 0.0625 - a - c\right)\right]\cos\left(\theta_3 + \theta_{4'} + 90\right) = x\end{aligned} \tag{4.11}$$

Note from Figure 4.13 that two things change the magnitude of the *x* vector: the incremental displacement of the actuator toggle linkage, which is what we're trying to find (the "input stroke"), and (half) the output stroke. In other words, we can't just look at the change in *x* per degree, but need to account for the lengthening of the caliper toggles as well.

4.4.3 Required Output Stroke

The required output stroke is the sum of the air gap between pads and rotor, any backlash in the self-adjustment mechanism, material/link deflections, and the incremental wear-induced excess clearance. While the total air gap of 0.006 in. was already given in section 4.2.2, the other elements that contribute to output stroke have yet to be discussed. In section 4.5, the mechanical advantage is calculated, including analysis on how much force is actually needed. In section 4.6, the selected self-adjustment method is presented and backlash and excess clearance are discussed. Finally, in section 4.7, stress analysis is conducted to calculate the amount of elastic deflection through the force flow path, another contributor to the necessary output stroke.

4.5 Mechanical Advantage

The transmission ratio, or mechanical advantage, was reviewed in section 2.7. Application to the MUSCLE Brake with regard to how much force is necessary and how much mechanical advantage the toggle links can provide are discussed below.

4.5.1 How Much is Necessary?

A brake system can be sized as long as the basic brake variables are known, which are: location of center of gravity ψ and χ (defined in section 4.1.2), vehicle weight W, brake lining (pad) coefficient of friction μ_L, the rolling radius of the tire rr, the effective radius of the rotor r_{eff}, and the required peak performance (maximum deceleration, in g's). With a

characteristic brake factor of $2\mu_L$ for a disc brake [42], we set half the dynamic axle torque from Equation 4.4 equal to the torque generated by the applied force F_A, then solve for F_A

$$F_A(2\mu_L)r_{eff} = \frac{1}{2}rr\left(\frac{a}{g}\right)\left(1-\psi+\chi\frac{a}{g}\right)W$$

or

$$F_A = \frac{rr\left(\frac{a}{g}\right)\left(1-\psi+\chi\frac{a}{g}\right)W}{4\mu_L r_{eff}} \tag{4.12}$$

Equation 4.12 is fundamental to the design of the disc brake caliper. It represents the force that the mechanism needs to generate so that the brake meets required performance standards. It is the force used in most of the stress calculations. This force causes material deflections, which need to be accounted for in the output stroke. A force directed design should start with this equation and then develop the kinematics to efficiently achieve these force requirements.

Figure 4.14 provides the required application force F_A for various levels of deceleration. The results are based on a compact car with inputs shown where weight is the GVWR of the vehicle, distances are in feet, and ψ and χ are approximate based on other examples from the literature [42].

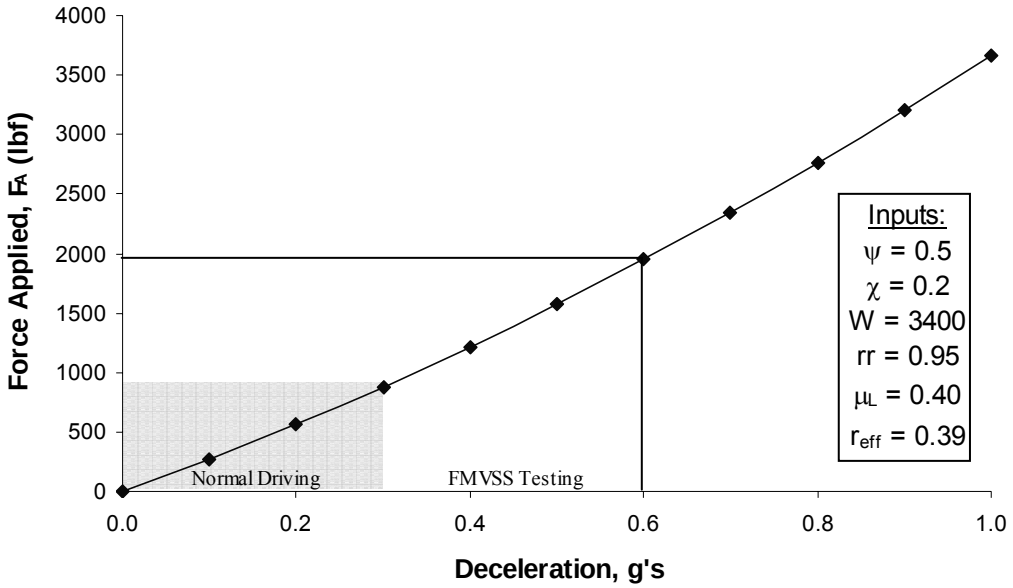

Figure 4.14 Application force required, F_A, normal to the rotor for various levels of deceleration (measured in g's) of a compact car with the given specifications.

4.5.2 Toggle Linkages

From Equation 2.27 and Figure 2.25, it can be shown that the mechanical advantage for a toggle linkage becomes, in theory, infinite as α approaches 90º (i.e. V_B approaches zero). Frictional forces reduce this ideal of "infinite" mechanical advantage, but forces are still relatively high at the toggle point.

With the input stroke and the output stroke both defined for each degree of caliper toggle rotation, we can now calculate the mechanical advantage for the brake mechanism throughout its range of motion. Using a numerical solver and spreadsheet macro, the vector loops were calculated for each degree of rotation for both the input stroke (actuator toggle) and the output stroke (caliper toggles). It can be shown that the mechanical advantage at any point in the stroke is $(dx/d\theta)_{input}$ divided by $(dx/d\theta)_{output}$, where the generalized coordinate

used here is the angle of the caliper toggles, θ_3, which is equal to 90º - α. The results are shown in Figure 4.15.

As shown, large mechanical advantages near the toggle point are typical of toggle linkages because the output stroke approaches zero. For the MUSCLE Brake design, the mechanical advantage is 1 at 20º, becomes significant at 10º, and increases exponentially at 5º. Total available output stroke and mechanical advantage as a function of eccentricity are plotted in Figure 4.16.

It's worth noting that whether circular rolling contacts are used or elliptical links with high eccentricity, adjacent links will produce exponentially increasing mechanical advantage as they approach the toggle position. Figure 4.16 simply illustrates the added effect of eccentricity on displacement and mechanical advantage. For many designs, the primary advantage of eccentricity will be the larger radius for reduced Hertzian and stabilization member stresses, and the main compromise will be output displacement.

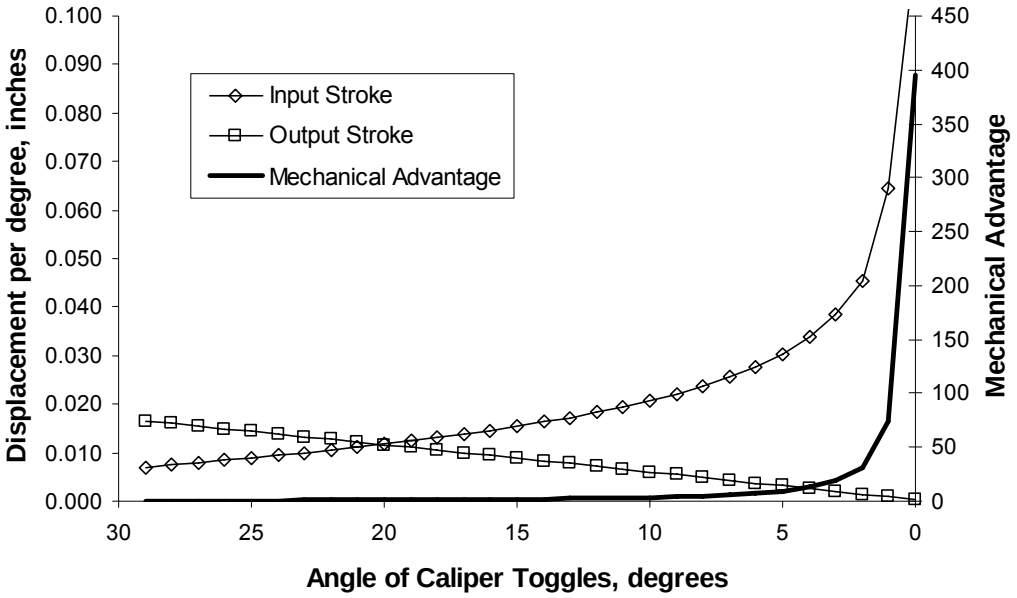

Figure 4.15 Mechanical advantage for MUSCLE Brake ($\varepsilon = 0.333$).

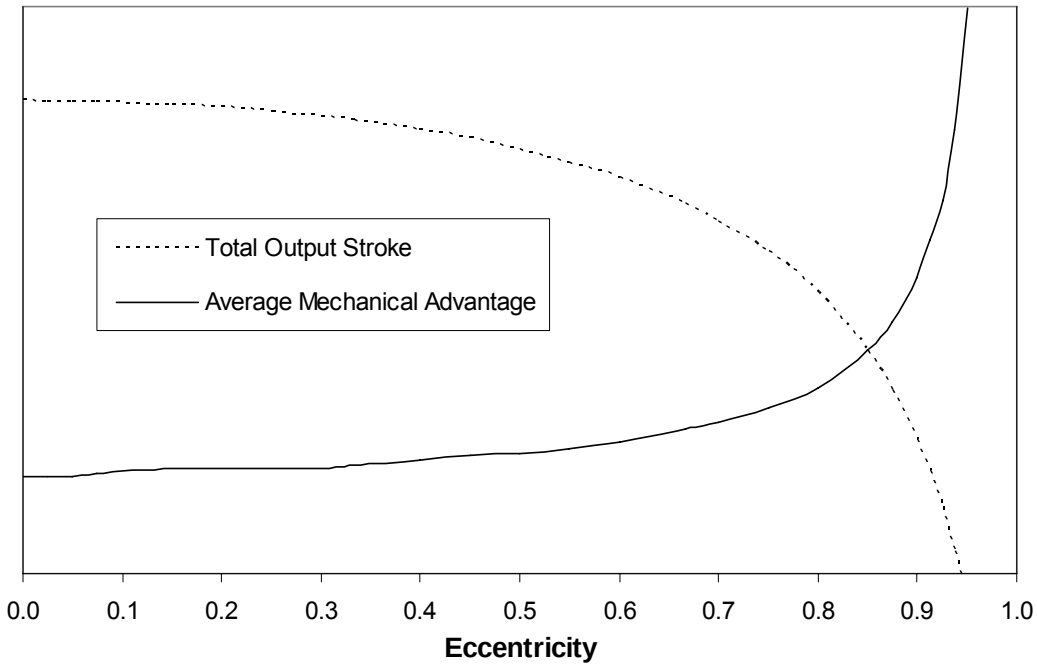

Figure 4.16 Relationship between total output stroke and average mechanical advantage as a function of eccentricity.

If one of the goals of the MUSCLE Brake mechanism was to generate sufficient force to stop a vehicle, toggle linkages can provide the necessary force, provided the linkage is properly adjusted and force transmission becomes large as contact is made with the rotor. Self-adjustment is the topic of the next section.

4.6 Self-adjustment Methods

In Chapter 2, self-adjustment strategies were discussed and several examples were provided of self-adjustment in grasping devices (pliers and clamps). Hydraulic seals between the wheel cylinder and the brake piston, along with the reserve in the master cylinder reservoir, have been cited as the source of self-adjustment in conventional hydraulic disc brakes. Perhaps the most relevant example of self-adjustment comes from parking brakes.

Figure 4.17 provides an example of how some parking brakes achieve self-adjustment. Essentially, links B and C have mating cammed surfaces that are joined such

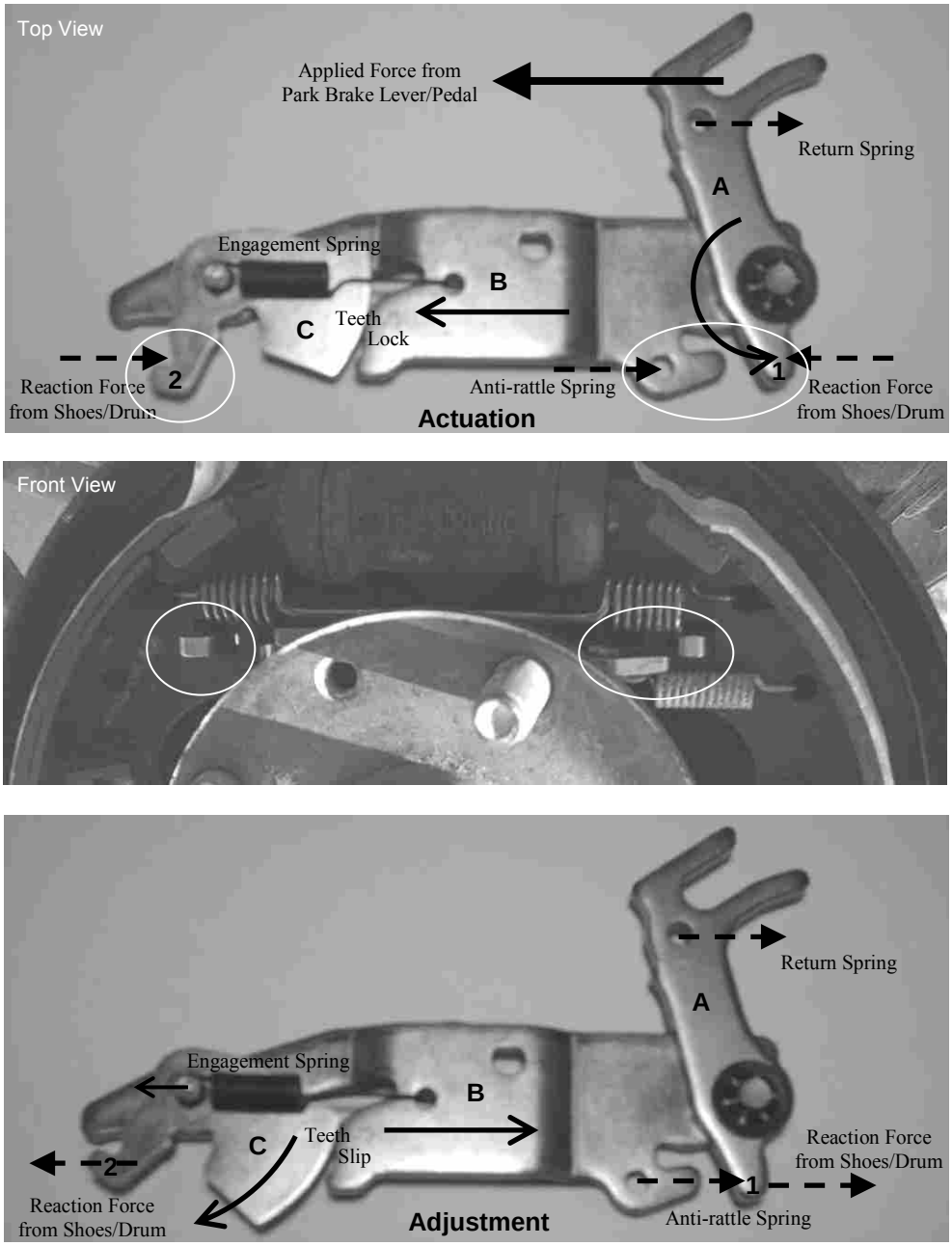

Figure 4.17 Parking brake self-adjustment mechanism for a 1996 Ford Escort (Ford Service Part #: F2CZ-2A637-A). The "Front View" shows the mechanism mounted inside the drum—between the shoes—where points 1, 2, and the anti-rattle spring attachment point are visible.

that they lock in compression (when the park brake is applied) and slip or adjust in tension (when the hydraulic brake is applied).

When the parking brake lever or pedal is applied, link A rotates counterclockwise, creating a highly leveraged force against the shoe/drum reaction at 1. The reaction at 1 and applied force shift the whole mechanism to the left, forcing link B into locking contact with link C. Thus, the applied force effectively spreads the shoes apart at 1 and 2, which is resisted by reactions from the shoe and drum at both points. Further actuation simply increases the brake force between the shoes and the drum.

Adjustment occurs when the hydraulic brake is applied. Near the top of the drum, the shoes mate up with the hydraulic wheel cylinder; thus they can be actuated with either the hydraulic brakes or with the park brake or "emergency" brake. When the driver puts his foot on the brake pedal, pressure builds up in the wheel cylinders and the shoes are pushed apart until the linings contact the drum. This spreading of the shoes also applies tension to the park brake self-adjustment mechanism, pulling it apart at points 1 and 2. Where the mating cammed surfaces of B and C lock in compression, they slip (and C rotates clockwise) in tension. Consequently, daily driving and normal braking regularly adjusts the park brake mechanism without the need for manual adjustment, all based on the principle of locking in compression and slipping in tension.

In the sections that follow, a self-adjustment method is selected, applied to the MUSCLE Brake, and analyzed for proper functionality.

4.6.1 Continuous Adjustment: Self-locking Plates

For automotive brakes, the preferred configuration would have the same input stroke each and every time (drivers and actuators prefer consistency) and incremental self-adjustment (rotors and pads wear very slowly). Although the self-adjustment used in the Craftsman AutoLock Pliers arguably represents the most reliable solution, it requires an input stroke that covers the full range of possible output strokes. In order to achieve large mechanical advantages on the MUSCLE Brake, the input stroke would have to cover a multiple of the range of the output stroke, which, with wear over the service life, is approximately 0.70 in. for a compact car. Thus, the required input stroke would be very large for this design. The Craftsman AutoLock Pliers use a 4-bar design with a triangle-shaped output link to increase the output stroke (width between the jaws), but the input stroke is a 90º rotation of handle/coupler and requires that the jaw surfaces pivot through 35º of relative rotation. Such large input strokes and non-parallel clamping surfaces would not work for brake caliper mechanisms.

Finally, continuous adjustment is preferred over discrete adjustment for consistent performance and ease of manufacture (teeth tend to be harder to make than smooth surfaces). With discrete adjustment, there is some small tradeoff made when the desired output stroke is halfway between two discrete choices. This compromise is exacerbated for small, precision displacements. Also, smooth surfaces are not only easier to manufacture but exhibit predictable, consistent performance over time and are less prone to wear.

Of the self-adjustment methods analyzed, the one that satisfies the preferences outlined is the bar clamp self-locking plates. This solution provides continuous, incremental self-adjustment without requiring full-range adjustment with each actuation.

Figure 4.18 illustrates how the self-locking plates work together on the MUSCLE Brake to provide self-adjustment, though the principles are similar to those found in the Quick-Action Bar Clamp. In the actuation stroke, the geometry of the inboard toggles (on the right) causes them to lock, while the opposite geometry in the forward toggles (on the left) allows them to slide. Thus, the plates that lock against the caliper arms on the right move the connected outboard brake pad to the right until contact is made with the rotor, and the inner brake pad slides to the left and applies force on the inboard side. In the return stroke, the geometry creates just the opposite effect: upon retraction the forward toggles near

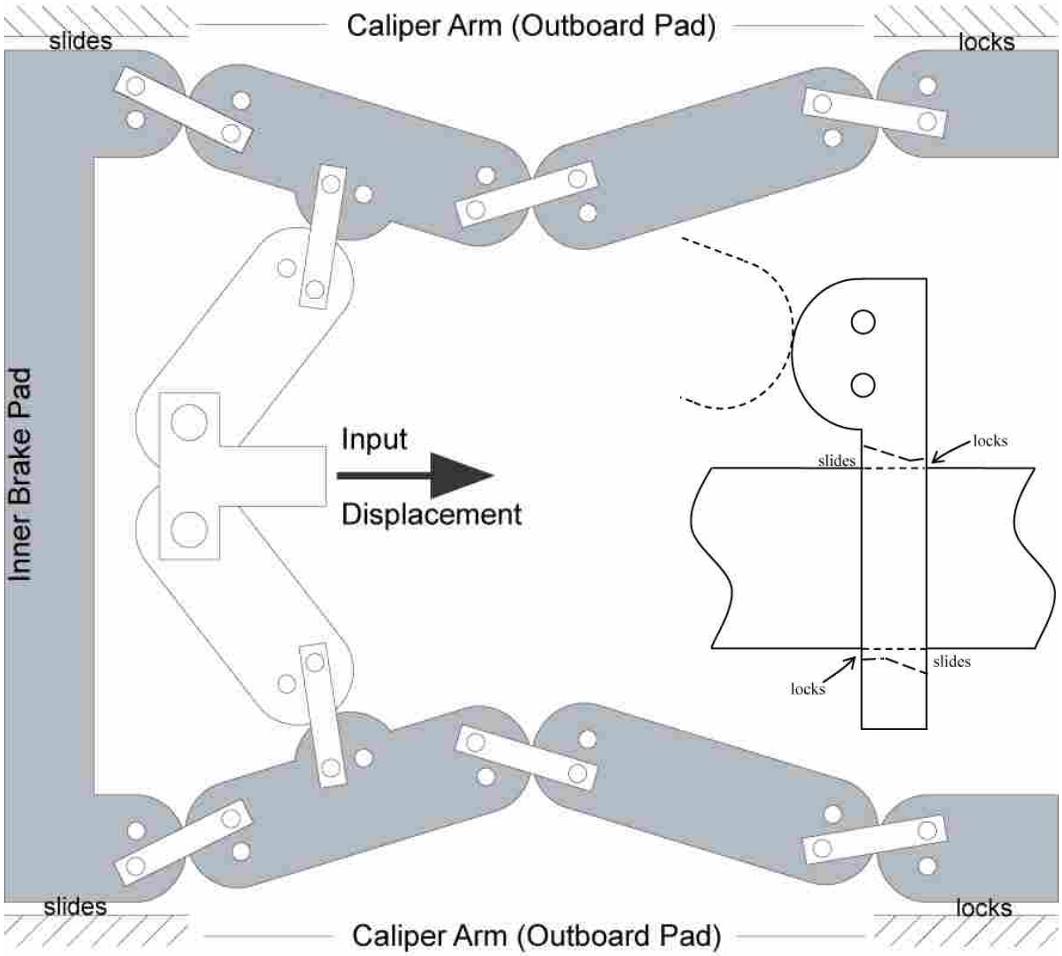

Figure 4.18 The MUSCLE Brake employs four binding plates (two per caliper toggle) to create incremental self-adjustment as the pads and rotor wear.

the inner pad (on the left) lock and the inboard toggles (on the right) slide. As a result, the caliper toggles walk forward in incrementally small steps as the pads and rotor wear.

Some of the challenges presented by this design are self-locking (binding) reliability and the required actuator movement, which will be addressed in the sections that follow.

4.6.2 Self-locking Reliability

Figure 4.19 shows the self-locking plates developed for the MUSCLE Brake caliper toggle output links in greater detail. Self-locking is ensured using the governing equation from Chapter 2 for tip before slip, Equation 2.6. The chosen distance ℓ between the elliptical link and the bar the MUSCLE Brake self-adjusting link slides on as shown in Figure 4.19 can be increased as necessary to satisfy the inequality below. For $d = \ell + a + x$ where x is defined in Equation 3.14, we have

$$d = \ell + a(1+\varepsilon) + r_{ji}\cos\theta_{ji} \geq \left(\frac{H}{2} + \mu c_{bar}\right)\tan\left(\frac{\theta_j}{2}\right) + \frac{H}{2\mu} - c_{bar} \tag{4.13}$$

where c_{bar} is used to distinguish from the parameter c used to define elliptical eccentricity. For the simplified case where $\theta_j = 0$, we have

$$d = \ell + a \geq \frac{H}{2\mu} - c_{bar} \tag{4.14}$$

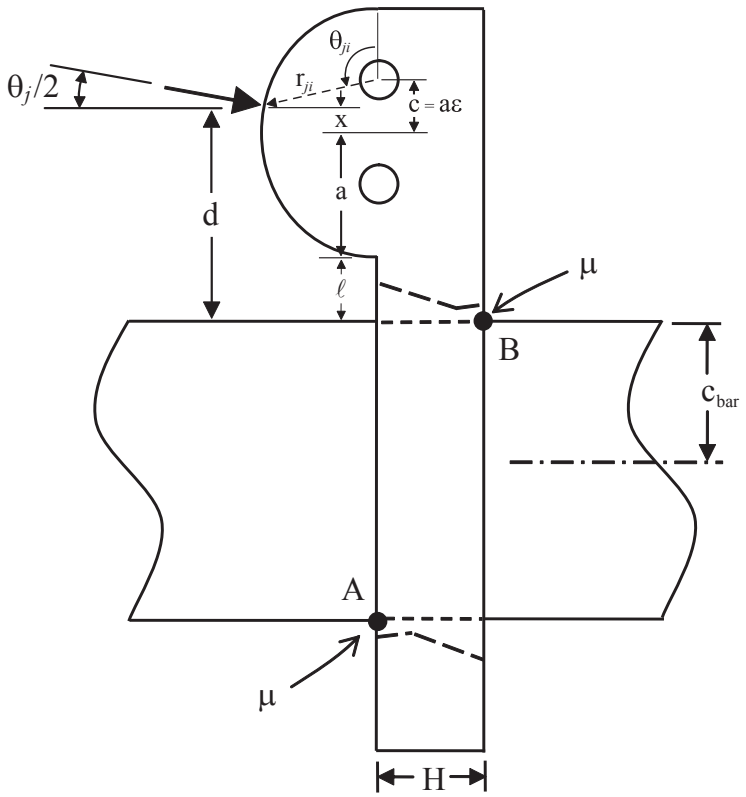

Figure 4.19 Self-locking plate design for MUSCLE Brake self-adjustment.

For the MUSCLE Brake design, $a = 0.188$ in., $\varepsilon = 0.333$, $\ell = 0.125$ in., $H = 0.125$ in., and $c_{bar} = 0.188$ in. A conservative coefficient of friction μ between 0.1 and 0.2 was assumed for "greasy" hard steel on hard steel [50], and θ_j ranges from 0 to 30º. Equation 4.14 can be viewed as the y-intercept for the graph of d as a function of θ_j where the left-hand side represents the y-intercept for d_{actual} and the right-hand side represents the y-intercept for $d_{required}$. As discussed in Chapter 2, the y-intercept for $d_{required}$ decreases as H decreases, μ increases, and/or c_{bar} increases. For the small range of caliper link rotation in the MUSCLE Brake design, the increase in required lever arm length d from the *tan* θ_j term in Equation 4.13 is insignificant (i.e. the required d is flat over the range of input angles). Moreover, the left-hand side of the inequality in Equation 4.13 (d_{actual}) increases faster than the right-hand side ($d_{required}$), especially for elliptical surfaces with large eccentricities. Consequently,

Equation 4.14 can be used for sizing d. Where the safety factor, SF, can be defined as $d_{actual}/d_{required}$, we have $SF_{\mu=0.1} = 0.71$ or $SF_{\mu=0.2} = 2.51$. As expected, binding is quite sensitive to the coefficient of friction. A second iteration on the MUSCLE Brake design should consider lengthening ℓ or increasing c_{bar}. Unfortunately, both of these solutions decrease the usable space between the brake caliper mounting bolts on the steering knuckle, and so tradeoffs have to be made.

For completeness, it's worth explaining the slight increase in required length d with increasing input angle θ_j. Binding of the plates on the bar is a strong function of the normal force at contact points A and B, and the direction of the applied force contributes to these large normal forces. As θ_j increases, the (non-perpendicular) direction of the contact on the lever arm reduces the moment on the bar and thus the normal force at points A and B (see Equation 4.15, derived from Equation 2.4). In short, binding of the plates is more likely when the normal forces at A and B are a result of the moment generated from a perpendicular force as opposed to directly pushing the link downward into the bar.

$$N_B = \frac{F_c\left(\cos\frac{\theta_j}{2} + \mu\sin\frac{\theta_j}{2}\right)}{2\mu} \tag{4.15}$$

Self-adjustment for the Quick-Action Bar Clamp is enabled by self-locking plates that are on the verge of locking. Compliant members—helical springs in this case—maintain this near-locked position. Being on the verge of lock has two important benefits: any small perturbation either way will cause the plate to lock or slide, and, perhaps more importantly, backlash in the actuation stroke is negligible. With small, precision outputs, it was critical

that the self-locking plates on the MUSCLE Brake be on the verge of locking. Several concept ideas were entertained, including the small length flexural pivots shown in the sketch in Figure 4.9. Nevertheless, for simplicity in developing a prototype, a tension spring was attached to the bottom of each self-locking plate. Whichever method is used, this is a critical aspect when designing self-locking plates with minimal backlash; otherwise, a significant portion of the output stroke will be used to overcome all of the gaps, in which case the output link may not move at all.

It should also be noted that increased angles θ_j create tangential forces that generate tensile forces in the connecting link (or bands). These tensile forces apply a moment opposite the desired direction of rotation for binding, thus reducing the propensity to self-lock. Similarly, stiffness in the joint from friction at the foci or the compliant flexures will also tend to rotate the self-adjusting link the wrong way. In both cases, a compliant member or spring of sufficient stiffness that maintains the plates on the verge of self-lock can counter these undesirable moments.

Bar clamps associated with the prior art are designed so that the locking plate/bar interface allows stress concentrations that create plastic deformation between the plate and the bar. At the micro-level, these stress concentrations cause the plates to plough into the bar and thus avoid sliding. For an automobile with an extended service life, this is an unacceptable solution. The goal was to design the interface to minimize wear by avoiding plastic deformation, relying on the frictional forces at the contacts and plate self-adjusting link geometry to ensure self-locking.

4.6.3 Actuator Mobility

The combination of incremental adjustment and the same input or actuation stroke each and every time requires that the actuator move with the mechanism. For the Quick-Action Bar Clamp in Figure 2.10, this means that actuation handles 124 and 118 must move along the bar together with the self-locking plate and the rest of the right-side jaw.

If we decompose the MUSCLE Brake into two subsystems as discussed previously, we have the multi-toggle ("slider crank") portion that moves towards the rotor as the pads and rotor wear. Likewise, the caliper arms that go up and over the rotor and are linked to the outside pad translate inboard as the pads and rotor wear. This relative movement, or self-adjustment, between the multi-toggle portion and the caliper arms requires that the actuator move along with the toggle linkages, so that the input stroke can be consistent. One way to accomplish this is to attach the actuator to the two joints, one on either side, where the caliper toggles come together, as shown in Figure 4.9.

4.7 Stress Analysis

The prototype that was built did not follow a force directed design approach, but took a more movement directed approach, as many of the principles discussed in this thesis were not well understood by the author at the time the first prototype was manufactured. More specifically, Hertz contact stresses were not considered, nor were the required apply forces accurately quantified. Consequently, the Hertzian stresses produced by the large application forces required in Figure 4.14 are excessive for the first MUSCLE Brake prototype. The purpose of this section remains to identify the stresses and associated deflections in the

mechanism and discuss methods to reduce stress concentrations. For this discussion, the force required for average everyday driving—566 lbs for 0.2 g deceleration—will be used. Later, design changes will be suggested that improve the MUSCLE Brake's function throughout the required range of forces and deceleration. A second prototype would build on lessons learned from this work and optimize the MUSCLE Brake design.

One of the motivations for using elliptical rolling contact joints in toggle link designs that oscillate back and forth is that they provide light compression, quick rotation across areas of large curvature (e.g. to close the gap between pad and rotor) and heavy compression, slow rotation over areas of small curvature (e.g. for large apply forces at the pad-rotor contact). Note from Figure 4.12 and Figure 4.15 that the MUSCLE Brake does not generate significant forces until the last 10º of caliper toggle rotation or 0.030 in. of output stroke, and forces only increase exponentially over the final 5º or 0.007 in. of travel. This is an important point to remember as stresses are analyzed, that is, understanding that large forces are only present near the toggle point.

4.7.1 Elliptical Rolling Contact Stresses

Applying Equation 2.22 to the MUSCLE Brake design, we can find the Hertz stress at the contact. The results, along with intermediate calculations derived from the inputs, are provided in Table 4.1 (verified in ANSYS to be accurate within 6%). Note that for twin elliptical cylinders in rolling contact, Equations 2.22 through 2.24 become

$$p_0 = 0.564\sqrt{\frac{2F_n}{R_s L\Delta}} \tag{4.16}$$

$$\Delta = \frac{2-2\nu^2}{E} \tag{4.17}$$

$$2b = 2.26\sqrt{\frac{R_s F_n \Delta}{2L}} \tag{4.18}$$

In section 4.4.3, several contributors to the required output stroke were listed, including material/link deflections. Although stresses at the contact are excessive, deflections—as shown in Table 4.1—are minimal. The maximum deflection was calculated using the contact width from Equation 4.18 and the following equation for any point (x, y) on an ellipse

$$y = b\left(1-\frac{x^2}{a^2}\right)^{1/2} \tag{4.19}$$

Maximum loading occurs when $\theta_j = 0°$. Instead of using Equation 4.19 to find the *y* coordinate of the contact point, it can be used unconventionally to find the *y* coordinate of the edge

Table 4.1 Hertz contact stress and deflection inputs and results for the MUSCLE Brake.

Inputs		*Intermediate Calculations*		*Results*	
a	0.1875 inches	θ_{ij}	109.5 degrees	Hertz stress	280 ksi
b	0.1768 inches	r_{ij}	0.187 inches	contact width, 2b	0.007 inches
c	0.0624 inches	r'	0.177 inches	deflection/joint	0.00006 inches
ε	0.333	θ'	90.0 degrees		
θ_j	0 degrees	t	90.0 degrees		
F	566 lbf	κ	288.1 degrees/inch		
L	0.375 inches	R_s	0.199 inches		
ν	0.28	Δ	6.1E-08 psi^{-1}		
E	3.0E+07 psi	ψ_c	0.0 degrees		

of the contact patch. The half-width from Equation 2.24 (or 4.18, in this case) can be substituted for x in Equation 4.20. Thus, the deflection for a toggle joint in elliptical rolling contact is given in Equation 4.21, where a and b are properties of the ellipse, and x is the half-width of the contact patch from Equation 2.24 (see Figure 4.20).

$$\Delta y = 2b - 2b\left(1 - \frac{x^2}{a^2}\right)^{1/2} \tag{4.21}$$

As shown in Table 4.1, Hertz contact stresses are excessive, especially when you consider that the applied force is just enough to provide 0.2 g deceleration in everyday driving, far short of the forces required in aggressive driving or panic braking. One solution would be to increase the eccentricity of the elliptical surfaces, which increases the area of the contact patch. However, the design tradeoff for increased eccentricity is reduced output stroke. In order to provide the necessary performance at 0.8 g, we would need five times the

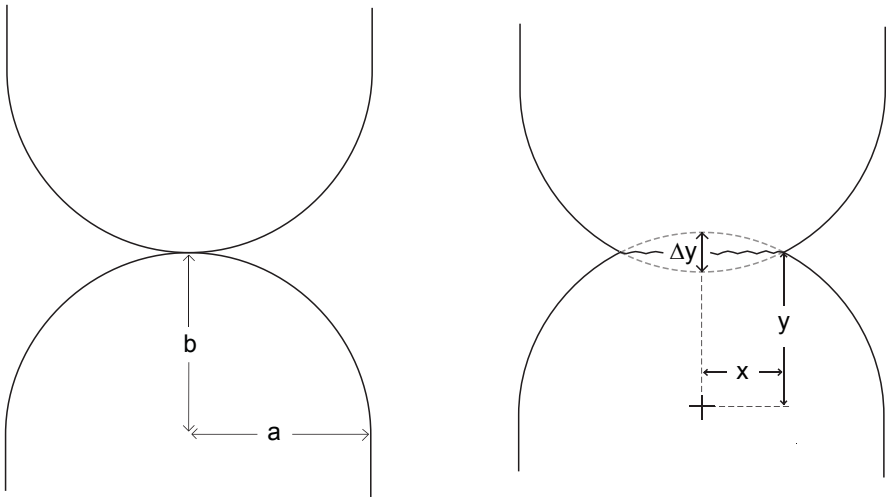

Figure 4.20 Hertz contact deflections Δy can be calculated using the half-width of the contact patch x and the equation of an ellipse.

force required for the 0.2 g stop (2766 lbf vs 566 lbf). The MUSCLE Brake design cannot produce this five-fold increase in force and still provide the output stroke necessary.

Another solution stems from the idea of using the principle of isolation to allow compliant mechanisms to bear high compressive loads. Recall that the large forces required are only available in the last few degrees of travel, and remember also that the toggle linkages have one-way, back-and-forth motion into toggle and out again (i.e. they never go past the toggle point $\theta_j = 0^\circ$). Consequently, half of the elliptically-shaped surface can be squared off to create a large contact surface at $\theta_j = 0^\circ$ (see Figure 4.21). This also ensures the toggle linkages don't lock by preventing them from moving beyond the toggle point.

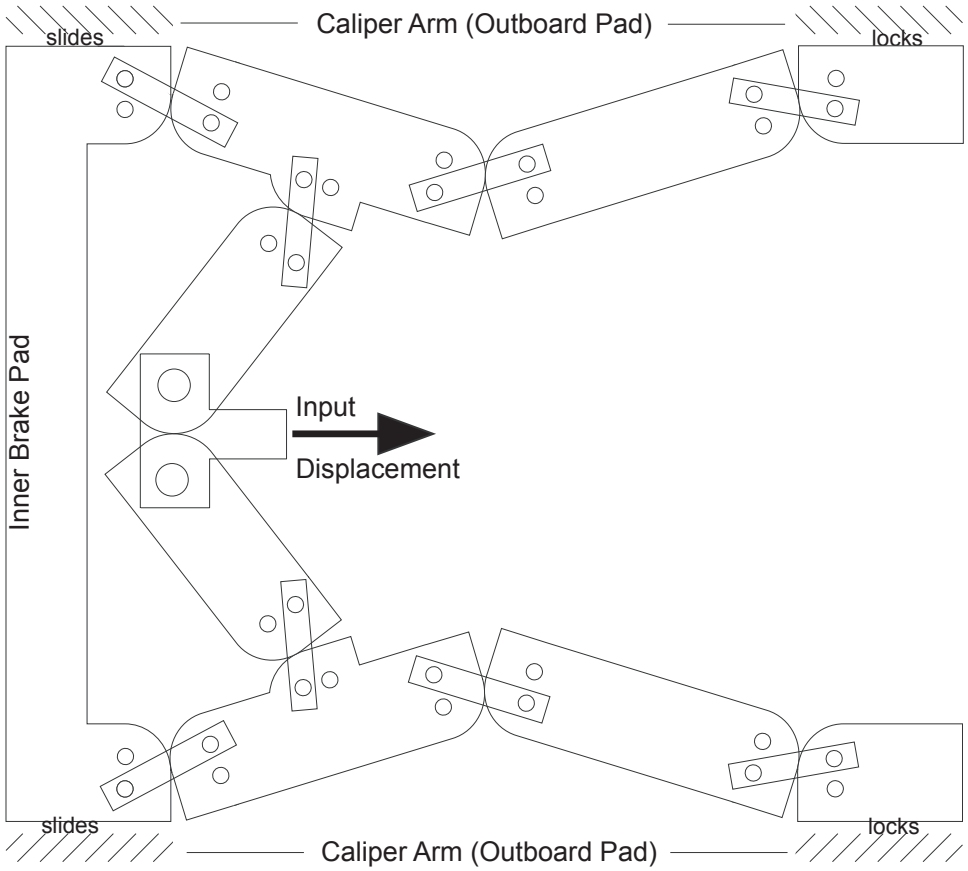

Figure 4.21 Squared-off links reduce stress in the toggle position and limit unintended locking from overtravel.

The stress in the connecting links (or flexures, if stabilization bands had been used) is maximum at the largest angle of rotation, which by design is $\theta_j = 30°$. The results of applying Equations 3.26 and 3.30 to the flexures and connecting links, respectively, are shown in Table 4.2.

Although the tensile stress is higher in the connecting links due to the *cos* γ term in the denominator of Equation 3.30, connecting links are not subject to bending or compression, so the combined stress is greater for flexures. However, the stresses in the flexures do not impede motion, whereas the tensile force in the connecting links magnifies the effect of friction at the foci. Remember that *cos* γ is equal to the elliptical eccentricity ε at $\theta_j = 0°$ and decreases as θ_j increases. Fortunately, for small rotations, *cos* γ decreases very little.

4.7.2 Self-locking Plates

The critical stresses in the self-locking plates are bending and contact stress at the interface between the bar and the plate. With reference to Figure 4.19, the equation for bend-

Table 4.2 Inputs and results for tensile stresses in connecting links (or combined stresses in stabilization bands, if used).

Inputs			*Intermediate Calculations*						*Results*		
a	0.1875	inches	θ_{ij}	123.8	degrees	ψ_s	5.7	degrees	Hertz stress	277	ksi
b	0.1768	inches	θ_{ji}	93.8	degrees	ψ_c	15.0	degrees	contact width, 2b	0.007	inches
c	0.0624	inches	r_{ij}	0.205	inches	F_t	146	lbf	deflection/joint	0.00029	inches
ε	0.333		r_{ji}	0.170	inches	F_n	547	lbf	$\sigma_{bending,flexures}$	153	ksi
θ_j	30	degrees	r'	0.178	inches	$F_{t(friction)}$	55	lbf	$\sigma_{compression,flexures}$	214	ksi
μ	0.1		θ'	73.2	degrees	$F_{t(flexures)}$	92	lbf	$\sigma_{tensile,flexures}$	122	ksi
F	566	lbf	t	105.9	degrees	γ	71	degrees	$\sigma_{bend\_tens,flexures}$	196	ksi
L	0.375	inches	κ	291.8	degrees/inch	cos γ	0.32		$\sigma_{comp\_tens,flexures}$	390	ksi
h	0.002	inches	R_s	0.196	inches				$\sigma_{tensile,connecting\ links}$	73	ksi
A_{CL}	0.004	$inches^2$									
ν	0.28										
E	3.0E+07	psi	Δ	6.1E-08	psi^{-1}						

ing of a rectangular beam is

$$\sigma_{bending} = \frac{Mc}{I} \tag{4.22}$$

where M is equal to the perpendicular contact force times the lever arm d, c is half the plate thickness H, and I is the out-of-plane width of the plate times the thickness H cubed divided by 12.

To find the contact stress at the interface between the bar and the plate, we use the normal force at the contact points from Equation 4.15 where $N_B = -N_A$. These normal forces act over an area equal to half the plate thickness H times the width of the bar at the contact L. Inputs and results for stresses on the self-locking plates are presented in Table 4.3.

Note that for 0.2 g deceleration the stresses are acceptable; however, they are directly proportional to the applied force, so if F_A must increase five-fold in order to achieve design level brake torque for panic stops and aggressive driving, these stresses will be much too large. The binding plates will only work with such high forces if their geometry is altered to withstand bending in the plates and compression at the contacts.

Table 4.3 Bending and contact stress calculations for the self-locking plates.

Inputs			***Intermediate Calculations***			***Results***	
F	566 lbf		M	248 in-lbs		$\sigma_{bending}$	190 ksi
θ_j	0 degrees		c	0.063 inches		σ_{shear}	9 ksi
d	0.438 inches		I	8.1E-05 inches^4		$\sigma_{von\ Mises}$	191 ksi
H	0.125 inches		$N_B = -N_A$	2830 lbf		$\sigma_{contact}$	137 ksi
b	0.5 inches						
L	0.33 inches						
μ	0.1						

There are significant tradeoffs between self-locking reliability and resistance to bending and contact stress (e.g. increasing *H* and decreasing *d*). However, an improved design would increase *H* without decreasing self-locking reliability by adding material in the out-of-plane direction on either side of the self-locking plates while maintaining the perpendicular distance between contact points A and B the same (see Figure 4.22). Contact stresses can be reduced by increasing the surface area in contact between the plates and the bar.

4.7.3 Deflections and Output Stroke

The caliper arms that straddle the rotor to apply force to the outboard pad deflect because of the large reaction forces at the pads. Castigliano's method helps quantify these de-

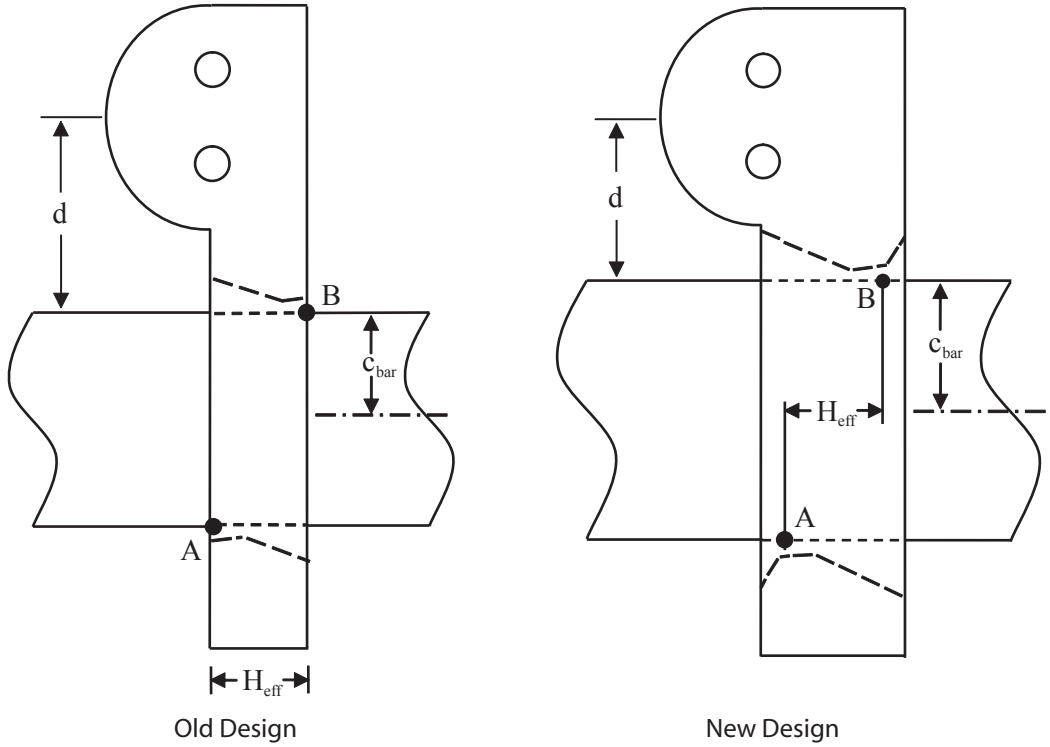

Figure 4.22 Proposed modifications to the geometry of the locking plate that will improve resistance to bending in the plates and compression at the contacts.

flections, and we observe 0.005 in. deflection for 0.2 g deceleration and 0.010 in. deflection for a 0.8 g stop.

For disc brakes, a significant contributor to required output stroke is the compressibility of the brake pads. Damped pads are used for reduced brake noise but are softer, with compressibility on the order of 9.0×10^{-6} in./psi [42]. Assuming a wheel cylinder diameter of 2 in., that equates to 0.003 in. of lost travel for a 0.2 g stop and 0.016 in. lost for a 0.8 g stop.

The MUSCLE Brake design proposes to eliminate backlash by maintaining the self-locking plates on the verge of locking, so it is assumed that binding requires no incremental output stroke. Similarly, wear for any one stop is assumed to be negligible, since pads and rotors with 0.70 in. available wear tend to last two to three years with tens of thousands of stops.

Combining the air gap closure with material and link deflections, we have a minimum required output stroke of 0.015 in. for 0.2 g deceleration and 0.036 in. for 0.8 g deceleration, as shown in Table 4.4. From Figure 4.12, the MUSCLE Brake—with eccentricity of 0.333—appears to provide sufficient output stroke to meet these minimum requirements.

Table 4.4 Summary of deflections through the MUSCLE Brake force flow path, including minimum requirements for a functional prototype.

Elements of Output Stroke (inches)		
Air Gap Closure	0.006	
Material Deflections	0.2 g stop	0.8 g stop
Elliptical Rolling Contact Joints	-	0.001
Self-Locking Plates	0.001	0.003
Caliper Arms	0.005	0.010
Compressibility of Pads	0.003	0.016
Minimum Required Output Stroke	0.015	0.036

However, it is important to consider deflections and compressibility, which act like a spring. Just as a brake system can only generate as much brake force as the road surface will allow (e.g. ice versus asphalt), a caliper can only clamp down as hard as the reactions push back, and if the path of force flow passes through "soft" materials or encounters backlash, the caliper mechanism may not generate the force required to provide the desired deceleration. Similarly, if the mechanism meets resistance before it has enough mechanical advantage to overcome that resistance, it may be rendered inoperable. Thus, self-adjustment is essential in maintaining the mechanism in the position that allows maximum force generation when and where it's needed, neither too early nor too late.

The MUSCLE Brake prototype is pictured in Figure 4.23. A test stand was built that the front corner module could be mounted to for future testing, and the wheel was custom-made with a negative offset so the brake components are in plain view for evaluation and analysis.

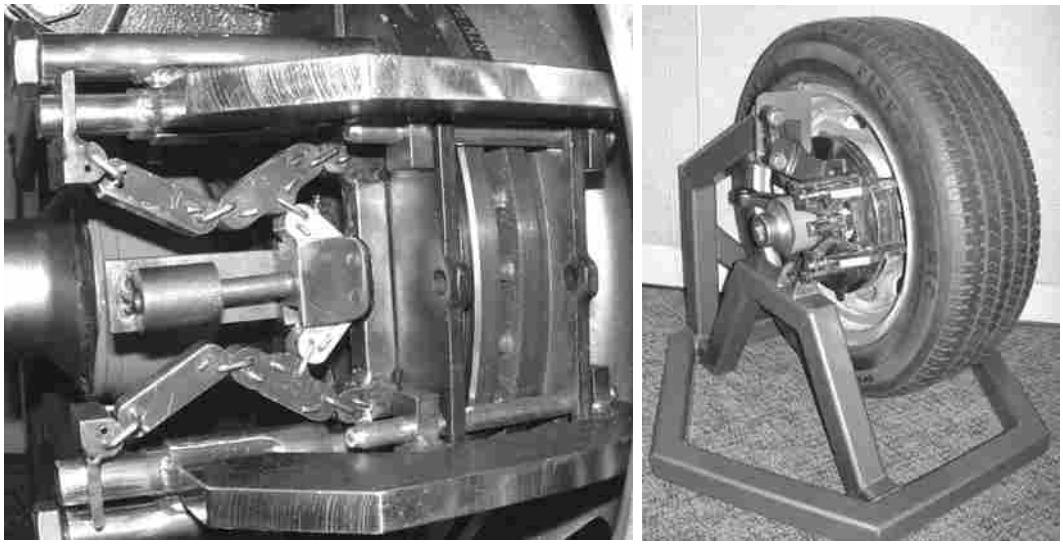

Figure 4.23 The MUSCLE Brake prototype.

CHAPTER 5 CONCLUSIONS AND RECOMMENDATIONS

The objective of this thesis has been to develop the kinematics for rolling link mechanisms with elliptical contact surfaces and identify the benefits, challenges, and trade-offs as applied generally and, more specifically, to the MUSCLE Brake electromechanical disc brake caliper. Toggle mechanisms were implemented for mechanical advantage and underactuation, and self-adjustment methods were analyzed.

In Chapter 3, connecting link angles were derived as a function of the elliptical eccentricity and relative link angle. These angles were then used to define critical characteristics at the contact point, including: polar angle to the contact point from the geometric center of the ellipse, curvature, radius of curvature, Hertz contact stress, and stress in the connecting links. If these characteristics are functions of the connecting link angles, and the connecting link angles are functions of the relative link angle, it follows that each of these characteristics are now tied to the relative link angle and can be incorporated into the design of mechanisms using standard generalized coordinates and other kinematic variables. Vector loops can be constructed through linkages containing multiple elliptical rolling contact joints to provide position analysis and its derivatives, which was demonstrated for the MUSCLE Brake.

5.1 Benefits of Elliptical Rolling Contact

Benefits of using elliptical rolling contact joints or elliptical rolling link mechanisms are similar to those of circular rolling contact joints, namely: low friction and backlash for high quality force transmission, large contact angles resisted by stabilizing constraints, and compact/simplified design. However, additional benefits are derived when elliptical rolling contact surfaces are used, including the following:

- Larger radii across the semi-minor axes yield lower Hertz contact stresses and flexure stresses.
- Changing radii across the surface of the joint as a function of elliptical eccentricity can create a customizable, variable output for quick rotation and then smooth, powerful compression. The curvature ratio characteristic of elliptically eccentric contact surfaces quantifies the relative distribution of rotation.
- For small oscillatory strokes, elliptical surfaces maximize the use of the whole available surface, not just the few degrees subtended by the same rotation on a circular contact surface.
- For toggle linkages, the force is maximum at the toggle point, which is within the friction wedge. Since forces generated by toggle linkages are not significant at large angles, tangential loads and stresses in the stabilization members are minimal.
- Compared to conventional revolute joints, elliptical rolling contact joints with connecting links have more “pin joints”, but much lower forces on those joints as they are isolated from bearing the force directly.
- Stress in the connecting links is relatively small for large eccentricities and small contact angles. Stress in the flexures does not inhibit motion.

- While circular rolling contact requires distinct provision for both tractive rolling (gear teeth or friction) and engagement (connecting link between centers of curvature), elliptical rolling contact is constrained for pure rolling and engagement by the connecting links only and does not require an additional constraint.
- Eccentricity can be selected to produce increased mechanical advantage at certain points in the range of motion.

5.2 Challenges Implementing Elliptical Rolling Contact

Mechanisms that incorporate elliptical rolling contact joints are relatively difficult to design and manufacture when compared to mechanisms that use conventional joints or even circular rolling contact. Due to the added complexity of elliptical surfaces, many designs of elliptical gears, for example, often aren't even ellipses but the combination of a few different circular radii that approximate the ellipse, a compromise made for ease of design and manufacture. The use of connecting links increases the number of "pin joints" by a factor of four. Using contact-aided compliant flexures requires the manufacture of monolithic layers that are subsequently stacked and assembled or an accurate method of separately attaching the flexures to the surfaces. It is anticipated, however, that the benefits described in this thesis will more than offset the added complexity for certain applications.

Another challenge cited by prior authors and confronted in this work is that of small link sizes with their relatively small radii creating large Hertz contact stresses as well as excessive bending stresses in the flexures. For the latter, the elliptical dimension c is definitive since $c = a\varepsilon$; therefore, increasing either a (link size) or ε (elliptical eccentricity of the contact surface) can reduce the stress at the contact.

Finally, rolling contact joints with thin stabilizing flexures are beneficial for large compressive loads over a relatively small range of motion. At large angles, they are limited by the combination of bending (due to the radius of curvature of the contact surface) and tension (as a result of large tangential forces at large contact angles).

5.3 MUSCLE Brake Lessons Learned

The initial MUSCLE Brake design required excessive actuation force and did not produce the brake torque anticipated. Two conceptual errors have been identified that, when combined with manufacturing complexity and variation, led to binding of the mechanism. For completeness, they are mentioned here, both as key takeaways relevant to mechanism design in general and also as next steps for future work on this project.

- The actuator toggles were originally designed to contact the caliper toggles at the contact joining the caliper toggle linkage (see Figure 4.9), not half-way down one of the links as manufactured (see Figure 4.18 and Figure 4.23). This change was incorporated to package longer actuator toggle links, but creates unfavorable transmission ratios between the actuator toggles and the adjacent links as well as large transmission angles between the actuator toggles and the most inboard caliper toggle link, L_4.
- The actuation stroke was constrained to slide back and forth inside a cylinder fixed perpendicular to the link connected to the inboard pad (see Figure 4.23). This constraint does not force simultaneous toggle or mirrored actuation across the line of symmetry; rather, one caliper toggles before the other and the inboard pad is canted and binds on the slide pins. Again, the concept from Figure 4.9 would have been a better execution, but three-way attachment in rolling contact is not well understood.

- The inboard pad is pushed against the rotor by 3/8 in. square bar stock that spans the width of the multi-toggle mechanism but contacts the pad approximately 1 in. below the slide pins (see Figure 4.23). Applying the governing equation for tip before slide, this configuration is self-locking. With the current hydraulic brake caliper architecture, brake pads don't bind on the slide pins because the wheel cylinder has a large diameter that creates a very short lever arm *d* and applies a force that is relatively uniform across a large portion of the backing plate. Thus, the pads are maintained perpendicular to the slide pins throughout their range of motion.
- Designing a mechanism with as much symmetry as the MUSCLE Brake is relatively easy; manufacturing such a mechanism to these symmetric specifications with little tolerance for error is very difficult, especially with prototyping where welds are used to join what might otherwise be monolithic cast or forged parts. Assuming the welder is expert in his trade and aligns everything as it should be, warping and movement due to heat are still typical. Consequently, the caliper arms didn't always slide within the mounting bolt brackets as designed.
- Future designs would also benefit from increased elliptical eccentricity and squared-off contact surfaces on the side opposite rotation (see Figure 4.21) so that large forces can be generated with reduced contact stress.

It is believed that these modifications will eliminate binding and allow the mechanism to move freely as intended; however, the ultimate success of this concept hinges on accurate self-adjustment since the MUSCLE Brake generates most of its force in the last 10º of caliper toggle rotation (0.030 in. of travel). If not accurately adjusted, the MUSCLE Brake will toggle too early or too late and produce inadequate application force to generate the brake torque necessary to stop the vehicle.

5.4 Recommendations for Future Work

One of the goals of this research was to seek a simplified design that leveraged the advantages of compliant mechanisms mentioned in Chapter 2. An improved method for accurately attaching stabilization bands would be beneficial as flexures provide the least amount of friction in the joint and allow non-identical ellipses and other dissimilar non-linear continuous surfaces to be joined in rolling contact. The 'CL' in MUSCLE was intended to be "compliant-linked", not "connecting-linked", and the former represents the ideal.

An adjacent category of toggle mechanism concepts that was not discussed are those concepts that derive high mechanical advantage coming *out* of toggle (in tension) as opposed to going *into* toggle (compression). One can imagine mechanical advantage curves that start at the infinite ideal (very large) and decrease exponentially, just the opposite of what is exhibited by the MUSCLE Brake. As long as the mechanical advantage is available where it's needed in the stroke, when it's needed, this is an equally viable solution. Loading links and joints in tension enables the use of a wider array of joints and linkage types. Several familiar mechanisms are examples of this type of "toggle mechanism", everything from a bow and arrow to conventional transverse-cable type cantilever bike brakes.

This thesis focused on elliptical surfaces whose major axes were perpendicular to the length or dominate dimension of the link. Some applications may benefit from elliptical surfaces whose major axes are not perpendicular, but skewed at some angle.

The elliptical contact joints analyzed herein assumed mating elliptical surfaces were identical, as required for elliptical gearing when connecting links are used. Further research should consider the benefits of pairing surfaces with different elliptical eccentricities or other dissimilar non-linear continuous surfaces, which are possible when flexures are used.

The elliptical rolling contact joint parameters and forward kinematics developed here provide a starting point for developing more extensive, generalized kinematics for elliptical rolling link mechanisms.

As discussed previously, one of the goals of this research was to build a prototype, mount it on a test stand, and validate the brake torque and functionality projected by the design. This remains an important aspect of design verification and is integral to future work on mechanical braking concepts.

REFERENCES

[1] Buchholz, K., 2004, "Escape Hybrid's Stopping Technology," *Automotive Engineering International*, December 2004, p. 20.

[2] Sutton, M., 2007, "Siemens Wedge Brake Shines in Winter Testing." http://subscribers.wardsauto.com/ar/siemens_wedge_brake/index.html (April 20, 2007).

[3] Kelling, N. A., and Leteinturier, P., 2003, "X-by-Wire: Opportunities, Challenges and Trends," *SAE Technical Paper Series*, 2003-01-0113.

[4] Sundar, M., and Plunkett, D., 2006, "Brake-by-Wire, Motivation and Engineering - GM Sequel," *SAE Technical Paper Series*, 2006-01-3194.

[5] Yoshikawa, T., 1996, "Passive and Active Closures by Constraining Mechanisms," in *Proceedings of the 1996 13th IEEE International Conference on Robotics and Automation*, vol. 2, Minneapolis, Minnesota, pp. 1477-1484.

[6] Brooks, S. H., 2003, "Design of Compliant Mechanisms for Grasping with Application to Mechanical Disc Brakes," M.S. Thesis, Brigham Young University, Provo, Utah.

[7] Brooks, S. H., Magleby, S. P., and Howell, L. L., 2005, "Grasping Mechanisms with Self-centering and Force-balancing Characteristics," in *Proceedings of the 2005 ASME Design Engineering Technical Conferences*, DETC2005-85478.

[8] Laliberté, T., and Gosselin, C.M., 1998, "Simulation and Design of Underactuated Mechanical Hands," *Mechanism & Machine Theory*, vol. 33, no. 1-2, pp. 39-57.

[9] Birglen, L., and Gosselin, C. M., 2006, "Force Analysis of Connected Differential Mechanisms: Application to Grasping," *International Journal of Robotics Research*, vol. 25, no. 10, pp. 1033-1046.

[10] Fetherston, D., 2007, "Automobile." http://encarta.msn.com/encyclopedia_76157-6902/Automobile.html (May 14, 2007).

[11] Society of Automotive Engineering, 1999, *Driving Safety Systems*, Robert Bosch GmbH, Stuttgart, Germany.

[12] Birglen, L., and Gosselin, C. M., 2004, "Kinetostatic Analysis of Underactuated Fingers," *IEEE Transactions on Robotics and Automation*, vol. 20, no. 2, pp. 211-221.

[13] Warheit, W. A., 1987, "Self-adjusting Utility Plier," United States Patent No. 4651598.

[14] Hostetter, J. L., 1964, "Self-adjusting Plier-type Toggle Locking Wrench," United States Patent No. 3116656.

[15] Sorensen, J. A., and Gatzemeyer, D. L., 1990, "Quick-action Bar Clamp," United States Patent No. 4926722.

[16] Myszka, D. H., 2005, *Machines and Mechanisms: Applied Kinematic Analysis*, 3rd Ed., Pearson Prentice Hall, Upper Saddle River, New Jersey.

[17] Howell, L. L., 2001, *Compliant Mechanisms*, John Wiley & Sons, Inc., New York, New York.

[18] Guérinot, A. E., Magleby, S. P., Howell, L. L., and Todd, R. H., 2005, "Compliant Joint Design Principles for High Compressive Load Situations," *Journal of Mechanical Design*, vol. 127, no. 4, pp. 774-781.

[19] Wilkes, D. F., 1967, "Rolamite: A New Mechanical Design Concept," Report SC-RR-67-656A, Sandia Laboratory, Albuquerque, New Mexico.

[20] Kuntz, J. P., 1995, "Rolling Link Mechanisms," Ph.D. Dissertation, Delft University of Technology, Delft, Netherlands.

[21] Chironis, N. P., and Sclater, N., 1996, *Mechanisms & Mechanical Devices Sourcebook*, 2nd Ed., McGraw-Hill, New York, New York.

[22] Collins, C. L., 2003, "Kinematics of Robot Fingers with Circular Rolling Contact Joints," *Journal of Robotic Systems*, vol. 20, no. 6, pp. 285-296.

[23] Herder, J. L., 1998, "Force Directed Design of Laparoscopic Forceps," in *Proceedings of the 1998 ASME Design Engineering Technical Conferences*, DETC98/MECH-5978.

[24] van der Pijl, A. J., and Herder, J. L., 2001, "Development of 5mm-trocar Laparoscopic Forceps with Mechanical Force Feedback," in *Proceedings of the 2001 ASME Design Engineering Technical Conferences*, DETC2001/DAC-21070.

[25] Visser, H. de, and Herder, J. L., 2000, "Force-directed Design of a Voluntary Closing Hand Prosthesis," *Journal of Rehabilitation Research and Development*, vol. 37, no. 3, pp. 261-271.

[26] Jeanneau, A., Herder, J. L., Laliberté, T., and Gosselin, C. M., 2004, "A Compliant Rolling Contact Joint and its Application in a 3-DOF Planar Parallel Mechanism with Kinematic Analysis," in *Proceedings of the 2004 ASME Design Engineering Technical Conferences*, DETC2004-57264.

[27] Collins, C. L., 2002, "Kinematics of a Spatial Three Degree-of-Freedom Robot with Rolling Contact Joints," in *Proceedings of the 2002 ASME Design Engineering Technical Conferences*, DETC2002/MECH-34250.

[28] Cannon, J. R., Lusk, C. P., and Howell, L. L., 2005, "Compliant Rolling-contact Element Mechanisms," in *Proceedings of the 2005 ASME Design Engineering Technical Conferences*, DETC2005-84073.

[29] Weisstein, E. W., 2005, "Ellipse." http://mathworld.wolfram.com/Ellipse.html (June 10, 2005).

[30] Halverson, P. A., 2007, "Multi-stable Compliant Rolling-contact Elements," M.S. Thesis, Brigham Young University, Provo, Utah.

[31] Juvinall, R. C., 1967, *Engineering Considerations of Stress, Strain, and Strength*, McGraw-Hill, New York, New York.

[32] Norton, R. L., 2000, *Machine Design: An Integrated Approach*, 2nd Ed., Prentice Hall, Upper Saddle River, New Jersey.

[33] Balli, S. S., and Chand, S., 2002, "Transmission Angle in Mechanisms (Triangle in Mech)," *Mechanism and Machine Theory*, vol. 37, no. 2, pp. 175-195.

[34] Salamon, B.A., and Midha, A., 1998, "Introduction to Mechanical Advantage in Compliant Mechanisms," *Journal of Mechanical Design*, vol. 120, no. 2, pp. 311-315.

[35] Paul, B., 1979, *Kinematics and Dynamics of Planar Machinery*, Prentice Hall, Englewood Cliffs, New Jersey.

[36] Norton, R. L., 2004, *Design of Machinery: An Introduction to the Synthesis and Analysis of Mechanisms and Machines*, 3rd Ed., McGraw-Hill, New York, New York.

[37] Munem, M. A., and Foulis, D. J., 1984, *Calculus with Analytic Geometry*, 2nd Ed., Worth Publishers, New York, New York.

[38] Brembo SpA, 1998, *Automotive Disc Brake Manual*, Haynes Techbook Series No. 3542, Haynes Publishing, Somerset, England.

[39] Lumpkin, W. R., and Mayberry, M. T., 2003, "Caliper Drive for a Bicycle Ball Bearing Mechanical Disc Brake Caliper," United States Patent No. 6527089.

[40] "History of the Automobile: Brakes." http://www.motorera.com/history/hist-07.htm (September 24, 2005).

[41] Kowalski, M. F., 2003, "Hydraulic Brake Systems," *SAE Seminars*, Troy, Michigan.

[42] Limpert, Rudolf, 1999, *Brake Design and Safety*, 2nd Ed., Society of Automotive Engineers, Warrendale, Pennsylvania.

[43] Hartmann, H., Schautt, M., Pascucci, A., and Gombert, B., 2002, "eBrake - The Mechatronic Wedge Brake," *SAE Technical Paper Series*, 2002-01-2582.

[44] Roberts, R., Schautt, M., Hartmann, H., and Gombert, B., 2003, "Modelling and Validation of the Mechatronic Wedge Brake," *SAE Technical Paper Series*, 2003-01-3331.

[45] Huang, H., Miller, J., and Nicastri, P., 1999, "Automotive Electrical System in the New Millennium," *SAE Technical Paper Series*, 1999-01-3747.

[46] Ho, L. M., Roberts, R., Hartmann, H., and Gombert, B., 2006, "The Electronic Wedge Brake - EWB," *SAE Technical Paper Series*, 2006-01-3196.

[47] Fox, J., Roberts, R., Baier-Welt, C., Ho, L. M., Lacraru, L., and Gombert, B., 2007, "Modeling and Control of a Single Motor Electronic Wedge Brake," *SAE Technical Paper Series*, 2007-01-0866.

[48] Schwarz, R., Isermann, R., Bohm, J., Nell, J., and Rieth, P., 1999, "Clamping Force Estimation for a Brake-by-Wire Actuator," *SAE Technical Paper Series*, 1999-01-0482.

[49] Maron, C., Dieckmann, T., Hauck, S., and Prinzler, H., 1997, "Electromechanical Brake System: Actuator Control Development System," *SAE Technical Paper Series*, 970814.

[50] Marks, L. S., 1996, *Marks' Standard Handbook for Mechanical Engineers*, 10th Ed., McGraw-Hill, New York, New York.